Metabolic capabilities are highly conserved among human nasal-associated *Corynebacterium* species in pangenomic analyses

Authors: Tommy H. Tran[a], Isabel F. Escapa[a*], Ari Q. Roberts[a*], Wei Gao[b,c,^], Abiola C. Obawemimo[a], Julia A. Segre[d], Heidi H. Kong[e], Sean Conlan[d], Matthew S. Kelly[f], Katherine P. Lemon[a,g#]

Affiliations

[a]Alkek Center for Metagenomics & Microbiome Research, Department of Molecular Virology & Microbiology, Baylor College of Medicine, Houston, Texas, USA

[b]The Forsyth Institute (Microbiology), Cambridge, MA, USA

[c]Department of Oral Medicine, Infection and Immunity, Harvard School of Dental Medicine, Boston, MA, USA

[d]Microbial Genomics Section, Translational and Functional Genomics Branch, National Human Genome Research Institute, National Institutes of Health, Bethesda, MD, USA

[e]Dermatology Branch, National Institute of Arthritis and Musculoskeletal and Skin Diseases, National Institutes of Health, Bethesda, MD, USA

[f]Division of Pediatric Infectious Diseases, Duke University School of Medicine, Durham, NC, USA

[g]Division of Infectious Diseases, Texas Children's Hospital, Department of Pediatrics, Baylor College of Medicine, Houston, Texas, USA

Running Title: Nasal *Corynebacterium* spp. share metabolic abilities

[#]Address correspondence to Katherine P. Lemon, katherine.lemon@bcm.edu

Present affiliation:

*Equal contribution

^W.G. is now at Illumina Inc. (of San Diego, CA, USA) in Melbourne, Australia

Abstract word count: 248

Text word count: 7303

Keywords: nasal microbiota, phylogenetics, pangenomics, metabolism, *Corynebacterium accolens*, *Corynebacterium propinquum*, *Corynebacterium pseudodiphtheriticum*, *Corynebacterium tuberculostearicum, Corynebacterium*

ABSTRACT

Corynebacterium species are globally ubiquitous in human nasal microbiota across the lifespan. Moreover, nasal microbiota profiles typified by higher relative abundances of *Corynebacterium* are often positively associated with health. Among the most common human nasal *Corynebacterium* species are *C. propinquum*, *C. pseudodiphtheriticum, C. accolens*, and *C. tuberculostearicum*. To gain insight into the functions of these four species, we identified genomic, phylogenomic, and pangenomic properties and estimated the metabolic capabilities of 87 distinct human nasal *Corynebacterium* strain genomes: 31 from Botswana and 56 from the USA. *C. pseudodiphtheriticum* had geographically distinct clades consistent with localized strain circulation, whereas some strains from the other species had wide geographic distribution spanning Africa and North America. All species had similar genomic and pangenomic structures. Gene clusters assigned to all COG metabolic categories were overrepresented in the persistent versus accessory genome of each species indicating limited strain-level variability in metabolic capacity. Based on prevalence data, at least two *Corynebacterium* species likely coexist in the nasal microbiota of 82% of adults. So, it was surprising that core metabolic capabilities

46 were highly conserved among the four species indicating limited species-level metabolic
47 variation. Strikingly, strains in the USA clade of *C. pseudodiphtheriticum* lacked genes for
48 assimilatory sulfate reduction present in most of the strains in the Botswana clade and in
49 the other studied species, indicating a recent, geographically related loss of assimilatory
50 sulfate reduction. Overall, the minimal species and strain variability in metabolic capacity
51 implies coexisting strains might have limited ability to occupy distinct metabolic niches.

52 **IMPORTANCE**

53 Pangenomic analysis with estimation of functional capabilities facilitates our
54 understanding of the full biologic diversity of bacterial species. We performed systematic
55 genomic, phylogenomic, and pangenomic analyses with qualitative estimation of the
56 metabolic capabilities of four common human nasal *Corynebacterium* species, along with
57 focused experimental validations, generating a foundational resource. The prevalence of
58 each species in human nasal microbiota is consistent with the common coexistence of at
59 least two species. We identified a notably high level of metabolic conservation within and
60 among species indicating limited options for species to occupy distinct metabolic niches,
61 highlighting the importance of investigating interactions among nasal *Corynebacterium*
62 species. Comparing strains from two continents, *C. pseudodiphtheriticum* had restricted
63 geographic strain distribution characterized by an evolutionarily recent loss of assimilatory
64 sulfate reduction in USA strains. Our findings contribute to understanding the functions of
65 *Corynebacterium* within human nasal microbiota and to evaluating their potential for
66 future use as biotherapeutics.

67 **INTRODUCTION**

68 Nasal *Corynebacterium* species are frequently associated with health in compositional
69 studies of human nasal microbiota. *Corynebacterium* are gram-positive bacteria in the
70 phylum Actinobacteria (Actinomycetota). Based on studies from five continents,
71 *Corynebacterium* species begin colonizing the human nasal passages before two months
72 of age (1-13). *Corynebacterium* colonize both the skin-coated surface of the nasal
73 vestibule (aka nostrils/nares) and the mucus-producing nasal respiratory epithelium
74 coating the nasal passages posterior of the limen nasi through the nasopharynx (14-19).
75 The bacterial microbiota of the human nasal passages from the nostrils through the
76 nasopharynx is highly similar, and we refer to it herein as the human nasal microbiota.

77 Pediatric nasal microbiota profiles characterized by a high relative abundance of
78 *Corynebacterium* are often associated with health rather than a specific disease or
79 disease-risk state in children (1, 2, 4, 7, 11-13, 20-30). In young children, the genus
80 *Corynebacterium* (alone or with the genus *Dolosigranulum*) is negatively associated with
81 *Streptococcus pneumoniae* nasal colonization, which is important because *S.*
82 *pneumoniae* colonization is a necessary precursor to invasive pneumococcal disease (13,
83 20, 22, 25, 28). For example, in young children in Botswana, the genus *Corynebacterium*
84 is negatively associated with *S. pneumoniae* colonization both in a cross-sectional study
85 of children younger than two years (25) and in a longitudinal study of infants followed from
86 birth to one year of age (13). In contrast to these genus-level associations, little is known
87 about species-level prevalence and relative abundance of nasal *Corynebacterium* in
88 children. However, in a cultivation-based study, *C. pseudodiphtheriticum* is positively
89 associated with ear and nasal health in young Indigenous Australian children (age 2-7
90 years), as is *D. pigrum* (29).

91 In adult nasal microbiota, the prevalence of the genus *Corynebacterium* is as high as
92 98.6%, with highly prevalent species including *C. accolens* (prevalence of 82%), *C.*
93 *tuberculostearicum* (93%), *C. propinquum* (18%), and *C. pseudodiphtheriticum* (20%),
94 based on 16S rRNA V1-V3 sequences (Tables S4A-B and S7 in (31)). In these data, 82%
95 of the adult nostril samples contained ≥ 2 of these 4 *Corynebacterium* species, 30%
96 contained ≥ 3, and 2.4% contained all 4 species. Thus, there is a high probability of
97 coexistence of these *Corynebacterium* species in nasal microbial communities. Like
98 children, some adults have nasal microbiota profiles characterized by a high relative
99 abundance of *Corynebacterium* (18, 32). At least 23 validly published species of
100 *Corynebacterium* can be cultivated from the adult nasal passages (17, 33). However,
101 among these, *C. accolens* and *C. tuberculostearicum* (and/or other members of the *C.*
102 *tuberculostearicum* species complex (34)) followed by *C. propinquum* and *C.*
103 *pseudodiphtheriticum* are the most common in human nasal microbiota, in terms of both
104 prevalence and relative abundance (15, 17, 31, 33). Indeed, the human nasal passages
105 appear to be a primary habitat for *C. accolens, C. propinquum*, and *C.*
106 *pseudodiphtheriticum,* whereas *C. tuberculostearicum* is also prevalent, often at high
107 relative abundances, at other human skin sites (31, 34-37).

108 Nasal *Corynebacterium* interact with other common commensal/mutualistic nasal
109 microbionts (38, 39) and with nasal pathobionts (22, 40-42). Some studies of healthy adult
110 nasal microbiota report a negative association between *Staphylococcus aureus* and
111 either the genus *Corynebacterium* or specific species of *Corynebacterium* (14, 31, 32, 43-
112 47), although others do not (which might reflect strain-level variation and/or differences in
113 populations studied). Furthermore, several small human studies support the potential use

114 of *Corynebacterium* species to inhibit or eradicate pathobiont colonization of the human
115 nasal passages (43, 48). This is of particular interest for *S. aureus* in the absence of an
116 effective vaccine, since *S. aureus* nasal colonization increases the risk of invasive
117 infection at distant body sites and the infection isolate matches the colonizing isolate in
118 ~80% of cases (49-52). Studies in mouse models further support potential benefits of
119 nasal *Corynebacterium* for the prevention/treatment of respiratory syncytial virus and
120 pneumococcal infections (53, 54). Inhibition of *S. pneumoniae* or *S. aureus in vitro* by
121 nasal *Corynebacterium* species displays strain-level variation, highlighting the importance
122 of sequencing the genomes of multiple strains per species (13, 14, 28, 55). An increasing
123 number of these inhibitory interactions are characterized (22, 40, 41, 54).

124 Some interactions between *Corynebacterium* species and other nasal microbionts are
125 related to metabolism/metabolites. For example, *C. accolens* strains secrete the
126 triacylglycerol lipase LipS1 to hydrolyze host-surface triacylglycerols releasing
127 nutritionally required free fatty acids that also inhibit *S. pneumoniae in vitro* (22, 54).
128 Additionally, a positive metabolic interaction, such as cross-feeding, might be how *C.*
129 *accolens*, *C. pseudodiphtheriticum,* and *C. propinquum* enhance the growth yield of the
130 candidate mutualist *D. pigrum in vitro* (38). These examples highlight the importance of
131 sequencing the genomes of multiple strains of each species to elucidate their metabolic
132 capabilities, and the variation, that might influence interspecies interactions and
133 contribute to promoting health-associated nasal microbiome compositions.

134 Overall, their ubiquity, frequent positive associations with health, and potential therapeutic
135 use raise fundamental questions about the role of *Corynebacterium* species in human
136 nasal microbiota. To increase genomic and metabolic knowledge of these, we performed

systematic phylogenomic and pangenomic analyses of four common human nasal-associated *Corynebacterium* species. To increase the generalizability of our findings, we analyzed genomes of 87 nasal strains collected across two continents from both children and adults. Nasal strains of *C. pseudodiphtheriticum* overwhelmingly partitioned into clades by country of origin, consistent with geographically restricted strain circulation. Comparison of the core versus accessory genome of each of these four *Corynebacterium* species demonstrated that all COG categories associated with metabolism were enriched in the core genome, indicating limited strain-level metabolic variation within each species. To provide broader context, we compare the predicted metabolic abilities of nasal *Corynebacterium* species to two well-studied *Corynebacterium* species, *C. diphtheriae* and *C. glutamicum*, and to common nasal species from other bacterial genera. Metabolic estimation revealed that these four species share the majority of KEGG modules with few species-specific, or even clade-specific, metabolic abilities. However, we found that the clade of *C. pseudodiphtheriticum* dominated by strains from the USA lacked the module for assimilatory sulfate reduction, which is key for biosynthesis of sulfur-containing amino acids, and two representative USA strains were unable to grow under conditions requiring sulfate assimilation. We also validated the predictions that *C. tuberculostearicum,* alone of the four nasal species, accumulated intracellular glycogen and that *C. tuberculostearicum* and *C. accolens* generated all 20 amino acids since both grew in their absence.

RESULTS

158 ***Corynebacterium pseudodiphtheriticum* displays geographically restricted strain**
159 **circulation.** To compare the genomic content and phylogenomic relationships among
160 and within four *Corynebacterium* species commonly found in human nasal microbiota, we
161 isolated strains from the nasal vestibule (nostrils) of generally healthy children and adults
162 in the USA and from nasopharyngeal swabs of mother-infant pairs in Botswana. We
163 compared 87 distinct nasal strain genomes to publicly available genomes of the type
164 strain plus several other reference strains of each species, for a total of 20 reference
165 genomes (39, 56-60) (**Table S1A**).

166 To confidently assign each new nasal isolate to a species, we first generated a maximum-
167 likelihood phylogenomic tree based on the 632 single-copy core gene clusters (GCs)
168 shared by the 107 strain genomes (**Fig. S1A**) and determined that each new nasal isolate
169 was in a clade with the type strain of one of the nasal species (**Fig. S1B**; type strains in
170 bold). *C. macginleyi* is the closest relative of *C. accolens* and these two species are
171 challenging to distinguish by partial 16S rRNA gene sequences. Therefore, we included
172 three *C. macginleyi* genomes in this phylogenomic analysis to confidently assign
173 candidate *C. accolens* strains to a species. This five-species phylogenomic tree contained
174 two major clades (**Fig. S1B**) confirming that *C. propinquum* and *C. pseudodiphtheriticum*
175 are more closely related to each other, whereas *C. macginleyi*, *C. accolens*, and *C.*
176 *tuberculostearicum* are more closely related to each other, with *C. macginleyi* closest to,
177 yet distinct from *C. accolens.* Furthermore, these two major clades are distinctly separate
178 from each other in a broader phylogenomic representation of the genus *Corynebacterium*
179 (**Fig. S1C**, **Table S1C**). Next, we confirmed that each strain had a pairwise average
180 nucleotide identity (ANI) of ≥ 95% for core GCs compared to the type strain of its assigned

181 species (**Fig. S2A**). For each species, the pairwise ANIs for core GCs were very similar
182 to those for all shared CoDing Sequences (CDS) (**Fig. S2B**).

183 To assess the evolutionary relationships between nasal isolates from both the USA and
184 Botswana, we produced individual maximum-likelihood phylogenomic trees for each
185 species (**Fig. 1**) based on its conservative core genome (**Fig. S2C**). These species-
186 specific phylogenies provided a refined view of the relationships between strains based
187 on the larger number of shared single-copy core GCs within each species (ranging from
188 1345 to 1788). To better approximate the root of each species-specific tree (**Fig. 1**), we
189 used the type strain of the most closely related species in the multispecies phylogenomic
190 trees (**Fig. S1**) as the outgroup (**Fig. S2D**). With a relatively even representation of
191 Botswana and USA strains (40% vs. 58%), the phylogenomic tree for *C.*
192 *pseudodiphtheriticum* had two large, well-supported clades dominated respectively by
193 nasal strains from Botswana (15/15) or from the USA (20/22), indicating a restricted
194 distribution of strains by country (**Fig. 1B**). We avoided calculating geographic proportions
195 within major clades for *C. propinquum* (**Fig. 1A**) and *C. accolens* (**Fig. 1C**) because of
196 the disproportionately high representation of USA strains (80%) and for *C.*
197 *tuberculostearicum* (**Fig. 1D**) because there were only 6 nasal strains, 5 of which were
198 from Botswana. Within these limitations, the phylogenomic analysis of these three
199 species revealed some remarkably similar strains present in samples collected in the USA
200 and Botswana based on their residing together in terminal clades. This raises the
201 possibility that a subset of strains from each of these three species might have a wide
202 geographic distribution, spanning from at least Botswana to Massachusetts.

203 **The sizes of the core genomes of four common nasal *Corynebacterium* species**
204 **have leveled off.** Based on rarefaction analysis, the core genomes of *C. propinquum, C.*
205 *pseudodiphtheriticum, C. accolens,* and *C. tuberculostearicum* have reached a stable size
206 and are unlikely to decrease much further with the sequencing of additional strains (**Fig.**
207 **2Ai-Aiv**). Based on the respective Tettelin curves (red line), the *C. tuberculostearicum*
208 core genome stabilized first at ~7 genomes; however, with the fewest genomes at 8 this
209 might be an upper bound that will continue to decrease with additional strain genomes.
210 In comparison, *C. pseudodiphtheriticum* had the largest number of strain genomes at 43,
211 with pairwise ANIs of ≥ 96.2% (**Fig. S2Aii**), and its core genome stabilized last at ~37
212 genomes.

213 The proportion of an individual genome of each of these nasal *Corynebacterium* species
214 devoted to conservative core GCs ranged from 72% for *C. pseudodiphtheriticum*
215 (1517/2105) to 79% for *C. tuberculostearicum* (1788/2250). This is based on the average
216 number of CDS per genome (**Table 1**). The average / median genome size for each
217 species ranged from ~2.33 / 2.33 Mb for *C. pseudodiphtheriticum* to ~2.51 / 2.52 Mb for
218 *C. propinquum* with the average / median predicted CDS per genome ranging from 2105
219 / 2096 for *C. pseudodiphtheriticum* to 2265 / 2272 for *C. propinquum* (**Table 1**). These
220 sizes and proportions are consistent with the reduced genome size and the GCs per
221 genome of host-associated compared to environment-associated *Corynebacterium*
222 species. For example, Swaney et al. report that environmental *Corynebacterium* species
223 have a larger median genome size of 3.03 Mb and more GCs per genome (with an
224 average of 2664) compared to host-associated *Corynebacterium* species (61).

225 **The pangenomes of these four human nasal-associated *Corynebacterium* species**
226 **remain open.** With the number of strain genomes analyzed (**Table 1**), the pangenome of
227 each of the four species continued to increase with each additional new genome,
228 indicating that all are open (**Fig. 2Bi-Biv**). Parameters used to generate a pangenome
229 via rarefaction yielded an overly conservative estimate of its size in GCs. Therefore, we
230 used two other approaches to estimate the number of GCs in the pangenome for each
231 species. These pangenome composition estimates are a lower bound for each species
232 and will increase with sequencing of additional strain genomes. Starting with
233 GET_HOMOLOGUES, we estimated pangenome size using the COG triangle and OMCL
234 clustering algorithms. The pangenome size and its proportion contributed by core versus
235 accessory GCs for each species ranged from 3232 GCs with 56% core and 44%
236 accessory for *C. tuberculostearicum* to 4590 GCs with 33% core and 67% accessory for
237 *C. pseudodiphtheriticum* (**Table 2**). The 56% core percentage for *C. tuberculostearicum*
238 is likely an overestimate since this pangenome is based on only 8 genomes. This range
239 of 33% to 56% for core genes per pangenome is similar to estimates for other human
240 upper respiratory tract microbionts, such as *D. pigrum* (31%) (62), *S. aureus* (36%), and
241 *Streptococcus pyogenes* (37%) (63).

242 Next, we used anvi'o to estimate the core- and pangenomes (64). The number of GCs in
243 the core genome of each species estimated with GET_HOMOLOGUES was within 6-13%
244 of those estimated with anvi'o; however, the GET_HOMOLOGUES estimated
245 pangenome sizes were 11-24% larger (**Fig. S3A, File S1**). Consistent with this, the
246 estimated single-copy core as a proportion of the pangenome using anvi'o was higher for
247 each species ranging from 41% to 64% (**Fig. S3B**).

248 We also used anvi'o to visualize the strain-level variation in gene presence and absence
249 within the four human nasal-associated *Corynebacterium* species (**Fig. S3B**). Manually
250 arraying the genomes in anvi'o to correspond with their species-specific phylogenomic
251 tree (**Fig. 1**) showed that some blocks of gene presence/absence correlated with the core-
252 genome-based phylogenetic relationships among strains, but others did not (**Fig. S3B**).
253 This is consistent with gene gain and loss playing a role in strain diversification with some
254 of this due to mobile genetic elements and horizontal gene transfer (65, 66).

255 **Gene clusters assigned to the COG categories associated with metabolism are**
256 **highly enriched in the core genomes of common nasal *Corynebacterium* species.**
257 To predict and compare functions based on the pangenomes of each species, we
258 assigned GCs to COG categories and used PPanGGOLiN to define the persistent versus
259 the accessory genome (**Table S2**) (67). We used the PPanGGOLiN estimation of the
260 persistent genome rather than the traditionally defined core genome for this analysis
261 because PPanGGOLin limits the effect of technical artifacts and/or strain-level gene loss
262 events on the assessment of persistently shared gene clusters by considering the
263 genomic context via examining genetic contiguity. As is common in bacteria, only about
264 63-65% of the GCs in the persistent genome and 26-36% of the GCs in the accessory
265 genome of each species had an informative assignment to a definitive COG category
266 (**Figs. 3Ai-iv & S4Ai-iv**). There was also variability in the size of the accessory genome
267 among strains within each species (**Fig. S4A-B**). We next generated functional
268 enrichment plots for COG categories in the persistent versus the accessory genome of
269 each species (**Fig. 3Bi-vi**). GCs assigned to "Mobilome: prophages, transposons" (mobile
270 genetic elements (MGEs); orange bar **Fig. 3B**) were overrepresented in the accessory

271 genome of each species with the ratio of GCs in the accessory/persistent genome ranging
272 from 4.2 (*C. tuberculostearicum*) to 36.1 (*C. pseudodiphtheriticum*). GCs assigned to
273 "defense mechanisms" (purple bar **Fig. 3B**), which protect bacteria from MGEs, were
274 more evenly distributed with the ratio of GCs in the accessory/persistent genome ranging
275 from 1 (*C. tuberculostearicum*) to 2.9 (*C. pseudodiphtheriticum*). These findings are
276 consistent with pangenomic analyses of other bacterial species, including our prior
277 analysis of the candidate beneficial nasal bacterium *D. pigrum* (62).

278 Our COG-enrichment analysis also showed that all the COG categories associated with
279 metabolism, from "energy production and conversion" (pale orange) through "secondary
280 metabolites biosynthesis, transport, and catabolism" (pink) in **Fig. 3B,** were highly
281 overrepresented in the persistent (or core) genome of each species with ratios of
282 accessory/persistent ranging from 0.02 to 0.56 (median of 0.16). The exception was an
283 accessory/persistent GC ratio of 1.2 for "secondary metabolites biosynthesis, transport,
284 and catabolism" in *C. pseudodiphtheriticum*. The overrepresentation of metabolic
285 categories in the persistent genome of each species points to limited strain-level variation
286 in metabolic capabilities, such as carbohydrate or amino acid metabolism. This contrasts
287 with our previous analysis of *D. pigrum* in which GCs assigned to the COG category
288 "carbohydrate transport and metabolism" are enriched in the accessory genome (ratio
289 1.66) (62).

290 **Common human nasal-associated *Corynebacterium* species have a largely shared**
291 **metabolic capacity**. Based on 16S rRNA V1-V3 sequences, 82% of adults are colonized
292 with ≥ 2 of these 4 *Corynebacterium* species (see Tables S4A-B and S7 in (31)). This,
293 combined with the enrichment of GCs assigned to metabolism COG categories in each

294 persistent genome, led us to hypothesize that there would be much species-specific
295 variation in core metabolic capabilities enabling the different nasal *Corynebacterium*
296 species to occupy distinct metabolic niches within human nasal microbiota. To test our
297 hypothesis, we used anvi'o to assign genes to Kyoto Encyclopedia of Genes and
298 Genomes (KEGG) Orthology family (KO) annotations (**Table S3A**) and to estimate KEGG
299 module completeness (**Table S4A-B**). In contrast to our hypothesis, we learned that *C.*
300 *propinquum*, *C. pseudodiphtheriticum*, *C. accolens,* and *C. tuberculostearicum* encode
301 highly conserved core metabolic capabilities sharing 43 of 58 (74%) detected fully
302 complete KEGG modules (**Table 3**, **Fig. 4**). Next, we identified modules enriched in one
303 or more of the four species, with various combinations of three of the four species sharing
304 eleven additional modules (19%) and combinations of two of the four species sharing
305 three additional modules (**Table S4D**). There were a few differences between the *C.*
306 *propinquum-C. pseudodiphtheriticum* clade and the *C. accolens-C. tuberculostearicum*
307 clade (**Fig. S1B**), with one and eight clade-specific KEGG modules, respectively. Only *C.*
308 *tuberculostearicum*, which is broadly distributed across human skin sites as well as in the
309 nasal passages (31, 34-37), was predicted to encode one complete KEGG module that
310 was absent in the other three nasal species, as discussed in detail later.

311 **Nasal *Corynebacterium* species encode for central carbohydrate metabolism**. To
312 contextualize our findings within the genus *Corynebacterium*, we included in our anvi'o
313 analyses the genomes of the type strains of two well-studied *Corynebacterium* species:
314 *C. glutamicum* ATCC 13032 (*C. glutamicum*^{T}) (68) and *C. diphtheriae* NCTC11397 (*C.*
315 *diphtheriae*^{T}) (**Table S1D**). The metabolism of the soil bacterium *C. glutamicum* is the
316 best studied of *Corynebacterium* species (69). *C. diphtheriae* colonizes the human

317 pharynx and toxigenic strains cause the human disease diphtheria (70). Along with *C.*
318 *diphtheriae*^{T} and *C. glutamicum*^{T}**,** the four human nasal *Corynebacterium* species all
319 encoded complete modules for glycolysis and gluconeogenesis, the pentose phosphate
320 pathway and phosphoribosyl pyrophosphate, and the tricarboxylic acid (TCA) cycle as
321 part of central carbon metabolism (**Table 3**). In terms of other carbohydrate metabolism,
322 all four nasal species, plus *C. diphtheriae*^{T} and *C. glutamicum*^{T}, also encoded a complete
323 module for UDP-N-acetyl-D-glucosamine biosynthesis (M00909), a precursor of cell wall
324 peptidoglycan (71). All four species plus *C. diphtheriae*^{T}, but not *C. glutamicum*^{T}, also
325 encoded the module for the Leloir pathway for galactose degradation.

326 **Nasal *Corynebacterium* species encode for synthesis of key biosynthetic**
327 **cofactors, vitamins, and electron transport chain components.** The strain genomes
328 of all four species contained complete modules for biosynthesis of several cofactors and
329 vitamins required for synthesis of essential biomolecules and central metabolism (**Table**
330 **3**). These include coenzyme A (M00120), required for the TCA cycle; lipoic acid
331 (M00881), an organosulfur cofactor required in central metabolism (72); and C1-unit
332 interconversion (M00140), which is connected to biosynthesis of tetrahydrofolate.
333 Consistent with an intact TCA cycle, all four also had complete modules for the
334 biosynthesis of key compounds involved in the electron transport chain, including heme
335 (M00121, M00926), and riboflavin (M00125). *C. accolens* and *C. tuberculostearicum* also
336 encoded biosynthesis of pyridoxal 5'-phosphate (M00916), which is a coenzyme in many
337 transamination reactions (73); and tetrahydrofolate biosynthesis (M00126), which acts as
338 a carrier for single carbon groups (**Table 3**). We also detected the modules for coenzyme
339 A, lipoic acid, heme, riboflavin, and pyridoxal 5'-phosphate in both *C. glutamicum*^{T} and *C.*

340 *diphtheriae*^{T}. Of note, modules for the biosynthesis of cobalamin/vitamin B12 (M00925,
341 M00924, M00122) were incomplete or absent in all four nasal *Corynebacterium* species.
342 However, the nasal *Corynebacterium* species also encoded for the version of enzymes
343 that are expected to be cobalamin independent, e.g., *metE* rather than the B12-
344 dependent *metH*, so are unlikely to require cobalamin, consistent with predictions from
345 Shelton and colleagues (74).

346 **Nasal *Corynebacterium* species share necessary modules for nucleotide synthesis**
347 **and energy generation.** All four of these common nasal *Corynebacterium* species had
348 five complete modules related to nucleotide metabolism (yellow in **Table 3**) and three
349 complete modules involved in ATP synthesis (M00151, M00155, M00157). Lastly, all four
350 had complete modules for dTDP-L-rhamnose biosynthesis (M00793), a precursor to
351 rhamnose cell wall polysaccharides. Rhamnose is part of the polysaccharide linker
352 between peptidoglycan and arabinogalactan in members of *Mycobacteriales*, including
353 *Corynebacterium* (71). Many of these 9 KEGG modules are also present in other common
354 nasal microbionts with 8/9 in *Cutibacterium acnes* KPA171202 (75), 6/9 in *S. pneumoniae*
355 TIGR4 (76) and *S. aureus* USA300_FPR3757 (77), 5/9 in *Staphylococcus epidermidis*
356 RP62A (78), as well as 9/9 in *C. diphtheriae*^{T}, and *C. glutamicum*^{T}. However, all 9 of these
357 modules were incomplete or absent across all 27 *D. pigrum* strains (62). (**Table S4C**).

358 **Nasal *Corynebacterium* species encode for biosynthesis of UDP-glucose via UDP-**
359 **galactose.** The UDP-glucose biosynthesis module (M00549) was fully detected in *C.*
360 *tuberculostearicum* but was missing a step in the other nasal *Corynebacterium* and in *D.*
361 *pigrum* (and present in all the other species analyzed (**Table S4C**)). UDP-glucose is a
362 key part of central metabolism. It is the activated form of glucose that serves as a

363 precursor for other activated carbohydrates and is used by most organisms for glucosyl
364 transfers. Phosphoglucomutase (*pgm*) performs the second step in its three-step
365 biosynthesis module. We identified a GC that included *pgm* from *C. glutamicum*, *C.*
366 *tuberculostearicum,* and the skin-associated *Corynebacterium* species but lacked
367 sequences from the other nasal *Corynebacterium* species. However, all four nasal
368 *Corynebacterium* species encoded the module for UDP-galactose biosynthesis (M00554)
369 plus a UDP-glucose 4-epimerase (K01784) to covert UDP-galactose to UDP-glucose. In
370 contrast, the *D. pigrum* genomes encoded a *pgm* but lacked the third step, a UDP-sugar
371 pyrophosphorylase or a UTP--glucose-1-phosphate uridylyltransferase (*galU*), for
372 addition of glucose to UDP and also lacked the comparable step for addition of galactose
373 to UDP suggesting the genes encoding for these steps are not yet included in the KEGG
374 orthology.

375 ***C. tuberculostearicum* performs glycogen metabolism, unlike the other three nasal-**
376 **associated *Corynebacterium* species.** Based on anvi'o KEGG module reconstruction
377 (**Table S4A-B**), three of the nasal *Corynebacterium* strains had a stepwise completeness
378 score of zero for the modules for glycogen synthesis and degradation (M00854 and
379 M00855), whereas *C. tuberculostearicum* had scores of 0.5 and 0.67, respectively, for
380 these two modules. Likewise, *C. glutamicum*^{T} had completeness scores of 0.5 and 0.67
381 for these modules and was missing the same steps as *C. tuberculostearicum*. However,
382 published data indicate *C. glutamicum* both synthesizes and degrades glycogen pointing
383 to the use of glycogen for energy storage (79, 80). It encodes four genes for glycogen
384 synthesis (*glgC*, *glgA*, *glgB, glgE*) and three genes for glycogen degradation (*glgX* and
385 two copies of *glgP*). After identifying the predicted enzymatic function (KO number) that

386 anvi'o assigned to the product of each of these six genes, we noted that all of these KOs
387 are enriched in *C. tuberculostearicum* compared to the other three nasal
388 *Corynebacterium* species (**Table S3B**). However, the KEGG module definitions for
389 M00854 and M00855 lack the KOs corresponding to *glgA* (K16148), *glgE* (K16147), and
390 *glgX* (K01214) in *C. glutamicum*^{T} and *C. tuberculostearicum*, and likely other
391 *Corynebacterium* species. In fact, when we included these three KOs in the glycogen
392 metabolism predictions for representative strains of other *Corynebacterium* species and
393 non-*Corynebacterium* human nasal bacterial species, we identified complete glycogen
394 synthesis pathways in *Corynebacterium diphtheriae* NCTC11397, the three common skin
395 *Corynebacterium* species *Corynebacterium simulans* PES1 (81), *Corynebacterium*
396 *kroppenstedtii* DSM 44395 (82), and *Corynebacterium amycolatum* FDAARGOS_1108
397 (83) as well as in strains of other common nasal bacteria: *C. acnes* KPA171202 (75), *S.*
398 *pneumoniae* TIGR4 (76), and *D. pigrum* (26/27 strain pangenome) (62). Glycogen
399 degradation was complete in all of those strains except *C. kroppenstedtii* and *D. pigrum*,
400 which were missing enzymatic activities for the first or second steps, respectively, of the
401 module.

402 Based on this analysis, we predicted that *C. tuberculostearicum* can synthesize and
403 degrade glycogen like *C. glutamicum*. To test for this, we measured intracellular
404 concentrations of glycogen in the four nasal *Corynebacterium* species, using *C.*
405 *glutamicum*^{T} as a positive control. We grew each in a liquid chemically defined medium
406 (CDM) supplemented with all 20 amino acids and 5% glucose (**Fig. 5A**). We used a
407 standardized estimated number of cells, based on OD_{600}, to assay for intracellular

408 glycogen. Under these conditions, *C. tuberculostearicum* harbored increased intracellular
409 glycogen compared to the basal level observed in the other nasal strains (**Fig. 5B**).

410 **Nasal *Corynebacterium* species can synthesize proteinogenic amino acids.** Our
411 overall analysis estimated that the vast majority of the analyzed strains of these four
412 common human nasal *Corynebacterium* species can synthesize all 20 standard amino
413 acids. In most of the genomes, we detected complete biosynthetic modules for 11 amino
414 acids, including the hydrophobic amino acids (isoleucine, leucine, methionine, valine, and
415 tryptophan); the polar uncharged amino acids (serine and threonine); the charged amino
416 acids (arginine and lysine); cysteine; and proline (**Table 3**).

417 Based on anvi'o KEGG module reconstruction (**Table S4C**), the four nasal
418 *Corynebacterium* species and *C. glutamicum*^{T} ATCC13032 have incomplete modules for
419 phenylalanine (M00024) and tyrosine (M00025) due to lack of the corresponding aromatic
420 aminotransferase KO. However, published experimental data confirms that the protein
421 encoded by the *aroT* gene (NCgl0215 or CGL_RS01140) in *C. glutamicum*^{T} acts as an
422 aromatic aminotransferase on substrates phenylpyruvate (O-Phe) and 4-
423 hydroxyphenylpyruvate (O-Tyr) (84). Using anvi'o to cluster all of the genomes for the
424 four nasal *Corynebacterium* species plus *C. glutamicum*^{T}, we identified a GC that includes
425 *C. glutamicum aroT* (annotated as K00817) and has matches in all of the analyzed strains.
426 Based on this, we predicted that all four nasal *Corynebacterium* species should indeed
427 be able to synthesize phenylalanine and tyrosine in the same way as *C. glutamicum.*

428 Substrate specificity of aminotransferase enzymes is notoriously difficult to predict from
429 sequencing data due to the high degree of amino acid similarity within this enzyme family.

430 Moreover, substrate promiscuity often leads to nonobservable phenotypes for deletion
431 mutants of many aminotransferase genes (84-86). Both in *E.coli* (87) and *C. glutamicum*
432 (84) this substrate overlap is especially significant for hydrophobic amino acids, including
433 phenylalanine and tyrosine, which might explain why the initial anvi'o KEGG predictions
434 were inaccurate for *aroT*. In fact, the identified *aroT* gene had an anvi'o KOfam annotation
435 of histidinol-phosphate aminotransferase (K00817) and in *C. glutamicum*^{T} this motif is
436 predicted in both *aroT* and *hisC* (named cg0267 and cg2304 respectively in (85)). In that
437 study, *aroT* had higher similarity to a set of histidinol-phosphate aminotransferases with
438 broader substrate specificity, whereas *hisC* was most similar to an aminotransferase
439 specific for histidine biosynthesis. The *hisC* gene is also located in an operon with other
440 genes involved in histidine biosynthesis. In our genomes of interest we also identified
441 another GC including the *C. glutamicum*^{T} *hisC.*

442 The majority (91/102) of the genomes had a complete KEGG module for histidine
443 biosynthesis (M00026), except that all *C. tuberculostearicum* and 3 *C. accolens* genomes
444 were missing K01693. However, the gene cluster analysis revealed matches to this KO,
445 corresponding to *C. glutamicum*^{T} *hisB,* in all 11 of these genomes, leading us to predict
446 that all of the strains of interest can biosynthesize histidine.

447 **The *C. pseudodiphtheriticum* phylogeny revealed a recent and geographically**
448 **localized loss of assimilatory sulfate reduction**. In addition to the anabolic modules
449 for biosynthesis, production of cysteine (M00021) and methionine (M00017) (**Table 3**)
450 requires assimilatory sulfate reduction, which takes environmental sulfate and converts it
451 to a usable form in the cell (88). Anvi'o analysis detected stepwise completion scores of
452 only 0.5 for the assimilatory sulfate reduction module (M00176) for *C. glutamicum*^{T}, all *C.*

453 *accolens,* all *C. tuberculostearicum,* most *C. propinquum* (17/19), and 13 of 42 *C.*
454 *pseudodiphtheriticum* genomes. However, *C. glutamicum*^{T} has proven assimilatory
455 sulfate reduction capabilities via the *fpr2-cysIXHDNYZ* locus (89). This operon includes
456 genes for two subunits of a sulphate adenylyltransferase, *cysD* (K00957) and *cysN*
457 (K00956); an APS reductase, *cysH* (K00390); and a sulphite reductase, *cysI* (K00392).
458 Of note, in *E. coli,* two enzymatic steps are required for the release of sulfite from APS:
459 APS kinase (CysC) and PAPS reductase (CysH). Whereas, in *C. glutamicum*, *M.*
460 *tuberculosis*, and *B. subtilis,* CysH is an APS reductase that directly converts APS to
461 sulfite (89-91). However, the KEGG definition for M00176 currently fails to account for the
462 experimental evidence that a complete assimilatory sulfate reduction module in *C.*
463 *glutamicum*^{T} does not require an APS kinase. All the strains in our analysis with a
464 stepwise completion score of 0.5 for this module have the same four KOs in the module
465 as *C. glutamicum*^{T} and are, therefore, predicted to perform assimilatory sulfate reduction.
466 However, this module was completely absent in all the *C. pseudodiphtheriticum* strains
467 from the USA and 4 from Botswana (**Fig. 6A**), plus 2 *C. propinquum* strains, and *C.*
468 *diphtheriae*^{T}. The complete absence of the module for assimilatory sulfate reduction
469 predicts that this subset of *C. pseudodiphtheriticum* strains cannot synthesize methionine
470 or cysteine when sulfate is the only exogenous source of sulfur. To test this, we generated
471 a chemically defined agarose medium supplemented with 18 amino acids (lacking
472 cysteine and methionine) in which 75 mM sodium sulfate was the only exogenous source
473 of sulfur. As predicted *C. pseudodiphtheriticum* MSK311, isolated in Botswana, showed
474 growth under conditions requiring assimilatory sulfate reduction, whereas the USA
475 isolates *C. pseudodiphtheriticum* KPL1989 and KPL4025 did not (**Figs. 6B** and **S5A**).

476 These findings indicate a recent and geographically localized complete loss of the
477 assimilatory sulfate reduction module M00176 within the *C. pseudodiphtheriticum*
478 phylogeny.

479 **Nasal *Corynebacterium* species encode for glycine and amino acids involved in**
480 **nitrogen assimilation**. KEGG lacks module definitions for biosynthesis of six of the
481 standard amino acids: glycine, glutamate, glutamine, aspartate, asparagine, and alanine.
482 Based on gene cluster analysis and the known capabilities of *C. glutamicum*^{T}, we
483 predicted that all four nasal *Corynebacterium* species can generate these six amino acids.
484 In *C. glutamicum*^{T}, the gene *glyA* encodes the enzyme serine hydroxymethyltransferase
485 (SHMT) that generates glycine from L-serine (92). This essential gene corresponds with
486 K00600, which was present in all the analyzed *Corynebacterium* genomes. Production of
487 the remaining five amino acids is intertwined with nitrogen assimilation, which is well
488 studied in *C. glutamicum*.

489 We predicted that the four nasal *Corynebacterium* species can assimilate ammonium and
490 synthetize glutamate and glutamine using glutamate dehydrogenase and glutamine
491 synthetase based on genomic comparisons to *C. glutamicum*^{T}. Tesch et al. propose that
492 glutamine amidotransferase reactions are critical for the flux of NH_4^+ into biomass in *C.*
493 *glutamicum* based on ^{15}N-ammonium flux measurements showing that *C. glutamicum*^{T}
494 assimilates 72% of the NH_4^+ into glutamate using glutamate dehydrogenase and 28%
495 into glutamine via glutamine synthetase (93). Surprisingly, 2-oxoglutarate
496 aminotransferase (GOGAT) does not actively contribute to NH_4^+ assimilation in *C.*
497 *glutamicum*^{T} (93, 94). Moreover, *C. glutamicum*^{T} GOGAT mutations display only a slight
498 increase in doubling time in minimal medium with limiting amounts of ammonium or urea

499 as the nitrogen source, indicating GOGAT is nonessential for ammonium assimilation in
500 *C. glutamicum*^{T} (94). In fact, the genes encoding for the two subunits of the GOGAT in *C.*
501 *glutamicum*^{T} (*gltBD*) were absent in all of the nasal *Corynebacterium* strains, as were
502 matches to the corresponding KOs (K00265 and K00266). In contrast, using GC analysis,
503 we detected *C. glutamicum*^{T} *gdhA,* encoding glutamate dehydrogenase (K00262), and
504 *glnA,* encoding glutamine synthetase, in all of the nasal strains (except for three *C.*
505 *propinquum* strains that had a truncated *ghdA*), predicting that the four nasal
506 *Corynebacterium* species can assimilate ammonium and synthetize glutamate and
507 glutamine.

508 We predicted that the four nasal *Corynebacterium* species can all generate aspartate
509 because *C. glutamicum aspT* (which encodes for an aspartate aminotransferase that
510 interchangeably converts glutamate and oxaloacetate to 2-oxoglutarate and aspartate)
511 (84), clustered with genes from all of the nasal *Corynebacterium* strains. The *C.*
512 *glutamicum aspT* (aka *aspAT*) was recently recognized as part of the new subgroup 1c
513 of class I aspartate aminotransferases (95), which likely accounts for the lack of KEGG
514 annotation even though the COG and Pfam annotations are consistent with an aspartate
515 aminotransferase domain (COG1167; PF12897.11).

516 We predicted that the four nasal *Corynebacterium* species do not require exogenous
517 asparagine. We identified a GC including the *C. glutamicum*^{T} *asnB* gene plus genes from
518 all of the analyzed *Corynebacterium* genomes annotated as an asparagine synthase
519 (K01953). However, Hirasawa et al. report that the *C. glutamicum asnB* gene (aka *ltsA*,
520 GenBank: AB029550.1) fails to complement an *E. coli asnA asnB* double mutant
521 suggesting that it lacks asparagine synthetase activity, which led them to propose that it

522 encodes for a glutamine-dependent amidotransferase that modifies cell wall
523 component(s) involved in lysozyme and temperature sensitivity (96). The putative *asnB*
524 genes of *Mycobacterium tuberculosis* and *Bacillus subtilis* are more similar to *C.*
525 *glutamicum asnB* than to *E. coli asnB*, suggesting their gene products also lack an
526 asparagine synthase function (96). This agrees with the observation that *M. tuberculosis*
527 relies on the amidation of aspartate-tRNA to incorporate asparagine into proteins (97, 98).
528 Based on these data and that *C. glutamicum*^{T} grows in defined medium in the absence of
529 amino acids, we predicted the four nasal *Corynebacterium* species also do not require
530 asparagine.

531 We predicted that the four nasal *Corynebacterium* species can synthesize alanine since
532 they all encoded *alaT* (K14260), an aminotransferase that converts pyruvate and
533 glutamate to alanine and 2-oxoglutarate. *C. glutamicum*^{T} encodes two genes, *alaT* and
534 *avtA*, that can both generate alanine via an amino transferase reaction, and mutants with
535 a deletion of *alaT* have an L-alanine requirement under specific growth conditions (99).

536 To test our predictions, we assayed for growth on a base MOPS-buffered CDM agarose
537 supplemented with 2% glucose with *C. glutamicum*^{T} as a positive control. All four nasal
538 *Corynebacterium* species grew on MOPS-CDM agarose supplemented with all 20
539 proteogenic amino acids (**Figs. 7** and **S5B**). Along with *C. glutamicum*^{T}, *C. accolens* and
540 *C. tuberculostearicum* both grew in the absence of all 20 amino acids confirming the
541 metabolic predictions, whereas *C. pseudodiphtheriticum* and *C. propinquum* did not. We
542 hypothesized that MOPS-CDM lacking amino acids failed to support the growth in these
543 two species due to nitrogen limitation. Therefore, we tested whether urea, glutamine (File
544 S1), or asparagine, which are all easily bioavailable sources of nitrogen, would restore

545 growth; however, none did so (**Figs. 7** and **S5B**). This leaves open the possibility that
546 both *C. pseudodiphtheriticum* and *C. propinquum* are auxotrophic for at least one amino
547 acid due to either a misannotation or a point mutation(s) resulting in a loss of function, or,
548 alternatively, that under these specific growth conditions both fail to produce at least one
549 of the required amino acids due to regulatory issues.

550 **Human nasal *Corynebacterium* species have a broader metabolic capacity for**
551 **biosynthesis of amino acids and cofactors/vitamins than *Dolosigranulum pigrum*.**
552 Many compositional studies of human nasal microbiota show a positive association at the
553 genus level between *Corynebacterium* and *Dolosigranulum,* e.g., (1, 2, 4, 7, 24, 26, 38,
554 100). Nasal *Corynebacterium* species can enhance *in vitro* growth yields of *D. pigrum*, a
555 lactic acid producing bacterium (38). Together with other prior analyses (101), these data
556 indicate *D. pigrum* must access nutrients from its host and its microbial neighbors. As
557 hypothesized, the nasal *Corynebacterium* species with their larger genome sizes (2.3 to
558 2.6 Mb) had a greater number of complete KEGG modules per genome than *D. pigrum*
559 (1.9 Mb) (**Fig. 8**). Using anvi'o, we identified 15 complete modules shared by the majority
560 (≥ 78%) of the 27 *D. pigrum* strain genomes (**Table 3,** highlighted in light blue). These are
561 for the metabolism of amino acids (2), carbohydrates (8), energy (1), lipids (1), and
562 cofactors and vitamins (3). This is approximately 30% of the number of complete modules
563 found in the majority of each of the four *Corynebacterium* species' genomes (range 47 to
564 56). The module for glycogen biosynthesis (M00854) was the only one found in *D. pigrum*
565 and incomplete in all four *Corynebacterium* species (**Table 3**); however, as described
566 above, *C. tuberculostearicum* produces glycogen (**Fig. 5**). Of note, each *D. pigrum*
567 genome had at least one CDS annotated as a sialidase (K01186), which can release

568 sialic acid from sialylated glycans found in mucus providing bacteria with carbon and
569 nitrogen (102), whereas there were none in the nasal *Corynebacterium* genomes (**Table**
570 **S3A**). Only 10 complete KEGG modules were shared by *D. pigrum* and all 4
571 *Corynebacterium* species (**Table 3**, highlighted in pale yellow). In contrast, the 4
572 *Corynebacterium* species shared 12 modules for amino acid metabolism and 4 modules
573 for cofactor/vitamin metabolism in the majority of their genomes that were
574 absent/incomplete in *D. pigrum* (**Table 3**).

575 **DISCUSSION**

576 Here, we analyzed strain genomes of four common *Corynebacterium* species including
577 those of 87 distinct human nasal isolates collected in Africa and North America across
578 the human lifespan. Phylogenomic analysis showed *C. pseudodiphtheriticum* displays
579 geographically restricted strain circulation. This corresponded with a recent
580 geographically restricted loss of the KEGG module for assimilatory sulfate reduction in
581 strains isolated in the USA, since this module was present in the other three species and
582 in most *C. pseudodiphtheriticum* strains from Botswana. We confirmed the absence of
583 the *cysIXHDNYZ* operon in the USA *C. pseudodiphtheriticum* strains and experimentally
584 demonstrated that representative USA strains failed to grow under conditions requiring
585 assimilatory sulfate reduction, whereas a strain from Botswana grew (**Fig. 6**). Across the
586 four species, genomic analysis revealed average genome sizes of 2.3 to 2.5 Mb, with the
587 average CDS per genome ranging from 2105 to 2265 and with 72-79% of each individual
588 genome encoding GCs of the shared conservative core genome of the respective
589 species. For each species, the core genome size had leveled off while the pangenome
590 remained open. An informative assignment to a definitive COG category was possible

591 only for approximately 65% of the GCs in the persistent genome and 26-36% of the GCs
592 in the accessory genome of each species, which points to the need for ongoing
593 experimental research to identify the function of many bacterial GCs. GCs assigned to
594 the COG categories for metabolism were overrepresented in the persistent genome of
595 each species and all four species shared the majority (43 of 58) of complete KEGG
596 modules identified, which implies limited strain- and species-level metabolic variation
597 restricting the possibilities for strains to occupy distinct metabolic niches during the
598 common occurrence of cocolonization of the human nasal passages. We experimentally
599 validated the genome-based metabolic prediction that of the four species only *C.*
600 *tuberculostearicum* accumulates intracellular glycogen (**Fig. 5**). *Corynebacterium* species
601 are often positively associated with *Dolosigranulum* in human nasal microbiota. We found
602 human nasal *Corynebacterium* species have a broader metabolic capacity for
603 biosynthesis of amino acids and cofactors/vitamins than *D. pigrum,* supporting the
604 possibility that *Corynebacterium* might cross-feed or serve as a source of nutrients for *D.*
605 *pigrum,* and possibly other microbionts, in human nasal microbiota. We experimentally
606 validated that *C. accolens* and *C. tuberculostearicum* both grow on defined medium
607 lacking amino acids. Our findings combined with data showing that the majority of adults
608 likely host at least two *Corynebacterium* species in their nasal passages points to the
609 importance of future investigation into how *Corynebacterium* species interact with each
610 other and with other microbionts in human nasal microbiota.

611 By analyzing the extent and distribution of cobamide production in 11,000 bacterial
612 species, Shelton et al. report 86% of bacteria in their dataset have at least 1 of the 15
613 cobamide-dependent enzyme families, but only 37% are predicted to synthesize their own

614 cobamide (74) pointing to widespread interspecies cobamide sharing among bacteria.
615 Swaney et al. find de *novo* cobamide biosynthesis is enriched in host-associated
616 compared to environment-associated *Corynebacterium* species, with several human
617 skin-associated *Corynebacterium* species encoding complete biosynthesis pathways
618 (61). In contrast, all four nasal *Corynebacterium* species had nearly absent modules for
619 production of the corrin ring (M00925 or M00924) and the nucleotide loop (M00122)
620 (**Table S4A-B**). They also lacked cobamide-dependent enzymes. Furthermore, based on
621 Shelton and colleagues' analysis of representative genomes, the majority of the most
622 common human nasal bacteria are both likely nonproducers and lack B12-dependent
623 enzymes and B12 pfam binding domains (74), the exception being *C. acnes*, which is a
624 highly prevalent and abundant member of human nasal microbiota, especially in adults
625 (31), and produces the cobamide vitamin B12 (cobalamin) (103).

626 Limitations of this study include the uneven representation of strains from the USA and
627 Botswana for *C. propinquum* and *C. accolens*; the limited number of *C.*
628 *tuberculostearicum* strains; the inherent limitations of KEGG annotations; and the
629 predictive nature of genome-based metabolic estimations, some of which still require
630 future experimental validation. To our knowledge, this analysis includes the largest
631 number of strain genomes for *C. pseudodiphtheriticum, C. propinquum*, and *C. accolens*
632 to date, with the aforementioned smaller number for *C. tuberculostearicum*. However,
633 compared to the thousands of strain genomes that have been analyzed for nasal
634 pathobionts, e.g., *S. aureus* (104), there are still a limited number of available genomes
635 of nasal *Corynebacterium* species. This highlights the need to build large strain
636 collections of human-associated *Corynebacterium* species to better assess the potential

637 use of these strains for the promotion of human health. Similarly, although we included
638 genomes for strains isolated from two continents and from a range of ages, the
639 geographic sampling was limited compared to the distribution of human populations
640 globally and there has yet to be a systematic large-scale sampling of nasal microbiota
641 across the human lifespan.

642 Qualitatively, we isolated fewer *C. tuberculostearicum* from nasal swabs than expected
643 based on its prevalence and relative abundance estimated in our earlier reanalysis of 16S
644 rRNA gene V1-V3 sequences from human nasal samples (31). In contrast to using a
645 single gene, here, we assigned isolates to *C. tuberculostearicum* based on WGS with an
646 ANI of ≥ 95% to the type strain *C. tuberculostearicum* DSM 44922. Only a subset of our
647 isolates from the USA and Botswana with partial 16S rRNA gene Sanger sequences
648 (approximately V1-V3) matching to *C. tuberculostearicum* met this criterion after WGS.
649 This points to the existence of another common nasal *Corynebacterium* species that is
650 closely related to *C. tuberculostearicum.* Recent human skin metagenomic analyses by
651 Salamzade et al. identify metagenome-assembled genomes and the strain genome
652 LK1134 with ANI ≥ 95% to the genome called "*Corynebacterium kefirresidentii"* (105),
653 which is not a validly published species, and show via phylogenomic analysis these are
654 closely related to *C. tuberculostearicum* (34). Furthermore, using metagenomic analyses,
655 they show sequences matching the "*C. kefirresidentii"* genome are more prevalent on
656 nasal and nearby facial skin sites, whereas *C. tuberculostearicum* is more prevalent and
657 at higher relative abundance on foot-associated skin sites (34). Future work to validly
658 name the species currently identified by the genome called "*C. kefirresidentii*" with

659 designation and deposition of a type strain in publicly accessible stock centers is critical
660 for experiments seeking to identify the function of this species in human nasal microbiota.
661 Isolation and whole genome sequencing of multiple strains for microbial species
662 commonly detected in the human microbiome, such as this one, is an ongoing effort
663 across multiple body sites. Collections of genome-sequenced strains from the microbiota
664 are a critical resource for experimentally testing hypotheses generated from metagenomic
665 and metatranscriptomic studies to identify the functions of human microbionts and
666 mechanisms by which they persist in the microbiome. The Human Oral Microbiome
667 Database (eHOMD) is an early and ongoing example of a body-site focused resource for
668 the human microbiome based on a combination of culture-dependent and -independent
669 data (106). Originally focused on the oral cavity, eHOMD now serves the full human
670 respiratory tract (31). More recently, Saheb Kashaf et al. established the Skin Microbial
671 Genome Collection (SMGC), a combined cultivation- and metagenomic-based resource
672 for the human skin microbiome (107). These well-curated, body-site focused databases
673 serve a critical role in advancing microbiome research, including their importance in
674 shedding light on so-called microbial and metagenomic "dark matter." The data we
675 presented here serves as a foundational resource for future genomic, metagenomic,
676 phenotypic, metabolic, functional, and mechanistic research on the role of nasal
677 *Corynebacterium* species in human development and health.

678 **MATERIALS AND METHODS**

679 **Collecting new nasal *Corynebacterium* sp. isolates.** The USA *Corynebacterium*
680 strains with KPL in their name were collected in Massachusetts, USA under a protocol

681 approved by the Forsyth Institutional Review Board (FIRB #17-02) as described
682 previously (62). In brief, adults and children participating in scientific outreach events in
683 April 2017 and 2018 performed supervised self-sampling of their nostrils (nasal vestibule)
684 with sterile swabs. They then inoculated their swab onto up to two types of agar medium:
685 1) brain heart infusion with 1% Tween80 (BHIT) and 25 microgram/ml fosfomycin
686 (BHITF25) to enrich for *Corynebacterium* sp. and/or 2) BBL Columbia Colistin-Nalidixic
687 acid agar with 5% sheep's blood (CNA BAP). These were incubated at 37°C for 48 hrs
688 under either atmospheric (BHITF25) or 5% CO_2-enriched (CNA BAP) conditions. We
689 selected colonies with a morphology typical of nasal *Corynebacterium* species and
690 passed each two to three times for purification on BHIT with 100 ug/ml fosfomycin
691 (BHITF100) at 37°C prior to storage in medium with 15-20% glycerol at -80°C. (Isolates
692 from 2017 were picked from growth on BHITF100 at 37°C under atmospheric conditions
693 that had been inoculated from sweeps of the original mixed growth on agar medium and
694 stored at -80°C.)

695 The majority of the *Corynebacterium* strains with MSK in their name were cultured from
696 nasopharyngeal swab samples collected from mothers and infants in a birth cohort study
697 conducted in Botswana, as previously described (13), with a small number also collected
698 from mid-turbinate nasal swab samples from patients cared for within the Duke University
699 Health System (MSK074, MSK075, MSK076, MSK079, and MSK080). This work was
700 reviewed and considered exempt by the Duke Health Institutional Review Board
701 (Pro00102629). Bacteria were cultivated and isolated as previously described (13).

702 **Selection of nasal *Corynebacterium* isolates for Illumina sequencing.** For each KPL-
703 named new isolate, Sanger sequencing (Macrogen, USA) was performed using primer

704 27F on a V1-V3 16S rRNA gene colony-PCR amplicon (GoTaq Green, Promega) of
705 primers 27F and 519R. We assigned each initial isolate to a genus and a putative species
706 based on blastn of each sequence against eHOMDv15.1 (31). We then selected a subset
707 of these isolates for whole genome sequencing (WGS). For MSK-named new isolates, all
708 isolates preliminarily assigned to *Corynebacterium* based on MALDI and/or Sanger
709 sequencing of V1-V3 16S rRNA gene underwent WGS.

710 **Genomic DNA extraction.** We extracted genomic DNA (gDNA) from the KPL-named
711 USA strains using the MasterPure Gram Positive Genomic DNA Extraction Kit with the
712 following modifications to the manufacturer's protocol: 10 mg/mL lysozyme treatment at
713 37°C for 10 min and 2x 30 sec bead beat in Lysing Matrix B tubes (MP Biomedicals) at
714 setting 6 on a FastPrep24 (MP Bio) with 1-minute interval on ice. To assess gDNA quality,
715 we performed electrophoresis on 0.5% TBE agarose gel, used a NanoDrop
716 spectrophotometer to quantify 260/280 and 260/230 ratios, and used a Qubit Fluorometric
717 Quantification (Invitrogen) to measure concentration. We extracted gDNA from the MSK-
718 named strains collected in Botswana and North Carolina using the Powersoil Pro
719 extraction kit (Qiagen) following the manufacturer's instructions. DNA concentrations
720 were determined using Qubit dsDNA high-sensitivity assay kits (Thermo Fisher
721 Scientific).

722 **Whole genome sequencing and assembly.** For the KPL-named USA isolates, Nextera
723 XT (Illumina) libraries were generated from gDNA. Each isolate was sequenced using a
724 paired-end 151-base dual index run on an Illumina Novaseq6000 at the NIH Intramural
725 Sequencing Center. The reads were subsampled to achieve 80x coverage and then
726 assembled with SPAdes (version 3.13.0) (108) and polished using Pilon (version 1.22)

727 (109). For the MSK-named isolates, which are mostly from Botswana, library preparation
728 was performed using DNA Prep Kits (Illumina) and these libraries were sequenced on a
729 NovaSeq 6000 instrument (Illumina) configured for 150 base pair paired-end reads.
730 Adapter removal and read trimming were performed using Trimmomatic version 0.39
731 (110) to a Phred score of 30 across a 4-bp sliding window. Surviving reads shorter than
732 70 bp were discarded. The final quality of reads was assessed using FastQC version
733 0.11.9. Assembly was performed using SPAdes version 3.15.3 (111). The completeness
734 of the genomes was evaluated with checkM version 1.1.3 (112) and all genomes with a
735 completeness less than 95% were discarded. Genomic data are deposited under
736 BioProjects PRJNA842433 for the KPL-named isolates (which are a subset of 94
737 *Corynebacterium* isolated in MA, USA) and PRJNA804245 for the MSK-named isolates
738 (which are a subset of 71 genomes isolated from Botswana and the Duke University
739 Health System). **Table S1A** includes NCBI accession IDs.

740 **Selection of strain genomes for pangenomic analysis.** To the 165 assemblies
741 mentioned in the previous section, we added another 16 KPL-named *Corynebacterium*
742 sp. nasal-isolate genomes originally sequenced as part of the HMP and deposited by the
743 Broad at NCBI to consider for analysis (113). Furthermore, 31 reference assemblies for
744 relevant *Corynebacterium* species, including the genome of the type strain of *C.*
745 *propinquum*, *C. pseudodiphtheriticum*, *C. accolens,* and *C. tuberculostearicum* plus 3
746 strain genomes of *C. macginleyi,* were downloaded from NCBI using the PanACoTA
747 v1.4.1 (114) `prepare -s` subcommand. We used default parameters such that genomes
748 with MASH distances to the type strain outside of the range 1e-4 to 0.06 were discarded
749 to avoid redundant pairs or mislabeled assemblies and low-quality assemblies based on

750 L90 ≤ 100 and number of contigs ≤ 999 were filtered out. The collected 212 assemblies
751 were filtered using the `prepare --norefseq` subcommand as above to select higher
752 quality assemblies (L90 ≤ 100 and number of contigs ≤ 999) and to eliminate redundant
753 genomes defined by a MASH distance < 10^{-4} keeping the genome with the highest quality
754 score from each redundant set. Finally, we confirmed the species-level assignment of our
755 nasal isolates, and the nontype reference strains, based on an ANIb (nucleotide) of ≥ 95%
756 for all shared CDS regions compared to the respective type strain of each species using
757 GET_HOMOLOGUES (see below). For each species, this resulted in a set of distinct
758 strain genomes (including the type strain) that we used for subsequent analyses, which
759 totaled to 104 genomes: 19 *C. propinquum* genomes, 43 *C. pseudodiphtheriticum*
760 genomes, 34 *C. accolens* genomes, and 8 *C. tuberculostearicum* genomes. **Table S1A**
761 contains a list of these 104 strain genomes selected for further analysis plus 3 *C.*
762 *macginleyi* reference strains, and **Table S1B** the all-by-all MASH distance analysis result
763 of the PanACoTA analysis for all 107 genomes.

764 **Determination of the conservative core genome.** We annotated all bacterial genomes
765 with Prokka version 1.14.6 (115) with default parameters, including gene recognition and
766 translation initiation site identification using Prodigal (116). Then, we used the
767 `./get_homologues.pl` command from GET_HOMOLOGUES version 24082022 (117,
768 118) to determine a conservative core genome for the selected *Corynebacterium*
769 genomes based on the consensus of three algorithms: bidirectional best-hits (BDBH),
770 cluster of orthologs triangles (COGS) v2.1 (119), and Markov Cluster Algorithm
771 OrthoMCL (OMCL) v2.4 (120) (**Figs. S1A** and **S2C**). Each of the three algorithms
772 reported clustering at the protein level using blastp from NCBI BLAST v2.2 (121) with `-C

773 90` (min % coverage in BLAST pairwise alignments). The data output created from
774 running the three different clustering algorithms was used to identify the intersection of
775 the core GCs with the command `./compare_clusters.pl` with `-t # of genomes`. We ran
776 this last command twice, with and without the -n flag to generate both nucleotide and
777 protein outputs. Additional methods for genome annotations
778 (https://klemonlab.github.io/CorPGA_Pangenomics/Supplemental

779 Methods_Prokka_Annotations.html) and for the determination of the conservative core
780 genome are available online
781 (https://klemonlab.github.io/CorPGA_Pangenomics/SupplementalMethods_GET_HOM
782 OLOGUES.html).

783 **Determination of core, soft core, shell, and cloud genomes.** For this analysis to
784 identify the core genomes, we dropped the strains Cps_090104 and Cac_ATCC_49726
785 from their respective species because, although these both passed CheckM analysis,
786 their inclusion in the initial rarefaction analyses caused a splitting of data points towards
787 the lower end resulting in an aberrant lower bound. We separately analyzed the genomes
788 of each *Corynebacterium* species using GET_HOMOLOGUES with the command
789 `./get_homologues.pl` and flag`-t 0` (to get all the possible clusters), first with `-M`
790 (OrthoMCL) and a second time with `-G` (COGS). The COGS and OMCL results were
791 then used with `./compare_clusters.pl` with `-m` (produce intersection pangenome
792 matrices). Then the command `./parse_pangenome_matrix.pl` was used with `-s` (report
793 core, soft core, shell, and cloud clusters), and `-x` (produce matrix of intersection
794 pangenome clusters) (**Fig. S3Ai-iv**). In-depth code and descriptions to determine the
795 core, soft core, shell, and cloud genomes are available online

796 (https://klemonlab.github.io/CorPGA_Pangenomics/SupplementalMethods_GET_HOM
797 OLOGUES.html).

798 **Calculating the conservative core genome for each species with the addition of an**
799 **outgroup.** We chose the type strain genome of the most closely related species from the
800 phylogenomic tree in **Fig. S1B** to serve as the outgroup in each species-specific
801 phylogeny with *C. pseudodiphtheriticum* DSM 44287 for the *C. propinquum* phylogeny,
802 *C. propinquum* DSM 44285 for the *C. pseudodiphtheriticum* phylogeny, *C. macginleyi*
803 CCUG 32361 for the C. *accolens* phylogeny, and *C. accolens* ATCC 49725 for the *C.*
804 *tuberculostearicum* phylogeny. Addition of an outgroup resulted in four new datasets with
805 n + 1 total genomes, where n denotes the number of strain genomes for each species.
806 Each species-plus-outgroup dataset of genomes was analyzed as before using the
807 commands `. /get_homologues.pl` (with BDBH, COG triangles, and OrthoMCL) and
808 `./compare_clusters.pl`, but now with the outgroup genome included (**Fig. S2D**). For
809 construction of single-species trees (**Fig. 1**), we then combined this smaller conservative
810 core of GCs shared between the species and its outgroup (shared intersection of each
811 Venn diagram in Fig. S2D) with the subset of GCs belonging only to the conservative core
812 of each species (which is the intersection of each Venn diagram in Fig. S2C minus the
813 intersection of those in Fig. S2D). The code used to do this is available online
814 (https://klemonlab.github.io/CorPGA_Pangenomics/SupplementalMethods_GET_HOM
815 OLOGUES.html).

816 **Construction of phylogenomic trees.** We used GET_PHYLOMARKERS v.2.2.9.1 to
817 concatenate and align the single copy core GCs for each phylogeny (122). The command
818 `run_get_phylomarkers_pipeline.sh` was run with the flags: `-R 1 -t DNA -k 0.7 -m 0.7`

819 on both the protein and nucleotide GET_HOMOLOGUES outputs. The flag `-R` was used
820 to select optimal markers for phylogenomics; `-t` for whether the input is DNA or protein;
821 `-k` for kde stringency; and `-m` for the minimum average support values for trees to be
822 selected. The codon fasta alignments generated by GET_PHYLOMARKERS were
823 analyzed with IQ-TREE v2.1.3 (123) with: `-p`, (uses edge linked partition model and
824 ModelFinder functions (124-126)), `-alrt 1000` (perform replicate SH-like approximate
825 likelihood ratio test) and `-B 1000` (number of ultrafast bootstrap replicates). The
826 phylogenetic tool iTOL v6 (127) was used to visualize, scale, edit, annotate names, and
827 root the tree at the midpoint for each phylogeny. Detailed code and methods to create
828 these phylogenies are available online
829 (https://klemonlab.github.io/CorPGA_Pangenomics/SupplementalMethods_GET_HOM
830 OLOGUES.html).

831 **Rarefaction analysis and Average Nucleotide Identity (ANI) across strain genomes.**
832 For each species, with GET_HOMOLOGUES, we used rarefaction analysis to estimate
833 whether the core genome and pangenome were closed or open (**Fig. 2**). We modified
834 "$MIN_PERSEQID_HOM" and "$MIN_COVERAGE_HOM" values to equal 50 (inside
835 "marfil_homology.pm") so only protein sequences with identity and coverage ≥ 50% will
836 be called homologues.

837 Again, we made the decision to eliminate the two genomes, namely Cac_ATCC_49726
838 and Cps_090104 from this dataset. The reason for this action was that their core genome
839 size resulted in the preliminary graph getting divided while conducting random sampling.
840 This is because their core genome sizes were considerably lower, resulting in a
841 misleading lower bound. The clustering was redone for each species using

842 `./get_homologues.pl` and the following parameters: `-C 90`, `-c`, (genome composition
843 analysis) and `-M` for OMCL. The rarefaction curve .tab files were produced from the `-c`
844 flag. Rarefaction .tab files for each species were plotted into svg files using
845 `/plot_pancore_matrix.pl` with flags `-f core_both` (displays both Tettelin and Willenbrock
846 curves for core genome), and `-f pan` (curve for estimating pangenome size). Blastn
847 instead of blastp was used to report GCs for ANI heat plots. To generate the core and the
848 all shared CDS regions ANI .tab files, we used the command `./get_homologues.pl` with
849 flags: `-d`, `-A`, `-t`, `-a`, `-M`. Furthermore, to plot the ANI heatmaps the
850 `./plot_matrix_heatmap.sh` command was used.

851 **Functional analysis of four *Corynebacterium* pangenomes using anvi'o and**
852 **PPanGGOLiN.** The pangenome for each *Corynebacterium* species was analyzed using
853 anvi'o v8 (64, 128). We used a workflow that allowed us to import Prokka annotated
854 genomes into anvi'o
855 (https://klemonlab.github.io/CorPGA_Pangenomics/SupplementalMethods_Prokka_Ann
856 otations.html), followed by the addition of functional COG annotations using the `anvi-run-
857 ncbi-cogs` command with --sensitive flag (runs sensitive version of DIAMOND (129)) and
858 the 2020 updated COG20 database (130, 131). Various annotations were also applied to
859 each genome db file, such as KEGG/KOfam (132, 133), Pfam (134)Mistry, 2021 #3457]
860 and hmm-hits (135). The pangenome for each species was computed with the `anvi-pan-
861 genome` program (flags: --mcl-inflation 10, and --use-ncbi-blast) using blastp search
862 (136), muscle alignment (137) `minbit heuristic` (138) to filter weak hits, and the MCL
863 algorithm (139). A combined pangenome was also computed for 107 strains: the 102
864 nasal *Corynebacterium* genomes selected for metabolic analysis (Cac_ATCC_49726 &

865 Cps_090104 were excluded) plus 5 *Corynebacterium* listed in **Table S1D**. This high level
866 pangenomic analysis was used for gene cluster level comparisons of the KEGG results.
867 The functional and the geometric homogeneity index, and the rest of the layers shown
868 within the anvi'o pangenome *Corynebacterium* figures were determined from the standard
869 anvi'o pangenomic pipeline (https://merenlab.org/2016/11/08/pangenomics-v2/). The
870 core (genes contained in all genomes), soft core (genes contained in 95% of the
871 genomes), shell (genes contained in several genomes), and cloud (genes present in only
872 a few genomes) assignments from GET_HOMOLOGUES were uploaded into the anvi'o
873 pangenome for each species by creating bins in the anvi'o interactive interface. We also
874 manually rearranged the order of strains in each species-specific analysis to match the
875 order in our species-specific phylogenomic trees and imported our phylogenies into the
876 anvi'o figures. This facilitated visualizing the strain genomes from an evolutionary
877 standpoint and identifying GCs that might be unique to a strain or a group of strains in a
878 clade. The code used to generate the anvi'o pangenomic analysis can be found at
879 https://klemonlab.github.io/CorPGA_Pangenomics/SupplementalMethods_Anvio.html.
880 We then exported the summary files from the anvi'o pangenomic analyses to synchronize
881 gene cluster identities with PPanGGOLiN v1.2.74 (67) (**Table S2**) (for detailed code see
882 https://klemonlab.github.io/CorPGA_Pangenomics/SupplementalMethods_PPanGGOLi
883 N.html). GCs were defined as persistent or accessory by PPanGGOLiN and then we used
884 an in-house R script
885 (https://github.com/KLemonLab/CorPGA_Pangenomics/blob/main/SupplementalMethod
886 s_COGS.Rmd) to clean up and retrieve informative COG20 annotated GCs and to
887 generate the functional enrichment plots shown in **Fig 3** and **Fig S4**.

888 **Estimation of metabolic capabilities using anvi'o v8.** We then used `anvi-estimate-
889 metabolism` (140) to estimate gene enzymatic functions (**Table S3A**) and the
890 completeness of KEGG modules in each of the four *Corynebacterium* genomes for the
891 selected 102 strains, in each of 27 *D. pigrum* strain genomes (62), in each reference
892 genome of the 9 other species listed in Table S1D, using their original NCBI annotations.
893 The complete KEGG modules estimation output in tabular format is provided in Table
894 S4A, including stepwise and pathwise completeness scores, and, for easier readability,
895 in Table S4B as a matrix summarizing module stepwise completeness by genome. Table
896 S4C includes the module estimations averaged by species. For the data summaries
897 presented in Table 3 and Figure 4, we excluded modules that were complete in < 12.5%
898 of the strains of each species, across all analyzed species. Additional detailed methods
899 and code, including the code for generating Table 3 and Figure 8, are available online
900 (https://klemonlab.github.io/CorPGA_Pangenomics/SupplementalMethods_Anvio.html).

901 **Determining KEGG module enrichment.** We used `anvi-display-functions` and `anvi-
902 compute-metabolic-enrichment`(141), with a module stepwise completeness score of 1
903 for the latter, to identify individual KOs (**Table S3B**) and KEGG modules (**Table S4D**)
904 enriched across the four *Corynebacterium* species. Modules with an adjusted q-value <
905 1e-9 were considered enriched in their associated group. Modules both with an adjusted
906 q-value > 1e-9 and complete in at least 87% of the analyzed genomes were considered
907 shared. Additional detailed methods and code are available online
908 (https://klemonlab.github.io/CorPGA_Pangenomics/SupplementalMethods_Anvio.html).

909 **Bacterial strains and growth conditions.** *C. propinquum* KPL3953, *C.*
910 *pseudodiphtheriticum* MSK311, KPL1989, and KPL4025, *C. accolens* KPL1818, *C.*

911 *tuberculostearicum* MSK074, and *C. glutamicum* DSM 20300^T were each grown from a -
912 80 °C freezer stock on Difco Brain Heart Infusion (BHI) agar medium supplemented with
913 1% Tween80 (BHIT) for 36-48 hours at 34 °C in a 5% CO_2 CellXpert C170 incubator
914 (Eppendorf, # 6734010015) with a humidification pan. Subsequently, for each strain, we
915 carefully collected 10-20 single colonies from BHIT agar and pooled these for
916 resuspension in individual 5 ml Eppendorf tubes containing 4.5 ml of either phosphate
917 buffered saline (PBS) for the glycogen experiments or Earle's Balanced Salt Solution
918 (EBSS) for the growth assays with amino acid supplementation.

919 **MOPS-buffered chemically defined medium base.** We used a base chemically defined
920 medium (CDM) buffered with 3-(N-morpholino)propanesulfonic acid (MOPS) into which
921 we supplemented specific concentrations of glucose, varying amino acids, and/or other
922 supplements, as detailed below, to generate sterile chemically defined media. MOPS-
923 buffered base CDM is a 2X solution of a Teknova medium prepared from Teknova 10X
924 MOPS Buffer (M2101), Teknova 10X AGCU solution (M2103), Teknova 100X Vitamin
925 Stock I (V1015), and Teknova 0.132 M Potassium Phosphate Dibasic (M2102) plus
926 1000X ferric chloride, 400X lipoic acid, and Tween80 with the following final
927 concentrations: 80 mM MOPS, 8 mM tricine, 2.64 mM potassium phosphate dibasic
928 anhydrous, 3 mM potassium hydroxide, 0.398 mM adenine, 0.398 mM cytosine, 0.398
929 mM uracil, 0.398 mM guanine, 0.02 mM ferrous (Iron II) sulfate heptahydrate, 19 mM
930 ammonium chloride, 0.552 mM potassium sulfate, 0.001 mM calcium chloride dihydrate,
931 1.05 mM magnesium chloride hexahydrate, 100 mM sodium chloride, 5.84E-07 mM
932 ammonium molybdate, 8.00E-05 mM boric acid, 6.04E-06 mM cobalt chloride
933 hexahydrate, 1.92E-06 mM copper sulfate pentahydrate, 1.62E-05 mM manganese (II)

934 chloride tetrahydrate, 1.95E-06 mM zinc sulfate heptahydrate, 0.2 mM ferric chloride
935 hexahydrate, 0.408 mM choline chloride, 0.406 mM nicotinic acid, 1.46E-02 mM
936 pyridoxine HCl, 3.94E-02 mM calcium pantothenate, 0.3732 mM PABA, 0.1048 mM
937 thiamine HCl, 8.18E-04 mM biotin, 1.48E-05 mM cyanocobalamin, 3.16E-04 mM folic
938 acid, 2.06E-02 mM riboflavin, 0.0192 mM lipoic acid, 0.1% Tween80. The pH of the
939 medium is 7 to 7.5.

940 **20 amino acid mix.** We prepared a 5X solution mixture of 20 amino acids in MilliQ H_2O
941 such that the final concentration of each after addition to base CDM was as follows: 1.6
942 mM L-alanine, 10.4 mM L-arginine, 0.8 mM L-asparagine, 0.8 mM L-aspartic Acid, 0.2
943 mM L-cysteine, 1.2 mM L-glutamic acid, 1.2 mM L-glutamine, 1.6 mM L-glycine, 0.4 mM
944 L-histidine, 0.8 mM L-isoleucine, 1.6 mM L-leucine, 0.8 mM L-lysine, 0.4 mM L-
945 methionine, 0.8 mM L-phenylalanine, 0.8 mM L-proline, 20 mM L-serine, 0.8 mM L-
946 threonine, 0.2 mM L-tryptophan, 0.4 mM L-tyrosine, 1.2 mM L-valine.

947 **Determination of intracellular glycogen concentration.** Bacteria were resuspended in
948 PBS as described above then washed twice by centrifugation at 16,000 RCF (relative
949 centrifugal force) at 4 °C for 10 minutes using a 5430R centrifuge (Eppendorf #
950 022620689) and resuspended in 4.5 ml of PBS. Next, we used PBS to adjust the OD_{600}
951 to 2 for each strain and then inoculated 1.25 ml of each as a monoculture into 50 ml base
952 phosphate-buffered CDM supplemented with 5% glucose and the 20 amino acid mix in a
953 250 ml flask. Cultures were grown in a shaking incubator at 250 RPM and 34 °C. At 24,
954 28, 32, and 48 hours, we measured the OD_{600} and collected 4 ml aliquots of each strain.
955 Samples were centrifuged, resuspended in PBS, and washed twice as above. After

956 washing, the samples were resuspended in 400 µl PBS and the OD_{600} was measured
957 and adjusted with PBS to ~ 0.5 to assay an equal biomass per strain. We recorded the
958 OD_{600} values and used these to normalize the assayed glycogen per unit of OD_{600}. A 300
959 µl aliquot of each strain was then combined with 150 µl of HCl in a 2 ml lysis matrix B
960 tube (MP Biomedicals, # 116911050-CF) and heated at 95 °C for 5 minutes. To lyse the
961 bacteria, we bead beat the samples 3 times at 6.5 m/s for 45 seconds each time using a
962 FastPrep-24 5G (MP Biomedicals # 116005500). After mechanical lysis, 150 µl of Tris
963 buffer was added to each tube. The samples were then centrifuged at 16,000 RCF at 4
964 °C for 20 minutes. The supernatant was recovered and 25 µl of each sample was
965 aliquoted into 6 separate wells per strain in a white 96-well plate with clear bottom
966 (Greiner Bio-One # 655074) and assayed for glycogen with the Glycogen-Glo Assay kit
967 (Promega # J5051). Per the manufacturer's instructions, we prepared a glycogen titration
968 curve with two-fold serial dilutions in PBS from 20 to 0 µg/ml and we added 25 µl of each
969 of these standards to the 96-well plate for each time point: one set of standards for the
970 glucoamylase assay and one as the control. We then added either 25 µl of glucoamylase
971 solution or buffer alone to each sample (three technical replicates each) and standard
972 well. Plates were incubated at room temp for one hour to allow the glucoamylase to digest
973 glycogen into free glucose. Following incubation, 50 µl of glucose detection reagent was
974 added to each well. Luminescence was measured after 70 minutes using a BioTek
975 Synergy H1 microplate reader (Agilent # SH1M-SN) with default settings. The average
976 luminescence for glucoamylase-treated and buffer-only samples was calculated from
977 three technical replicates for each strain at each timepoint for each independent
978 experiment. The average value from the buffer-only samples was subtracted from the

979 glucoamylase-treated samples for each sample to correct for background levels of free
980 glucose. The glycogen titration curve was derived by subtracting the luminescence of the
981 buffer-only negative controls from the glucoamylase positive standards to establish a
982 best-fit regression curve. The average differences in luminescence values from bacterial
983 samples with and without glucoamylase treatment were input into the corresponding best-
984 fit curve equation to determine total glycogen concentration (μg/ml) per sample. These
985 were normalized to μg/ml per OD_{600} of the bacterial suspension measured before
986 mechanical lysis to approximate the glycogen concentration per cell biomass of each
987 strain. Statistics were performed using a linear mixed model with species as the fixed
988 effect and time point as a random effect fit by restricted maximum likelihood with t-tests
989 using Satterthwaite's method with R packages lme4 (142) and afex. Additional detailed
990 methods and code, including the code for generating Figure 5A-B, are available online
991 https://klemonlab.github.io/CorPGA_Pangenomics/SupplementalMethods_Glycogen.ht
992 ml.

993 **Sequence alignment for the *fpr2-cysIXHDNYZ* operon.** We manually inspected KO
994 assignments for all the enzymes encoded in the *C. glutamicum fpr2-cysIXHDNYZ* operon
995 (89) that absent from the KEGG definition of the assimilatory sulfate reduction module
996 (M00176). Genes annotated as K00528 (*fprA*) were identified in all the *Corynebacterium*
997 genomes. A manual exploration of the gene annotations in the genomic region around
998 the putative *fprA* gene in all *C. pseudodiphtheriticum* strains identified *hchA* as a common
999 gene downstream the *fpr2-cysIXHDNYZ* operon. We used BEDTools (143, 144) to extract
1000 the genomic sequence flanked by *fprA* and *hchA* and performed multiple sequence
1001 alignment using MAFFT (145, 146). AliView (147) was used for sequence inspection and

1002 generation of a reverse-complemented alignment. The final visualization in Figure 6A was
1003 generated in R with the package msavisr. Additional detailed methods and code, are
1004 available online
1005 https://klemonlab.github.io/CorPGA_Pangenomics/SupplementalMethods_Anvio.html

1006 **Assay for growth under conditions requiring assimilatory sulfate reduction**. We
1007 generated a phosphate-buffered version of base CDM with 75 mM (f.c.) sodium sulfate
1008 as the only source of sulfur (KS-CDM) by replacing the Teknova MOPS buffer with a
1009 phosphate buffer consisting of potassium phosphate monobasic, potassium phosphate
1010 dibasic, and sodium phosphate dibasic and trace minerals (see below) since *C.*
1011 *glutamicum* can reportedly use MOPS as a source of sulfur (148). We supplemented the
1012 KS-CDM base with 2% glucose (Teknova 20% Glucose solution G0520) and an 18 amino
1013 acid mix, excluding cysteine and methionine, to generate KS-CDM 0.76% agarose. We
1014 also assayed for growth on KS-CDM agarose supplemented with a 75X cysteine and
1015 methionine solution to final concentrations of 2 mM cysteine and 4 mM methionine. Both
1016 conditions were tested with and without lipoic acid, as a potential additional sulfur source.
1017 Prior to inoculation for each experiment, each bacterial strain resuspended in EBSS (as
1018 described above) was centrifuged at 10,000 RCF for 10 minutes and then subjected to
1019 three washes of 4.5 ml EBSS. After the final wash, cells were resuspended in 500 µl
1020 EBSS to achieve a visibly turbid solution and 15 µl from the resuspension of each strain
1021 was inoculated and struck for single colonies onto KS-CDM 0.76% agarose (SeaKem LE
1022 Agarose, # 50004) prepared with the different variations and incubated at 34 °C in 5%
1023 CO2 incubator with a humidification pan. We used agarose because of its higher purity
1024 compared to agar. The KS-CDM agarose plates were imaged at 8 days to assess

1025 bacterial growth with each supplementation. We performed four independent experiments
1026 (**Figs. 6** and **S5A**). KS-CDM is a 2X solution of a Teknova medium prepared from
1027 Teknova 10X AGCU solution (M2103), and Teknova 100X Vitamin Stock I (V1015), plus
1028 50000X Trace Minerals I and 50X Trace Minerals II (File S1), 1000X ferric chloride, 1000X
1029 ferrous chloride, 10X phosphates, 10X NaCl, 100X tricine, 25X sodium sulfate, 400X
1030 lipoic acid, and Tween80. Final concentrations in KS-CDM were as follows: 37 mM
1031 potassium phosphate monobasic, 109 mM potassium phosphate dibasic, 63 mM sodium
1032 phosphate dibasic, 0.398 mM adenine, 0.398 mM cytosine, 0.398 mM uracil, 0.398 mM
1033 guanine, 8 mM tricine, 75mM sodium sulfate, 6.04E-06 mM cobalt chloride hexahydrate,
1034 1.92E-06 mM copper chloride dihydrate, 1.62E-05 mM manganese chloride tetrahydrate,
1035 5.84E-07 mM ammonium molybate, 1.95E-06 mM zinc chloride, 0.00008 mM boric acid,
1036 19 mM ammonium chloride, 0.001 mM calcium chloride, 1.05 mM magnesium chloride,
1037 0.2 mM ferric (Iron III) chloride hexahydrate, 0.02 mM ferrous (Iron II) chloride
1038 tetrahydrate, 35 mM sodium chloride, 1.6 mM L-alanine, 10.4 mM L-arginine, 0.8 mM L-
1039 asparagine, 0.8 mM L-aspartic Acid, 1.2 mM L-glutamic Acid, 1.2 mM L-glutamine, 1.6
1040 mM L-glycine, 0.4 mM L-histidine, 0.8 mM L-isoleucine, 1.6 mM L-leucine, 0.8 mM L-
1041 lysine, 0.8 mM L-phenylalanine, 0.8 mM L-proline, 20 mM L-serine, 0.8 mM L-threonine,
1042 0.2 mM L-tryptophan, 0.4 mM L-tyrosine, 1.2 mM L-valine, 0.1% Tween80.

1043 **Amino acid auxotrophy assays.** To test for amino acid auxotrophy, we used MOPS-
1044 buffered base CDM 0.76% agarose supplemented with 2% glucose and either lacking
1045 amino acids (0 AA) or supplemented with one of the following: the 20 amino acid mix, 5
1046 mM Urea, 10 mM glutamine, or 10 mM asparagine. Bacterial inocula were prepared and
1047 growth assays were performed as described above in testing for assimilatory sulfate

1048 reducing ability. The MOPS-CDM agarose plates were imaged at 8 days to assess
1049 bacterial growth with each supplementation. We performed four independent experiments
1050 (**Figs. 7** and **S5B**).

1051 **Data and code availability.** All genomes are available from NCBI in Bioprojects
1052 PRJNA842433 and PRJNA804245. Table S1 lists genome accession numbers. Code
1053 used is in our GitHub repository https://github.com/KLemonLab/CorPGA_Pangenomics.

1054 **Acknowledgments.** Thank you to all the individuals who donated nostril swab samples
1055 at a 2017 and 2018 science festival that were used to isolate KPL strains of
1056 *Corynebacterium* species. Their contributions continue to expand knowledge about
1057 human nasal microbiota. Thank you to lab members and colleagues who contributed to
1058 these outreach events, including Javier Fernandez Juarez, Kerry Maguire, Genevieve
1059 Holmes, Pallavi Murugkar, Pooja Balani, Sowmya Balasubramanian, Fan Zhu, Andrew
1060 Collins, Andy Kempczynski, Brian Klein, and Megan Lambert. For early planning and
1061 initial cultivation efforts we thank Silvio D. Brugger, Lindsey Bomar, Stephany Flores
1062 Ramos, and Sara M. Eslami for KPL strains; and Jhoanna N. Aquino and Christopher R.
1063 Polage for MSK strains. We also thank all of the individuals in the USA and Botswana
1064 who participated in the research studies that resulted in cultivation of the MSK strains.
1065 Thank you to Clay Deming and the NIH Intramural Sequencing Center for sequencing of
1066 the KPL strains. Thank you to Bruno Contreras-Moreira for advice on using
1067 GET_HOMOLOGUES; to A. Murat Eren for advice on using anvi'o; and to Ashlee M. Earl
1068 for early efforts to genome sequence nasal *Corynebacterium* isolates. Thank you to other
1069 members of our labs.

1070 **Authorship contributions:** Conceptualization: KPL, WG, IFE. New Strain isolation: WG.
1071 Investigation: THT, IFE, AQR, ACO, WG, SC, MSK. Bioinformatic analysis: THT, IFE,
1072 AQR, SC. Interpretation of data: THT, IFE, AQR, ACO, WG, JAS, HHK, SC, MSK, KPL.
1073 Visualization: THT, IFE, ACO, AQR. Wrote Original Draft: THT, AQR, IFE, ACO, KPL.
1074 Editing and review: KPL, MSK, SC, IFE, THT, ACO, AQR, WG, HHK, JAS. All authors
1075 read and approved the final manuscript. Supervision: KPL, IFE, MSK, HHK, JAS. Funding
1076 Acquisition: KPL, MSK, HHK, JAS.

1077 **Funding information:** This work was supported by the National Institutes of Health
1078 through the National Institute of General Medical Sciences (grants R35 GM141806 and
1079 R01 GM117174 to K.P.L) and the National Institutes of Allergy and Infectious Diseases
1080 (grant K23 AI135090 to M.S.K.); and through the Intramural Research Programs of the
1081 National Human Genome Research Institute (J.A.S.) and the National Institute of Arthritis
1082 and Musculoskeletal and Skin Diseases (H.H.K.). Additional funding was provided by the
1083 Forsyth Institute through a Pilot Grant (FPILOT45 to K.P.L.).

1084 **Table 1. Basic genomic information for four common human nasal-associated**
1085 ***Corynebacterium* species.**

Corynebacterium species	**# Strain Genomes (# Nasal isolates)**	**Average (median) genome size (Mb)**	**Average (median) CDS/genome**	**Average (median) G+C%**	**Conservative Core GCs/species[a]**	**Pangenome GCs/species[b]**	**Country #USA/#BWA**	**Age range (years) of nasal strains**
C. propinquum	19 (15)	2.51 (2.52)	2265 (2272)	56.47 (56.48)	1623	3777	12/3	0.3-72
C. pseudodiphtheriticum[c]	43 (39)	2.33 (2.33)	2105 (2096)	55.29 (55.29)	1345	4590[c]	22/17	0.2-55

C. accolens[d]	34 (32)	2.50 (2.49)	2304 (2294)	59.46 (59.44)	1561	4220[d]	25/7	0.1-62
C. tuberculostearicum	8 (6)	2.39 (2.39)	2250 (2253)	59.86 (59.88)	1788	3232	2/4	0.1-39

[a]GET_HOMOLOGUES conservative core GCs predicted from the consensus of BDBH, OMCL, and COGS algorithms.
[b]GET_HOMOLOGUES pangenome GCs predicted from the consensus of OMCL, and COGS algorithms.
[c]Cps_090104 removed from dataset for this analysis due to false % core lower bound.
[d]Cac_ATCC_49756 removed from dataset for this analysis due to false % core lower bound.

Table 2. Pangenomic estimation of human nasal-associated *Corynebacterium* species based on three different platforms.

Platform Species	Pangenome size (GCs)	% Core GCs/pangenome	% Accessory GCs/pangenome
GET_HOMOLOGUES[a]			
C. propinquum	3777	43%	57%
C. pseudodiphtheriticum[c]	4590	33%	67%
C. accolens[d]	4220	40%	60%
C. tuberculostearicum	3232	56%	44%
anvi'o			
C. propinquum	3108	59%	40%
C. pseudodiphtheriticum	3590	48%	51%
C. accolens	3427	57%	42%
C. tuberculostearicum	2907	66%	32%
PPanGGOLiN		% Persistent	
C. propinquum	[b]	63%	37%
C. pseudodiphtheriticum	[b]	49%	51%
C. accolens	[b]	59%	41%
C. tuberculostearicum	[b]	69%	31%

[a]GET_HOMOLOGUES pangenome size, % core, and % accessory are from the consensus of OMCL and COGS algorithms.
[b]Pangenome size was estimated in anvi'o then the GCs imported into PPanGGOLiN to estimate persistent vs. accessory genome percentages.
[c]Cps_090104 was removed from dataset only for this analysis due to an aberrant % core lower bound.
[d]Cac_ATCC_49756 was removed from dataset only for this analysis due to an aberrant % core lower bound.

Table 3. List of estimated complete KEGG modules.

Module[a]	**Module Name[b]**	% genomes with complete module				
		Cpr	**Cps**	**Cac**	**Ctu**	**Dpi**

M00015	Proline biosynthesis, glutamate => proline	100	100	100	100	0
M00028	Ornithine biosynthesis, glutamate => ornithine	100	100	100	50	0
M00844	Arginine biosynthesis, ornithine => arginine	100	100	100	100	0
M00970	Proline degradation, proline => glutamate	100	100	100	100	0
M00022	Shikimate pathway, phosphoenolpyruvate + erythrose-4P => chorismate	100	100	100	100	0
M00023	Tryptophan biosynthesis, chorismate => tryptophan	100	100	100	100	0
M00019	Valine/isoleucine biosynthesis, pyruvate => valine / 2-oxobutanoate => isoleucine	100	100	100	100	0
M00432	Leucine biosynthesis, 2-oxoisovalerate => 2-oxoisocaproate	100	100	100	100	0
M00570	Isoleucine biosynthesis, threonine => 2-oxobutanoate => isoleucine	100	100	100	100	0
M00017	Methionine biosynthesis, aspartate => homoserine => methionine	100	100	100	100	0
M00021	Cysteine biosynthesis, serine => cysteine	100	100	100	100	0
M00026	Histidine biosynthesis, PRPP => histidine	100	100	90.9	0	0
M00045	Histidine degradation, histidine => N-formiminoglutamate => glutamate	100	100	100	100	0
M00016	Lysine biosynthesis, succinyl-DAP pathway, aspartate => lysine	100	100	100	50	0
M00018	Threonine biosynthesis, aspartate => homoserine => threonine	100	100	100	100	81.5
M00020	Serine biosynthesis, glycerate-3P => serine	100	100	100	87.5	0
M00621	Glycine cleavage system	0	0	100	100	100
M00793	dTDP-L-rhamnose biosynthesis	100	100	100	100	0
M00096	C5 isoprenoid biosynthesis, non-mevalonate pathway	0	0	100	100	0
M00364	C10-C20 isoprenoid biosynthesis, bacteria	0	0	100	100	0
M00365	C10-C20 isoprenoid biosynthesis, archaea	0	0	100	100	0
M00001	Glycolysis (Embden-Meyerhof pathway), glucose => pyruvate	100	100	100	100	100
M00002	Glycolysis, core module involving three-carbon compounds	100	100	100	100	100
M00003	Gluconeogenesis, oxaloacetate => fructose-6P	100	100	100	100	0
M00004	Pentose phosphate pathway (Pentose phosphate cycle)	100	100	100	100	77.8
M00005	PRPP biosynthesis, ribose 5P => PRPP	100	100	100	100	100
M00006	Pentose phosphate pathway, oxidative phase, glucose 6P => ribulose 5P	100	100	100	100	100
M00007	Pentose phosphate pathway, non-oxidative phase, fructose 6P => ribose 5P	100	100	100	100	77.8
M00009	Citrate cycle (TCA cycle, Krebs cycle)	100	100	100	100	0
M00010	Citrate cycle, first carbon oxidation, oxaloacetate => 2-oxoglutarate	100	100	100	100	0
M00011	Citrate cycle, second carbon oxidation, 2-oxoglutarate => oxaloacetate	100	100	100	100	0
M00307	Pyruvate oxidation, pyruvate => acetyl-CoA	100	69	100	100	0
M00549	Nucleotide sugar biosynthesis, glucose => UDP-glucose	0	0	0	100	0
M00550	Ascorbate degradation, ascorbate => D-xylulose-5P	0	0	0	0	37

M00554	Nucleotide sugar biosynthesis, galactose => UDP-galactose	100	100	100	100	0
M00632	Galactose degradation, Leloir pathway, galactose => alpha-D-glucose-1P	100	100	100	100	0
M00854	Glycogen biosynthesis, glucose-1P => glycogen/starch	0	0	0	0	96.3
M00909	UDP-N-acetyl-D-glucosamine biosynthesis, prokaryotes, glucose => UDP-GlcNAc	100	100	100	100	100
M00151	Cytochrome bc1 complex respiratory unit	100	100	100	100	0
M00155	Cytochrome c oxidase, prokaryotes	100	100	100	100	0
M00157	F-type ATPase, prokaryotes and chloroplasts	100	100	100	100	0
M00579	Phosphate acetyltransferase-acetate kinase pathway, acetyl-CoA => acetate	0	0	100	100	100
M00083	Fatty acid biosynthesis, elongation	100	100	0	0	96.3
M00086	beta-Oxidation, acyl-CoA synthesis	100	100	100	100	0
M00120	Coenzyme A biosynthesis, pantothenate => CoA	100	100	100	100	100
M00121	Heme biosynthesis, plants and bacteria, glutamate => heme	100	100	100	100	0
M00123	Biotin biosynthesis, pimeloyl-ACP/CoA => biotin	21.1	92.9	100	0	0
M00125	Riboflavin biosynthesis, plants and bacteria, GTP => riboflavin/FMN/FAD	100	100	100	100	14.8
M00126	Tetrahydrofolate biosynthesis, GTP => THF	0	0	100	100	0
M00140	C1-unit interconversion, prokaryotes	100	97.6	100	100	100
M00577	Biotin biosynthesis, BioW pathway, pimelate => pimeloyl-CoA => biotin	21.1	92.9	100	0	0
M00881	Lipoic acid biosynthesis, plants and bacteria, octanoyl-ACP => dihydrolipoyl-E2/H	100	100	100	100	0
M00899	Thiamine salvage pathway, HMP/HET => TMP	0	0	100	100	100
M00916	Pyridoxal-P biosynthesis, R5P + glyceraldehyde-3P + glutamine => pyridoxal-P	0	0	100	100	0
M00926	Heme biosynthesis, bacteria, glutamyl-tRNA => coproporphyrin III => heme	100	100	100	100	0
M00048	De novo purine biosynthesis, PRPP + glutamine => IMP	100	100	100	100	0
M00049	Adenine ribonucleotide biosynthesis, IMP => ADP,ATP	100	100	100	100	0
M00050	Guanine ribonucleotide biosynthesis, IMP => GDP,GTP	100	100	100	100	0
M00053	Deoxyribonucleotide biosynthesis, ADP/GDP/CDP/UDP => dATP/dGTP/dCTP/dUTP	100	100	100	100	0
M00938	Pyrimidine deoxyribonucleotide biosynthesis, UDP => dTTP	100	100	100	100	0

[a]Modules are colored based on their KEGG module subcategory; red: “amino acid metabolism”, dark teal: “biosynthesis of terpenoids and polyketides”, green: “carbohydrate metabolism”, grey: “energy metabolism”, dark orange: “lipid metabolism”, orange: “metabolism of cofactors and vitamins”, yellow: “nucleotide metabolism”.

[b]PRPP is 5-phosphoribosyl diphosphate, DAP is diaminopimelate, FMN is flavin mononucleotide, FAD is flavin adenine dinucleotide, ACP is acyl-carrier protein, HMP is 4-amino-5-hydroxymethyl-2-methylpyrimidine, HET is 5-(2-hydroxyethyl)-4-methylthiazole and TMP is thiamine monophosphate.

1112 **SUPPLEMENTAL MATERIALS**

1113 **File S1 (text).** Supplemental text

1114 **Figure S1.** Phylogenomic trees

1115 **Figure S2.** Pairwise ANIs and conservative core GCs

1116 **Figure S3.** Pangenome estimates

1117 **Figure S4.** COG analysis of accessory genome by strain

1118 **Figure S5.** Additional data related to Figures 6 and 7

1119 **Table S1 (excel file).** Bacterial strain genome information

1120 **Table S2 (excel file).** PPanGGOLiN assignment of GCs to the persistent or accessory

1121 genome

1122 **Table S3 (excel file).** KO metabolic estimations and enrichment analysis by anvi'o

1123 **Table S4 (excel file).** KEGG module estimations and enrichment analysis by anvi'o

1124

1125 **Supplemental File S1**

1126 **Species assignment for *Corynebacterium* sp. KPL# previously submitted to NCBI.**

1127 The Broad Institute originally sequenced a set of *Corynebacterium* strains we had isolated

1128 from human nostril swabs, and we included in our current analyses any of these that were

1129 assigned to one of the four species of interest (113). The species assignment for each of

1130 these based on phylogenomic analyses (**Figs. 1** and **S1**) and ANI (**Figs. S2A-B**) are as

1131 follows: *C. accolens* KPL1818; *C. accolens* KPL1824; *C. accolens* KPL1996 (*C. accolens*

1132 KPL1986, KPL1998, and KPL2004); and *C. pseudodiphtheriticum* KPL1989 (*C.*

1133 *pseudodiphtheriticum* KPL1995). Isolates in parentheses are genomes listed in NCBI that

1134 have a MASH distance ≤ 10^{-4} to the strain genome listed immediately before the
1135 parentheses.

1136 **Comparing core genomes and pangenomes predicted by GET_HOMOLOGUES and**
1137 **anvi'o.** The difference in the outputs of gene clusters (GCs) from GET_HOMOLOGUES
1138 (consensus of OMCL and COGS algorithms) and anvi'o were measured using the percent
1139 difference formula $\frac{|V1-V2|}{\left[\frac{(V1+V2)}{2}\right]} \times 100 = \%\ difference$. Core and pangenomes sizes for both
1140 the pangenomic platforms are listed below for comparison, with their percentage
1141 differences.

Species	Core genome			Pangenome		
	GH	anvi'o	% diff.	GH	anvi'o	% diff.
C. propinquum	1624	1824	11.6%	3777	3108	19.4%
C. pseudodiphtheriticum	1515	1714	12.3%	4590	3590	24.4%
C. accolens	1688	1904	12.0%	4220	3427	20.7%
C. tuberculostearicum	1810	1915	5.6%	3232	2907	10.6%

1142

1143 **L-Glutamine is also an excellent nitrogen source in *C. glutamicum*.** Although the
1144 GOGAT enzyme is the main pathway involved in glutamine assimilation, it is not required
1145 for this, since in a *C. glutamicum* GOGAT deletion mutant, a glutaminase in conjunction
1146 with glutamate dehydrogenase appears to contribute to glutamine utilization, although
1147 primarily as a carbon and energy source (149, 150) In all the analyzed *Corynebacterium*
1148 genomes, except for *C. diphtheriae*^{T}, we identified genes annotated as a glutaminase

1149 (K01425) corresponding to the *C. glutamicum*^{T} *glsK* gene, which hydrolyzes glutamine
1150 producing ammonium and glutamate. Glutamine is also essential to produce carbamoyl
1151 phosphate, a precursor for the arginine and pyrimidine synthesis pathways. In *C.*
1152 *glutamicum* the glutamine-dependent carbamoyl phosphate synthetase II (CPS_II)
1153 encoded by the *carAB* operon converts HCO_3^-, ATP, and glutamine to carbamoyl
1154 phosphate (151). We identified K01956 and K01955 (*carA* and *carB*) annotations in all
1155 analyzed *Corynebacterium* species. Based on these findings, we predicted that addition
1156 of glutamine might improve the growth of nasal *Corynebacterium* species in defined
1157 medium lacking amino acids via enzymatic activities that use glutamine as a precursor,
1158 including, but probably not limited to, glutaminase, carbamoyl phosphate, and/or
1159 glutamine amidotransferase enzymes.

1160 **Trace Minerals Solutions.** The Trace Minerals I 50000X stock consists of the following:
1161 0.302 mM cobalt chloride hexahydrate, 0.096 mM copper chloride dihydrate, 0.81 mM
1162 manganese chloride tetrahydrate, 0.0292 mM ammonium molybdate, 0.0975 mM zinc
1163 chloride, 4 mM boric acid. The Trace Minerals II 50X stock consists of the following: 950
1164 mM ammonium chloride, 0.05 mM calcium chloride, 52.5 mM magnesium chloride.

1165

1166 **REFERENCES**
1167

1168 1. Biesbroek G, Bosch AA, Wang X, Keijser BJ, Veenhoven RH, Sanders EA,
1169 Bogaert D. 2014. The impact of breastfeeding on nasopharyngeal microbial
1170 communities in infants. Am J Respir Crit Care Med 190:298-308.
1171 2. Biesbroek G, Tsivtsivadze E, Sanders EA, Montijn R, Veenhoven RH, Keijser BJ,
1172 Bogaert D. 2014. Early respiratory microbiota composition determines bacterial
1173 succession patterns and respiratory health in children. Am J Respir Crit Care Med
1174 190:1283-92.

1175 3. Mika M, Mack I, Korten I, Qi W, Aebi S, Frey U, Latzin P, Hilty M. 2015. Dynamics
1176 of the nasal microbiota in infancy: a prospective cohort study. J Allergy Clin
1177 Immunol 135:905-912 e11.
1178 4. Teo SM, Mok D, Pham K, Kusel M, Serralha M, Troy N, Holt BJ, Hales BJ, Walker
1179 ML, Hollams E, Bochkov YA, Grindle K, Johnston SL, Gern JE, Sly PD, Holt PG,
1180 Holt KE, Inouye M. 2015. The infant nasopharyngeal microbiome impacts severity
1181 of lower respiratory infection and risk of asthma development. Cell Host Microbe
1182 17:704-15.
1183 5. Peterson SW, Knox NC, Golding GR, Tyler SD, Tyler AD, Mabon P, Embree JE,
1184 Fleming F, Fanella S, Van Domselaar G, Mulvey MR, Graham MR. 2016. A Study
1185 of the Infant Nasal Microbiome Development over the First Year of Life and in
1186 Relation to Their Primary Adult Caregivers Using cpn60 Universal Target (UT) as
1187 a Phylogenetic Marker. PLoS One 11:e0152493.
1188 6. Bosch AATM, Levin E, Van Houten MA, Hasrat R, Kalkman G, Biesbroek G, De
1189 Steenhuijsen Piters WAA, De Groot P-KCM, Pernet P, Keijser BJF, Sanders EAM,
1190 Bogaert D. 2016. Development of Upper Respiratory Tract Microbiota in Infancy is
1191 Affected by Mode of Delivery. EBioMedicine 9:336-345.
1192 7. Bosch A, de Steenhuijsen Piters WAA, van Houten MA, Chu M, Biesbroek G, Kool
1193 J, Pernet P, de Groot PCM, Eijkemans MJC, Keijser BJF, Sanders EAM, Bogaert
1194 D. 2017. Maturation of the Infant Respiratory Microbiota, Environmental Drivers,
1195 and Health Consequences. A Prospective Cohort Study. Am J Respir Crit Care
1196 Med 196:1582-1590.
1197 8. Shilts MH, Rosas-Salazar C, Tovchigrechko A, Larkin EK, Torralba M, Akopov A,
1198 Halpin R, Peebles RS, Moore ML, Anderson LJ, Nelson KE, Hartert TV, Das SR.
1199 2016. Minimally Invasive Sampling Method Identifies Differences in Taxonomic
1200 Richness of Nasal Microbiomes in Young Infants Associated with Mode of
1201 Delivery. Microb Ecol 71:233-42.
1202 9. Chu DM, Ma J, Prince AL, Antony KM, Seferovic MD, Aagaard KM. 2017.
1203 Maturation of the infant microbiome community structure and function across
1204 multiple body sites and in relation to mode of delivery. Nat Med 23:314-326.
1205 10. Salter SJ, Turner C, Watthanaworawit W, de Goffau MC, Wagner J, Parkhill J,
1206 Bentley SD, Goldblatt D, Nosten F, Turner P. 2017. A longitudinal study of the
1207 infant nasopharyngeal microbiota: The effects of age, illness and antibiotic use in
1208 a cohort of South East Asian children. PLoS Negl Trop Dis 11:e0005975.
1209 11. Ta LDH, Yap GC, Tay CJX, Lim ASM, Huang CH, Chu CW, De Sessions PF, Shek
1210 LP, Goh A, Van Bever HPS, Teoh OH, Soh JY, Thomas B, Ramamurthy MB, Goh
1211 DYT, Lay C, Soh SE, Chan YH, Saw SM, Kwek K, Chong YS, Godfrey KM, Hibberd
1212 ML, Lee BW. 2018. Establishment of the nasal microbiota in the first 18 months of
1213 life: Correlation with early-onset rhinitis and wheezing. J Allergy Clin Immunol
1214 142:86-95.
1215 12. Toivonen L, Hasegawa K, Waris M, Ajami NJ, Petrosino JF, Camargo CA, Jr.,
1216 Peltola V. 2019. Early nasal microbiota and acute respiratory infections during the
1217 first years of life. Thorax 74:592-599.
1218 13. Kelly MS, Plunkett C, Yu Y, Aquino JN, Patel SM, Hurst JH, Young RR, Smieja M,
1219 Steenhoff AP, Arscott-Mills T, Feemster KA, Boiditswe S, Leburu T, Mazhani T,
1220 Patel MZ, Rawls JF, Jawahar J, Shah SS, Polage CR, Cunningham CK, Seed PC.

1221 2022. Non-diphtheriae Corynebacterium species are associated with decreased
1222 risk of pneumococcal colonization during infancy. ISME J 16:655-665.
1223 14. Yan M, Pamp SJ, Fukuyama J, Hwang PH, Cho DY, Holmes S, Relman DA. 2013.
1224 Nasal microenvironments and interspecific interactions influence nasal microbiota
1225 complexity and *S. aureus* carriage. Cell host & microbe 14:631-40.
1226 15. Ramakrishnan VR, Feazel LM, Gitomer SA, Ir D, Robertson CE, Frank DN. 2013.
1227 The microbiome of the middle meatus in healthy adults. PLoS One 8:e85507.
1228 16. Biswas K, Hoggard M, Jain R, Taylor MW, Douglas RG. 2015. The nasal
1229 microbiota in health and disease: variation within and between subjects. Front
1230 Microbiol 9:134.
1231 17. Kaspar U, Kriegeskorte A, Schubert T, Peters G, Rudack C, Pieper DH, Wos-Oxley
1232 M, Becker K. 2016. The culturome of the human nose habitats reveals individual
1233 bacterial fingerprint patterns. Environ Microbiol 18:2130-42.
1234 18. Wos-Oxley ML, Chaves-Moreno D, Jauregui R, Oxley AP, Kaspar U, Plumeier I,
1235 Kahl S, Rudack C, Becker K, Pieper DH. 2016. Exploring the bacterial
1236 assemblages along the human nasal passage. Environ Microbiol 18:2259-71.
1237 19. De Boeck I, Wittouck S, Wuyts S, Oerlemans EFM, van den Broek MFL,
1238 Vandenheuvel D, Vanderveken O, Lebeer S. 2017. Comparing the Healthy Nose
1239 and Nasopharynx Microbiota Reveals Continuity As Well As Niche-Specificity.
1240 Front Microbiol 8:2372.
1241 20. Laufer AS, Metlay JP, Gent JF, Fennie KP, Kong Y, Pettigrew MM. 2011. Microbial
1242 communities of the upper respiratory tract and otitis media in children. mBio
1243 2:e00245-10.
1244 21. Pettigrew MM, Laufer AS, Gent JF, Kong Y, Fennie KP, Metlay JP. 2012. Upper
1245 respiratory tract microbial communities, acute otitis media pathogens, and
1246 antibiotic use in healthy and sick children. Appl Environ Microbiol 78:6262-70.
1247 22. Bomar L, Brugger SD, Yost BH, Davies SS, Lemon KP. 2016. *Corynebacterium*
1248 *accolens* Releases Antipneumococcal Free Fatty Acids from Human Nostril and
1249 Skin Surface Triacylglycerols. mBio 7:e01725-15.
1250 23. Kelly MS, Surette MG, Smieja M, Pernica JM, Rossi L, Luinstra K, Steenhoff AP,
1251 Feemster KA, Goldfarb DM, Arscott-Mills T, Boiditswe S, Rulaganyang I, Muthoga
1252 C, Gaofiwe L, Mazhani T, Rawls JF, Cunningham CK, Shah SS, Seed PC. 2017.
1253 The Nasopharyngeal Microbiota of Children With Respiratory Infections in
1254 Botswana. Pediatr Infect Dis J 36:e211-e218.
1255 24. Hasegawa K, Linnemann RW, Mansbach JM, Ajami NJ, Espinola JA, Petrosino
1256 JF, Piedra PA, Stevenson MD, Sullivan AF, Thompson AD, Camargo CA, Jr. 2017.
1257 Nasal Airway Microbiota Profile and Severe Bronchiolitis in Infants: A Case-control
1258 Study. Pediatr Infect Dis J 36:1044-1051.
1259 25. Kelly MS, Surette MG, Smieja M, Rossi L, Luinstra K, Steenhoff AP, Goldfarb DM,
1260 Pernica JM, Arscott-Mills T, Boiditswe S, Mazhani T, Rawls JF, Cunningham CK,
1261 Shah SS, Feemster KA, Seed PC. 2018. Pneumococcal Colonization and the
1262 Nasopharyngeal Microbiota of Children in Botswana. Pediatr Infect Dis J 37:1176-
1263 1183.
1264 26. Lappan R, Imbrogno K, Sikazwe C, Anderson D, Mok D, Coates H, Vijayasekaran
1265 S, Bumbak P, Blyth CC, Jamieson SE, Peacock CS. 2018. A microbiome case-

control study of recurrent acute otitis media identified potentially protective bacterial genera. BMC Microbiol 18:13.

27. Man WH, Clerc M, de Steenhuijsen Piters WAA, van Houten MA, Chu M, Kool J, Keijser BJF, Sanders EAM, Bogaert D. 2019. Loss of Microbial Topography between Oral and Nasopharyngeal Microbiota and Development of Respiratory Infections Early in Life. Am J Respir Crit Care Med 15:760-770.

28. Xu L, Earl J, Pichichero ME. 2021. Nasopharyngeal microbiome composition associated with *Streptococcus pneumoniae* colonization suggests a protective role of *Corynebacterium* in young children. PLoS One 16:e0257207.

29. Coleman A, Bialasiewicz S, Marsh RL, Grahn Hakansson E, Cottrell K, Wood A, Jayasundara N, Ware RS, Zaugg J, Sidjabat HE, Adams J, Ferguson J, Brown M, Roos K, Cervin A. 2021. Upper Respiratory Microbiota in Relation to Ear and Nose Health Among Australian Aboriginal and Torres Strait Islander Children. J Pediatric Infect Dis Soc 10:468-476.

30. Coleman A, Zaugg J, Wood A, Cottrell K, Hakansson EG, Adams J, Brown M, Cervin A, Bialasiewicz S. 2021. Upper Respiratory Tract Microbiome of Australian Aboriginal and Torres Strait Islander Children in Ear and Nose Health and Disease. Microbiol Spectr 9:e0036721.

31. Escapa IF, Chen T, Huang Y, Gajare P, Dewhirst FE, Lemon KP. 2018. New Insights into Human Nostril Microbiome from the Expanded Human Oral Microbiome Database (eHOMD): a Resource for the Microbiome of the Human Aerodigestive Tract. mSystems 3:e00187-18.

32. Liu CM, Price LB, Hungate BA, Abraham AG, Larsen LA, Christensen K, Stegger M, Skov R, Andersen PS. 2015. *Staphylococcus aureus* and the ecology of the nasal microbiome. Sci Adv 1:e1400216.

33. Teutsch B, Berger A, Marosevic D, Schonberger K, Lam TT, Hubert K, Beer S, Wienert P, Ackermann N, Claus H, Drayss M, Thiel K, van der Linden M, Vogel U, Sing A. 2017. *Corynebacterium* species nasopharyngeal carriage in asymptomatic individuals aged >/= 65 years in Germany. Infection 45:607-611.

34. Salamzade R, Swaney MH, Kalan LR. 2022. Comparative Genomic and Metagenomic Investigations of the *Corynebacterium tuberculostearicum* Species Complex Reveals Potential Mechanisms Underlying Associations To Skin Health and Disease. Microbiol Spectr doi:10.1128/spectrum.03578-22:e0357822.

35. Oh J, Byrd AL, Park M, Program NCS, Kong HH, Segre JA. 2016. Temporal Stability of the Human Skin Microbiome. Cell 165:854-66.

36. Salamzade R, Cheong JZA, Sandstrom S, Swaney MH, Stubbendieck RM, Starr NL, Currie CR, Singh AM, Kalan LR. 2023. Evolutionary investigations of the biosynthetic diversity in the skin microbiome using lsaBGC. Microb Genom 9.

37. Ahmed N, Joglekar P, Deming C, Program NCS, Lemon KP, Kong HH, Segre JA, Conlan S. 2023. Genomic characterization of the C. tuberculostearicum species complex, a prominent member of the human skin microbiome. mSystems 8:e0063223.

38. Brugger SD, Eslami SM, Pettigrew MM, Escapa IF, Henke MT, Kong Y, Lemon KP. 2020. *Dolosigranulum pigrum* Cooperation and Competition in Human Nasal Microbiota. mSphere 5:e00852-20.

1311 39. Stubbendieck RM, May DS, Chevrette MG, Temkin MI, Wendt-Pienkowski E,
1312 Cagnazzo J, Carlson CM, Gern JE, Currie CR. 2019. Competition among Nasal
1313 Bacteria Suggests a Role for Siderophore-Mediated Interactions in Shaping the
1314 Human Nasal Microbiota. Appl Environ Microbiol 85.
1315 40. Ramsey MM, Freire MO, Gabrilska RA, Rumbaugh KP, Lemon KP. 2016.
1316 *Staphylococcus aureus* Shifts toward Commensalism in Response to
1317 *Corynebacterium* Species. Frontiers in Microbiology 7:1230.
1318 41. Hardy BL, Dickey SW, Plaut RD, Riggins DP, Stibitz S, Otto M, Merrell DS. 2019.
1319 *Corynebacterium pseudodiphtheriticum* Exploits *Staphylococcus aureus* Virulence
1320 Components in a Novel Polymicrobial Defense Strategy. mBio 10.
1321 42. Zhao Y, Bitzer A, Power JJ, Belikova D, Torres Salazar BO, Adolf LA, Gerlach D,
1322 Krismer B, Heilbronner S. 2024. Nasal commensals reduce Staphylococcus
1323 aureus proliferation by restricting siderophore availability. ISME J 18.
1324 43. Uehara Y, Nakama H, Agematsu K, Uchida M, Kawakami Y, Abdul Fattah AS,
1325 Maruchi N. 2000. Bacterial interference among nasal inhabitants: eradication of
1326 *Staphylococcus aureus* from nasal cavities by artificial implantation of
1327 *Corynebacterium* sp. J Hosp Infect 44:127-33.
1328 44. Lina G, Boutite F, Tristan A, Bes M, Etienne J, Vandenesch F. 2003. Bacterial
1329 competition for human nasal cavity colonization: role of Staphylococcal agr alleles.
1330 Appl Environ Microbiol 69:18-23.
1331 45. Wos-Oxley ML, Plumeier I, von Eiff C, Taudien S, Platzer M, Vilchez-Vargas R,
1332 Becker K, Pieper DH. 2010. A poke into the diversity and associations within
1333 human anterior nare microbial communities. ISME J 4:839-51.
1334 46. Johnson RC, Ellis MW, Lanier JB, Schlett CD, Cui T, Merrell DS. 2015. Correlation
1335 between nasal microbiome composition and remote purulent skin and soft tissue
1336 infections. Infection and immunity 83:802-11.
1337 47. Blum FC, Whitmire JM, Bennett JW, Carey PM, Ellis MW, English CE, Law NN,
1338 Tribble DR, Millar EV, Merrell DS. 2022. Nasal microbiota evolution within the
1339 congregate setting imposed by military training. Sci Rep 12:11492.
1340 48. Kiryukhina NV, Melnikov VG, Suvorov AV, Morozova YA, Ilyin VK. 2013. Use of
1341 *Corynebacterium pseudodiphtheriticum* for elimination of *Staphylococcus aureus*
1342 from the nasal cavity in volunteers exposed to abnormal microclimate and altered
1343 gaseous environment. Probiotics and antimicrobial proteins 5:233-8.
1344 49. Kluytmans J, van Belkum A, Verbrugh H. 1997. Nasal carriage of *Staphylococcus*
1345 *aureus*: epidemiology, underlying mechanisms, and associated risks. Clin
1346 Microbiol Rev 10:505-20.
1347 50. von Eiff C, Becker K, Machka K, Stammer H, Peters G, Group FtS. 2001. Nasal
1348 carriage as a source of *Staphylococcus aureus* bacteremia. N Engl J Med 344:11-
1349 6.
1350 51. Wertheim HF, Vos MC, Ott A, van Belkum A, Voss A, Kluytmans JA, van Keulen
1351 PH, Vandenbroucke-Grauls CM, Meester MH, Verbrugh HA. 2004. Risk and
1352 outcome of nosocomial *Staphylococcus aureus* bacteraemia in nasal carriers
1353 versus non-carriers. Lancet 364:703-5.
1354 52. Young BC, Wu CH, Gordon NC, Cole K, Price JR, Liu E, Sheppard AE, Perera S,
1355 Charlesworth J, Golubchik T, Iqbal Z, Bowden R, Massey RC, Paul J, Crook DW,

Peto TE, Walker AS, Llewelyn MJ, Wyllie DH, Wilson DJ. 2017. Severe infections emerge from commensal bacteria by adaptive evolution. Elife 6.

53. Kanmani P, Clua P, Vizoso-Pinto MG, Rodriguez C, Alvarez S, Melnikov V, Takahashi H, Kitazawa H, Villena J. 2017. Respiratory Commensal Bacteria *Corynebacterium pseudodiphtheriticum* Improves Resistance of Infant Mice to Respiratory Syncytial Virus and *Streptococcus pneumoniae* Superinfection. Front Microbiol 8:1613.

54. Horn KJ, Jaberi Vivar AC, Arenas V, Andani S, Janoff EN, Clark SE. 2021. *Corynebacterium* Species Inhibit *Streptococcus pneumoniae* Colonization and Infection of the Mouse Airway. Front Microbiol 12:804935.

55. Menberu MA, Liu S, Cooksley C, Hayes AJ, Psaltis AJ, Wormald PJ, Vreugde S. 2021. *Corynebacterium accolens* Has Antimicrobial Activity against *Staphylococcus aureus* and Methicillin-Resistant *S. aureus* Pathogens Isolated from the Sinonasal Niche of Chronic Rhinosinusitis Patients. Pathogens 10.

56. Neubauer M, Šourek J, Rýc M, Boháček J, Mára M, Mňuková J. 1991. *Corynebacterium accolens* sp. nov., a Gram-Positive Rod Exhibiting Satellitism, from Clinical Material. Systematic and Applied Microbiology 14:46-51.

57. Riegel P, de Briel D, Prevost G, Jehl F, Monteil H. 1993. Proposal of *Corynebacterium propinquum* sp. nov. for *Corynebacterium* group ANF-3 strains. FEMS Microbiol Lett 113:229-234.

58. Karlyshev AV, Melnikov VG. 2013. Draft Genome Sequence of *Corynebacterium pseudodiphtheriticum* Strain 090104 "Sokolov". Genome Announc 1.

59. Bernier AM, Bernard K. 2018. Whole-Genome Sequences of *Corynebacterium macginleyi* CCUG 32361(T) and Clinical Isolates NML 080212 and NML 120205. Microbiol Resour Announc 7.

60. Zhang C, Song W, Ma HR, Peng X, Anderson DJ, Fowler VG, Jr., Thaden JT, Xiao M, You L. 2020. Temporal encoding of bacterial identity and traits in growth dynamics. Proc Natl Acad Sci U S A 117:20202-20210.

61. Swaney MH, Sandstrom S, Kalan LR. 2022. Cobamide Sharing Is Predicted in the Human Skin Microbiome. mSystems 7:e0067722.

62. Flores Ramos S, Brugger SD, Escapa IF, Skeete CA, Cotton SL, Eslami SM, Gao W, Bomar L, Tran TH, Jones DS, Minot S, Roberts RJ, Johnston CD, Lemon KP. 2021. Genomic Stability and Genetic Defense Systems in *Dolosigranulum pigrum*, a Candidate Beneficial Bacterium from the Human Microbiome. mSystems 6:e0042521.

63. McInerney JO, McNally A, O'Connell MJ. 2017. Why prokaryotes have pangenomes. Nat Microbiol 2:17040.

64. Eren AM, Kiefl E, Shaiber A, Veseli I, Miller SE, Schechter MS, Fink I, Pan JN, Yousef M, Fogarty EC, Trigodet F, Watson AR, Esen OC, Moore RM, Clayssen Q, Lee MD, Kivenson V, Graham ED, Merrill BD, Karkman A, Blankenberg D, Eppley JM, Sjodin A, Scott JJ, Vazquez-Campos X, McKay LJ, McDaniel EA, Stevens SLR, Anderson RE, Fuessel J, Fernandez-Guerra A, Maignien L, Delmont TO, Willis AD. 2021. Community-led, integrated, reproducible multi-omics with anvi'o. Nat Microbiol 6:3-6.

65. Oliveira PH, Touchon M, Cury J, Rocha EPC. 2017. The chromosomal organization of horizontal gene transfer in bacteria. Nat Commun 8:841.

1402 66. Iranzo J, Wolf YI, Koonin EV, Sela I. 2019. Gene gain and loss push prokaryotes
1403 beyond the homologous recombination barrier and accelerate genome sequence
1404 divergence. Nat Commun 10:5376.
1405 67. Gautreau G, Bazin A, Gachet M, Planel R, Burlot L, Dubois M, Perrin A, Medigue
1406 C, Calteau A, Cruveiller S, Matias C, Ambroise C, Rocha EPC, Vallenet D. 2020.
1407 PPanGGOLiN: Depicting microbial diversity via a partitioned pangenome graph.
1408 PLoS Comput Biol 16:e1007732.
1409 68. Kalinowski J, Bathe B, Bartels D, Bischoff N, Bott M, Burkovski A, Dusch N,
1410 Eggeling L, Eikmanns BJ, Gaigalat L, Goesmann A, Hartmann M, Huthmacher K,
1411 Kramer R, Linke B, McHardy AC, Meyer F, Mockel B, Pfefferle W, Puhler A, Rey
1412 DA, Ruckert C, Rupp O, Sahm H, Wendisch VF, Wiegrabe I, Tauch A. 2003. The
1413 complete *Corynebacterium glutamicum* ATCC 13032 genome sequence and its
1414 impact on the production of L-aspartate-derived amino acids and vitamins. J
1415 Biotechnol 104:5-25.
1416 69. Wolf S, Becker J, Tsuge Y, Kawaguchi H, Kondo A, Marienhagen J, Bott M,
1417 Wendisch VF, Wittmann C. 2021. Advances in metabolic engineering of
1418 Corynebacterium glutamicum to produce high-value active ingredients for food,
1419 feed, human health, and well-being. Essays Biochem 65:197-212.
1420 70. Oliveira A, Oliveira LC, Aburjaile F, Benevides L, Tiwari S, Jamal SB, Silva A,
1421 Figueiredo HCP, Ghosh P, Portela RW, De Carvalho Azevedo VA, Wattam AR.
1422 2017. Insight of Genus *Corynebacterium*: Ascertaining the Role of Pathogenic and
1423 Non-pathogenic Species. Front Microbiol 8:1937.
1424 71. Burkovski A. 2013. Cell envelope of corynebacteria: structure and influence on
1425 pathogenicity. ISRN Microbiol 2013:935736.
1426 72. Cronan JE. 2016. Assembly of Lipoic Acid on Its Cognate Enzymes: an
1427 Extraordinary and Essential Biosynthetic Pathway. Microbiol Mol Biol Rev 80:429-
1428 50.
1429 73. Tramonti A, Nardella C, di Salvo ML, Barile A, D'Alessio F, de Crecy-Lagard V,
1430 Contestabile R. 2021. Knowns and Unknowns of Vitamin B(6) Metabolism in
1431 Escherichia coli. EcoSal Plus 9.
1432 74. Shelton AN, Seth EC, Mok KC, Han AW, Jackson SN, Haft DR, Taga ME. 2019.
1433 Uneven distribution of cobamide biosynthesis and dependence in bacteria
1434 predicted by comparative genomics. ISME J 13:789-804.
1435 75. Bruggemann H, Henne A, Hoster F, Liesegang H, Wiezer A, Strittmatter A, Hujer
1436 S, Durre P, Gottschalk G. 2004. The complete genome sequence of
1437 *Propionibacterium acnes*, a commensal of human skin. Science 305:671-3.
1438 76. Tettelin H, Nelson KE, Paulsen IT, Eisen JA, Read TD, Peterson S, Heidelberg J,
1439 DeBoy RT, Haft DH, Dodson RJ, Durkin AS, Gwinn M, Kolonay JF, Nelson WC,
1440 Peterson JD, Umayam LA, White O, Salzberg SL, Lewis MR, Radune D,
1441 Holtzapple E, Khouri H, Wolf AM, Utterback TR, Hansen CL, McDonald LA,
1442 Feldblyum TV, Angiuoli S, Dickinson T, Hickey EK, Holt IE, Loftus BJ, Yang F,
1443 Smith HO, Venter JC, Dougherty BA, Morrison DA, Hollingshead SK, Fraser CM.
1444 2001. Complete genome sequence of a virulent isolate of *Streptococcus*
1445 *pneumoniae*. Science 293:498-506.
1446 77. Diep BA, Gill SR, Chang RF, Phan TH, Chen JH, Davidson MG, Lin F, Lin J,
1447 Carleton HA, Mongodin EF, Sensabaugh GF, Perdreau-Remington F. 2006.

1448 Complete genome sequence of USA300, an epidemic clone of community-
1449 acquired meticillin-resistant *Staphylococcus aureus*. Lancet 367:731-9.
1450 78. Gill SR, Fouts DE, Archer GL, Mongodin EF, Deboy RT, Ravel J, Paulsen IT,
1451 Kolonay JF, Brinkac L, Beanan M, Dodson RJ, Daugherty SC, Madupu R, Angiuoli
1452 SV, Durkin AS, Haft DH, Vamathevan J, Khouri H, Utterback T, Lee C, Dimitrov G,
1453 Jiang L, Qin H, Weidman J, Tran K, Kang K, Hance IR, Nelson KE, Fraser CM.
1454 2005. Insights on evolution of virulence and resistance from the complete genome
1455 analysis of an early methicillin-resistant *Staphylococcus aureus* strain and a
1456 biofilm-producing methicillin-resistant *Staphylococcus epidermidis* strain. J
1457 Bacteriol 187:2426-38.
1458 79. Seibold G, Dempf S, Schreiner J, Eikmanns BJ. 2007. Glycogen formation in
1459 Corynebacterium glutamicum and role of ADP-glucose pyrophosphorylase.
1460 Microbiology (Reading) 153:1275-1285.
1461 80. Seibold GM, Eikmanns BJ. 2007. The *glgX* gene product of *Corynebacterium*
1462 *glutamicum* is required for glycogen degradation and for fast adaptation to
1463 hyperosmotic stress. Microbiology (Reading) 153:2212-2220.
1464 81. Tsai YC, Conlan S, Deming C, Program NCS, Segre JA, Kong HH, Korlach J, Oh
1465 J. 2016. Resolving the Complexity of Human Skin Metagenomes Using Single-
1466 Molecule Sequencing. mBio 7:e01948-15.
1467 82. Tauch A, Schneider J, Szczepanowski R, Tilker A, Viehoever P, Gartemann KH,
1468 Arnold W, Blom J, Brinkrolf K, Brune I, Gotker S, Weisshaar B, Goesmann A,
1469 Droge M, Puhler A. 2008. Ultrafast pyrosequencing of *Corynebacterium*
1470 *kroppenstedtii* DSM44385 revealed insights into the physiology of a lipophilic
1471 corynebacterium that lacks mycolic acids. J Biotechnol 136:22-30.
1472 83. Sichtig H, Minogue T, Yan Y, Stefan C, Hall A, Tallon L, Sadzewicz L, Nadendla
1473 S, Klimke W, Hatcher E, Shumway M, Aldea DL, Allen J, Koehler J, Slezak T,
1474 Lovell S, Schoepp R, Scherf U. 2019. FDA-ARGOS is a database with public
1475 quality-controlled reference genomes for diagnostic use and regulatory science.
1476 Nat Commun 10:3313.
1477 84. Marienhagen J, Kennerknecht N, Sahm H, Eggeling L. 2005. Functional analysis
1478 of all aminotransferase proteins inferred from the genome sequence of
1479 Corynebacterium glutamicum. J Bacteriol 187:7639-46.
1480 85. McHardy AC, Tauch A, Ruckert C, Puhler A, Kalinowski J. 2003. Genome-based
1481 analysis of biosynthetic aminotransferase genes of Corynebacterium glutamicum.
1482 J Biotechnol 104:229-40.
1483 86. Koper K, Han SW, Pastor DC, Yoshikuni Y, Maeda HA. 2022. Evolutionary origin
1484 and functional diversification of aminotransferases. J Biol Chem 298:102122.
1485 87. Gelfand DH, Steinberg RA. 1977. Escherichia coli mutants deficient in the
1486 aspartate and aromatic amino acid aminotransferases. J Bacteriol 130:429-40.
1487 88. Lensmire JM, Hammer ND. 2019. Nutrient sulfur acquisition strategies employed
1488 by bacterial pathogens. Curr Opin Microbiol 47:52-58.
1489 89. Ruckert C, Koch DJ, Rey DA, Albersmeier A, Mormann S, Puhler A, Kalinowski J.
1490 2005. Functional genomics and expression analysis of the *Corynebacterium*
1491 *glutamicum fpr2-cysIXHDNYZ* gene cluster involved in assimilatory sulphate
1492 reduction. BMC Genomics 6:121.

1493 90. Williams SJ, Senaratne RH, Mougous JD, Riley LW, Bertozzi CR. 2002. 5'-
1494 adenosinephosphosulfate lies at a metabolic branch point in mycobacteria. J Biol
1495 Chem 277:32606-15.
1496 91. Berndt C, Lillig CH, Wollenberg M, Bill E, Mansilla MC, de Mendoza D, Seidler A,
1497 Schwenn JD. 2004. Characterization and reconstitution of a 4Fe-4S adenylyl
1498 sulfate/phosphoadenylyl sulfate reductase from Bacillus subtilis. J Biol Chem
1499 279:7850-5.
1500 92. Simic P, Willuhn J, Sahm H, Eggeling L. 2002. Identification of glyA (encoding
1501 serine hydroxymethyltransferase) and its use together with the exporter ThrE to
1502 increase L-threonine accumulation by Corynebacterium glutamicum. Appl Environ
1503 Microbiol 68:3321-7.
1504 93. Tesch M, de Graaf AA, Sahm H. 1999. In vivo fluxes in the ammonium-assimilatory
1505 pathways in corynebacterium glutamicum studied by 15N nuclear magnetic
1506 resonance. Appl Environ Microbiol 65:1099-109.
1507 94. Beckers G, Nolden L, Burkovski A. 2001. Glutamate synthase of Corynebacterium
1508 glutamicum is not essential for glutamate synthesis and is regulated by the
1509 nitrogen status. Microbiology (Reading) 147:2961-70.
1510 95. Son HF, Kim KJ. 2016. Structural Insights into a Novel Class of Aspartate
1511 Aminotransferase from *Corynebacterium glutamicum*. PLoS One 11:e0158402.
1512 96. Hirasawa T, Wachi M, Nagai K. 2000. A mutation in the Corynebacterium
1513 glutamicum ltsA gene causes susceptibility to lysozyme, temperature-sensitive
1514 growth, and L-glutamate production. J Bacteriol 182:2696-701.
1515 97. Javid B, Sorrentino F, Toosky M, Zheng W, Pinkham JT, Jain N, Pan M, Deighan
1516 P, Rubin EJ. 2014. Mycobacterial mistranslation is necessary and sufficient for
1517 rifampicin phenotypic resistance. Proc Natl Acad Sci U S A 111:1132-7.
1518 98. Agapova A, Serafini A, Petridis M, Hunt DM, Garza-Garcia A, Sohaskey CD, de
1519 Carvalho LPS. 2019. Flexible nitrogen utilisation by the metabolic generalist
1520 pathogen Mycobacterium tuberculosis. Elife 8.
1521 99. Marienhagen J, Eggeling L. 2008. Metabolic function of Corynebacterium
1522 glutamicum aminotransferases AlaT and AvtA and impact on L-valine production.
1523 Appl Environ Microbiol 74:7457-62.
1524 100. Copeland E, Leonard K, Carney R, Kong J, Forer M, Naidoo Y, Oliver BGG,
1525 Seymour JR, Woodcock S, Burke CM, Stow NW. 2018. Chronic Rhinosinusitis:
1526 Potential Role of Microbial Dysbiosis and Recommendations for Sampling Sites.
1527 Front Cell Infect Microbiol 8:57.
1528 101. Renz A, Widerspick L, Drager A. 2021. First Genome-Scale Metabolic Model of
1529 Dolosigranulum pigrum Confirms Multiple Auxotrophies. Metabolites 11.
1530 102. Adolf LA, Heilbronner S. 2022. Nutritional Interactions between Bacterial Species
1531 Colonising the Human Nasal Cavity: Current Knowledge and Future Prospects.
1532 Metabolites 12.
1533 103. Jang J, Forbes VE, Sadowsky MJ. 2022. Probable role of *Cutibacterium acnes* in
1534 the gut of the polychaete *Capitella teleta*. Sci Total Environ 809:151127.
1535 104. Howden BP, Giulieri SG, Wong Fok Lung T, Baines SL, Sharkey LK, Lee JYH,
1536 Hachani A, Monk IR, Stinear TP. 2023. *Staphylococcus aureus* host interactions
1537 and adaptation. Nat Rev Microbiol doi:10.1038/s41579-023-00852-y:1-16.

1538 105. Blasche S, Kim Y, Patil KR. 2017. Draft Genome Sequence of *Corynebacterium*
1539 *kefirresidentii* SB, Isolated from Kefir. Genome Announc 5.
1540 106. Chen T, Yu WH, Izard J, Baranova OV, Lakshmanan A, Dewhirst FE. 2010. The
1541 Human Oral Microbiome Database: a web accessible resource for investigating
1542 oral microbe taxonomic and genomic information. Database (Oxford)
1543 2010:baq013.
1544 107. Saheb Kashaf S, Proctor DM, Deming C, Saary P, Holzer M, Program NCS, Taylor
1545 ME, Kong HH, Segre JA, Almeida A, Finn RD. 2022. Integrating cultivation and
1546 metagenomics for a multi-kingdom view of skin microbiome diversity and functions.
1547 Nat Microbiol 7:169-179.
1548 108. Nurk S, Bankevich A, Antipov D, Gurevich AA, Korobeynikov A, Lapidus A,
1549 Prjibelski AD, Pyshkin A, Sirotkin A, Sirotkin Y, Stepanauskas R, Clingenpeel SR,
1550 Woyke T, McLean JS, Lasken R, Tesler G, Alekseyev MA, Pevzner PA. 2013.
1551 Assembling single-cell genomes and mini-metagenomes from chimeric MDA
1552 products. J Comput Biol 20:714-37.
1553 109. Walker BJ, Abeel T, Shea T, Priest M, Abouelliel A, Sakthikumar S, Cuomo CA,
1554 Zeng Q, Wortman J, Young SK, Earl AM. 2014. Pilon: an integrated tool for
1555 comprehensive microbial variant detection and genome assembly improvement.
1556 PLoS One 9:e112963.
1557 110. Bolger AM, Lohse M, Usadel B. 2014. Trimmomatic: a flexible trimmer for Illumina
1558 sequence data. Bioinformatics 30:2114-20.
1559 111. Bankevich A, Nurk S, Antipov D, Gurevich AA, Dvorkin M, Kulikov AS, Lesin VM,
1560 Nikolenko SI, Pham S, Prjibelski AD, Pyshkin AV, Sirotkin AV, Vyahhi N, Tesler G,
1561 Alekseyev MA, Pevzner PA. 2012. SPAdes: A New Genome Assembly Algorithm
1562 and Its Applications to Single-Cell Sequencing. Journal of Computational Biology
1563 19:455-477.
1564 112. Parks DH, Imelfort M, Skennerton CT, Hugenholtz P, Tyson GW. 2015. CheckM:
1565 assessing the quality of microbial genomes recovered from isolates, single cells,
1566 and metagenomes. Genome Res 25:1043-55.
1567 113. Human Microbiome Jumpstart Reference Strains C, Nelson KE, Weinstock GM,
1568 Highlander SK, Worley KC, Creasy HH, Wortman JR, Rusch DB, Mitreva M,
1569 Sodergren E, Chinwalla AT, Feldgarden M, Gevers D, Haas BJ, Madupu R, Ward
1570 DV, Birren BW, Gibbs RA, Methe B, Petrosino JF, Strausberg RL, Sutton GG,
1571 White OR, Wilson RK, Durkin S, Giglio MG, Gujja S, Howarth C, Kodira CD,
1572 Kyrpides N, Mehta T, Muzny DM, Pearson M, Pepin K, Pati A, Qin X, Yandava C,
1573 Zeng Q, Zhang L, Berlin AM, Chen L, Hepburn TA, Johnson J, McCorrison J, Miller
1574 J, Minx P, Nusbaum C, Russ C, Sykes SM, Tomlinson CM, et al. 2010. A catalog
1575 of reference genomes from the human microbiome. Science 328:994-9.
1576 114. Perrin A, Rocha EPC. 2021. PanACoTA: a modular tool for massive microbial
1577 comparative genomics. NAR Genom Bioinform 3:lqaa106.
1578 115. Seemann T. 2014. Prokka: rapid prokaryotic genome annotation. Bioinformatics
1579 30:2068-9.
1580 116. Hyatt D, Chen G-L, Locascio PF, Land ML, Larimer FW, Hauser LJ. 2010.
1581 Prodigal: prokaryotic gene recognition and translation initiation site identification.
1582 BMC Bioinformatics 11:119.

1583 117. Contreras-Moreira B, Vinuesa P. 2013. GET_HOMOLOGUES, a versatile
1584 software package for scalable and robust microbial pangenome analysis. Appl
1585 Environ Microbiol 79:7696-701.
1586 118. Vinuesa P, Contreras-Moreira B. 2015. Robust identification of orthologues and
1587 paralogues for microbial pan-genomics using GET_HOMOLOGUES: a case study
1588 of pIncA/C plasmids. Methods Mol Biol 1231:203-32.
1589 119. Kristensen DM, Kannan L, Coleman MK, Wolf YI, Sorokin A, Koonin EV,
1590 Mushegian A. 2010. A low-polynomial algorithm for assembling clusters of
1591 orthologous groups from intergenomic symmetric best matches. Bioinformatics
1592 26:1481-1487.
1593 120. Li L. 2003. OrthoMCL: Identification of Ortholog Groups for Eukaryotic Genomes.
1594 Genome Research 13:2178-2189.
1595 121. Altschul S. 1997. Gapped BLAST and PSI-BLAST: a new generation of protein
1596 database search programs. Nucleic Acids Research 25:3389-3402.
1597 122. Vinuesa P, Ochoa-Sanchez LE, Contreras-Moreira B. 2018.
1598 GET_PHYLOMARKERS, a Software Package to Select Optimal Orthologous
1599 Clusters for Phylogenomics and Inferring Pan-Genome Phylogenies, Used for a
1600 Critical Geno-Taxonomic Revision of the Genus Stenotrophomonas. Front
1601 Microbiol 9:771.
1602 123. Minh BQ, Schmidt HA, Chernomor O, Schrempf D, Woodhams MD, von Haeseler
1603 A, Lanfear R. 2020. IQ-TREE 2: New Models and Efficient Methods for
1604 Phylogenetic Inference in the Genomic Era. Mol Biol Evol 37:1530-1534.
1605 124. Chernomor O, von Haeseler A, Minh BQ. 2016. Terrace Aware Data Structure for
1606 Phylogenomic Inference from Supermatrices. Syst Biol 65:997-1008.
1607 125. Hoang DT, Chernomor O, von Haeseler A, Minh BQ, Vinh LS. 2018. UFBoot2:
1608 Improving the Ultrafast Bootstrap Approximation. Mol Biol Evol 35:518-522.
1609 126. Kalyaanamoorthy S, Minh BQ, Wong TKF, Von Haeseler A, Jermiin LS. 2017.
1610 ModelFinder: fast model selection for accurate phylogenetic estimates. Nature
1611 Methods 14:587-589.
1612 127. Letunic I, Bork P. 2021. Interactive Tree Of Life (iTOL) v5: an online tool for
1613 phylogenetic tree display and annotation. Nucleic Acids Res 49:W293-W296.
1614 128. Delmont TO, Eren AM. 2018. Linking pangenomes and metagenomes: the
1615 *Prochlorococcus* metapangenome. PeerJ 6:e4320.
1616 129. Buchfink B, Xie C, Huson DH. 2015. Fast and sensitive protein alignment using
1617 DIAMOND. Nat Methods 12:59-60.
1618 130. Tatusov RL, Natale DA, Garkavtsev IV, Tatusova TA, Shankavaram UT, Rao BS,
1619 Kiryutin B, Galperin MY, Fedorova ND, Koonin EV. 2001. The COG database: new
1620 developments in phylogenetic classification of proteins from complete genomes.
1621 Nucleic Acids Res 29:22-8.
1622 131. Galperin MY, Wolf YI, Makarova KS, Vera Alvarez R, Landsman D, Koonin EV.
1623 2021. COG database update: focus on microbial diversity, model organisms, and
1624 widespread pathogens. Nucleic Acids Res 49:D274-D281.
1625 132. Kanehisa M, Goto S. 2000. KEGG: kyoto encyclopedia of genes and genomes.
1626 Nucleic Acids Res 28:27-30.

133. Kanehisa M, Furumichi M, Sato Y, Kawashima M, Ishiguro-Watanabe M. 2023. KEGG for taxonomy-based analysis of pathways and genomes. Nucleic Acids Res 51:D587-D592.
134. Bateman A, Birney E, Durbin R, Eddy SR, Howe KL, Sonnhammer EL. 2000. The Pfam protein families database. Nucleic Acids Res 28:263-6.
135. Eddy SR. 2011. Accelerated Profile HMM Searches. PLoS Comput Biol 7:e1002195.
136. Altschul SF, Gish W, Miller W, Myers EW, Lipman DJ. 1990. Basic local alignment search tool. J Mol Biol 215:403-10.
137. Edgar RC. 2004. MUSCLE: multiple sequence alignment with high accuracy and high throughput. Nucleic Acids Res 32:1792-7.
138. Benedict MN, Henriksen JR, Metcalf WW, Whitaker RJ, Price ND. 2014. ITEP: an integrated toolkit for exploration of microbial pan-genomes. BMC Genomics 15:8.
139. van Dongen S, Abreu-Goodger C. 2012. Using MCL to Extract Clusters from Networks. *In* van Helden J, Toussaint A, Thieffry D (ed), Bacterial Molecular Networks Methods in Molecular Biology (Methods and Protocols), vol 804. Springer, New York, NY.
140. Veseli I, Chen YT, Schechter MS, Vanni C, Fogarty EC, Watson AR, Jabri B, Blekhman R, Willis AD, Yu MK, Fernandez-Guerra A, Fussel J, Eren AM. 2023. Microbes with higher metabolic independence are enriched in human gut microbiomes under stress. bioRxiv doi:10.1101/2023.05.10.540289.
141. Shaiber A, Willis AD, Delmont TO, Roux S, Chen LX, Schmid AC, Yousef M, Watson AR, Lolans K, Esen OC, Lee STM, Downey N, Morrison HG, Dewhirst FE, Mark Welch JL, Eren AM. 2020. Functional and genetic markers of niche partitioning among enigmatic members of the human oral microbiome. Genome Biol 21:292.
142. Bates D, Mächler M, Bolker B, Walker S. 2015. Fitting Linear Mixed-Effects Models Using lme4. Journal of Statistical Software 67:1 - 48.
143. Quinlan AR, Hall IM. 2010. BEDTools: a flexible suite of utilities for comparing genomic features. Bioinformatics 26:841-2.
144. Quinlan AR. 2014. BEDTools: The Swiss-Army Tool for Genome Feature Analysis. Curr Protoc Bioinformatics 47:11 12 1-34.
145. Katoh K, Misawa K, Kuma K, Miyata T. 2002. MAFFT: a novel method for rapid multiple sequence alignment based on fast Fourier transform. Nucleic Acids Res 30:3059-66.
146. Katoh K, Standley DM. 2013. MAFFT Multiple Sequence Alignment Software Version 7: Improvements in Performance and Usability. Molecular Biology and Evolution 30:772-780.
147. Larsson A. 2014. AliView: a fast and lightweight alignment viewer and editor for large datasets. Bioinformatics 30:3276-8.
148. Koch DJ, Ruckert C, Rey DA, Mix A, Puhler A, Kalinowski J. 2005. Role of the ssu and seu genes of Corynebacterium glutamicum ATCC 13032 in utilization of sulfonates and sulfonate esters as sulfur sources. Appl Environ Microbiol 71:6104-14.
149. Rehm N, Georgi T, Hiery E, Degner U, Schmiedl A, Burkovski A, Bott M. 2010. L-Glutamine as a nitrogen source for Corynebacterium glutamicum: derepression of

1673 the AmtR regulon and implications for nitrogen sensing. Microbiology (Reading)
1674 156:3180-3193.
1675 150. Buerger J, Rehm N, Grebenstein L, Burkovski A. 2016. Glutamine metabolism of
1676 Corynebacterium glutamicum: role of the glutaminase GlsK. FEMS Microbiol Lett
1677 363.
1678 151. Wang Q, Jiang A, Tang J, Gao H, Zhang X, Yang T, Xu Z, Xu M, Rao Z. 2021.
1679 Enhanced production of L-arginine by improving carbamoyl phosphate supply in
1680 metabolically engineered Corynebacterium crenatum. Appl Microbiol Biotechnol
1681 105:3265-3276.
1682

Main and Supplemental Figures (in order of appearance in text)

A

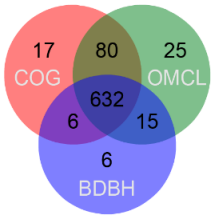

B Midpoint Rooted ML Phylogenomic Tree of 107 *Corynebacterium* Strain Genomes

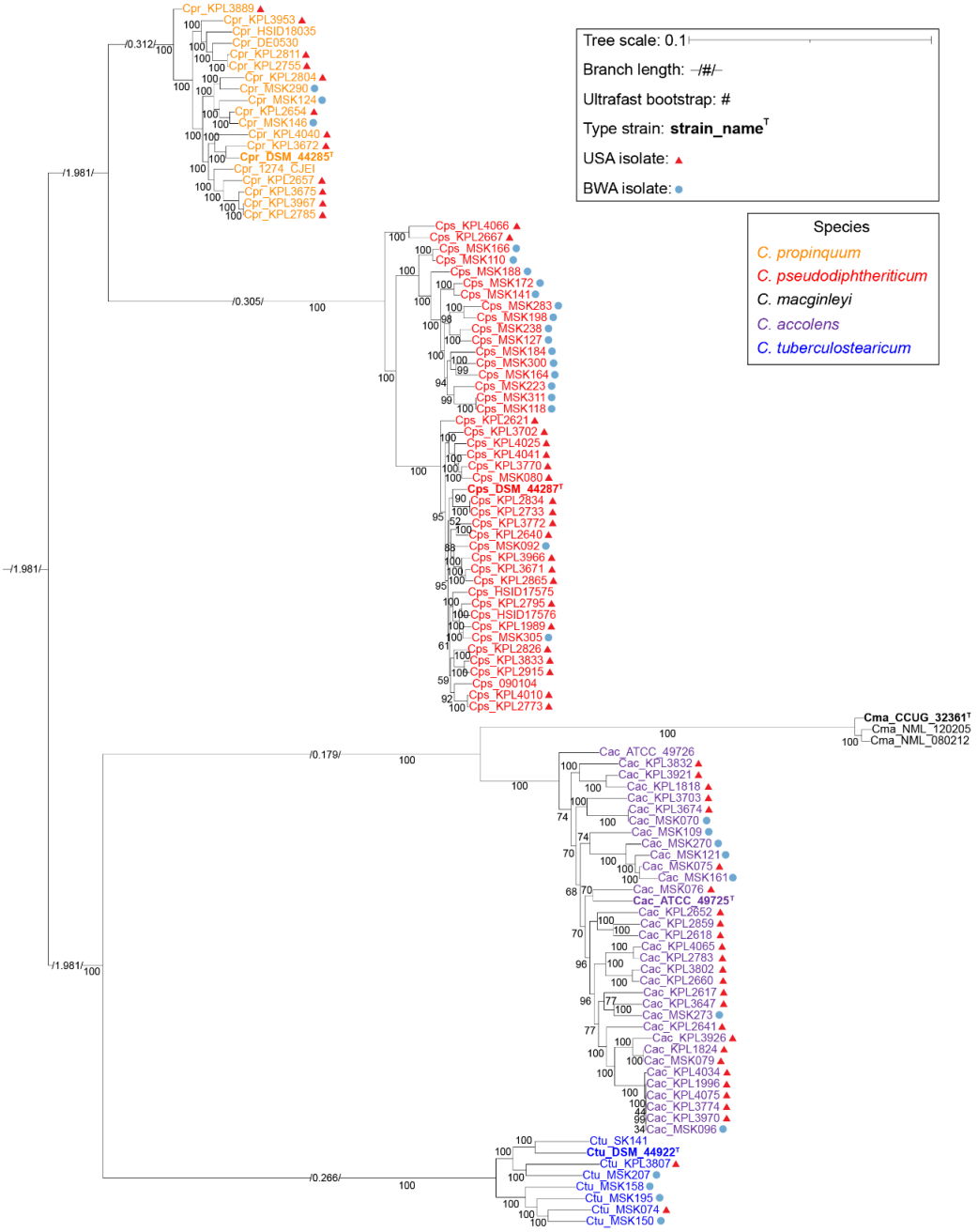

C Midpoint Rooted ML Phylogenomic Tree of 71 *Corynebacterium* Strain Genomes

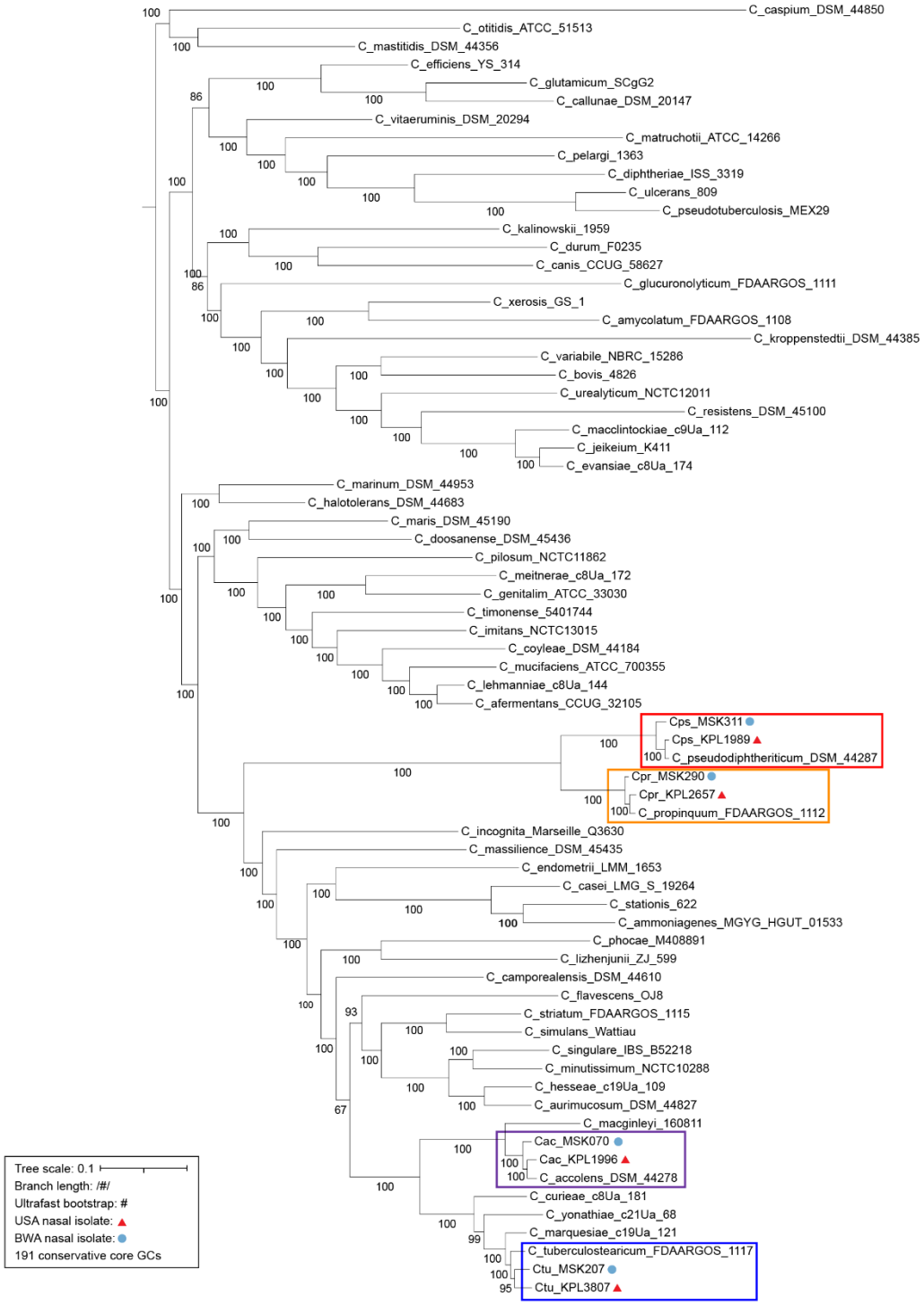

Figure S1. Phylogenomic trees, generated from the shared conservative core gene clusters, illustrate the evolutionary relationships among four human-nasal-associated *Corynebacterium* species and their relationship to other species within this genus. (**A**) Venn diagram showing 632 single-copy GCs are shared between 107 *Corynebacterium* strain genomes based on the consensus of BDBH, COG triangle, and OMCL algorithms using GET_HOMOLOGUES v24082022. (**B**) A maximum-likelihood phylogenomic tree constructed from 632 concatenated shared single-copy GCs from 107 *Corynebacterium* strain genomes. Species are indicated by name and color-code (see key) with type strains highlighted in bold. We used IQ-Tree v2.1.3 with model finder (BIC value 11679476.6345), edge-linked-proportional partition model, and 1,000 ultrafast rapid bootstraps (values on tree). Branch lengths are indicated (see key). The phylogeny contains 31 and 56 nasal-isolated strain genomes from Botswana (blue circles) and the USA (red triangles). Many branches are highly supported with ultrafast bootstrap values ≥ 95. (**C**) A maximum-likelihood phylogenomic tree of 63 *Corynebacterium* species illustrates the relationship of the four nasal species to other members of the genus. *C. propinquum*, *C. pseudodiphtheriticum*, *C. accolens*, and *C. tuberculostearicum* are each highlighted by a colored box. This is based on 191 shared conservative core GCs from 71 *Corynebacterium* strain genomes. Representative nasal strain genomes from Botswana (blue circle) and the USA (red triangle) are shown for each of the four species.

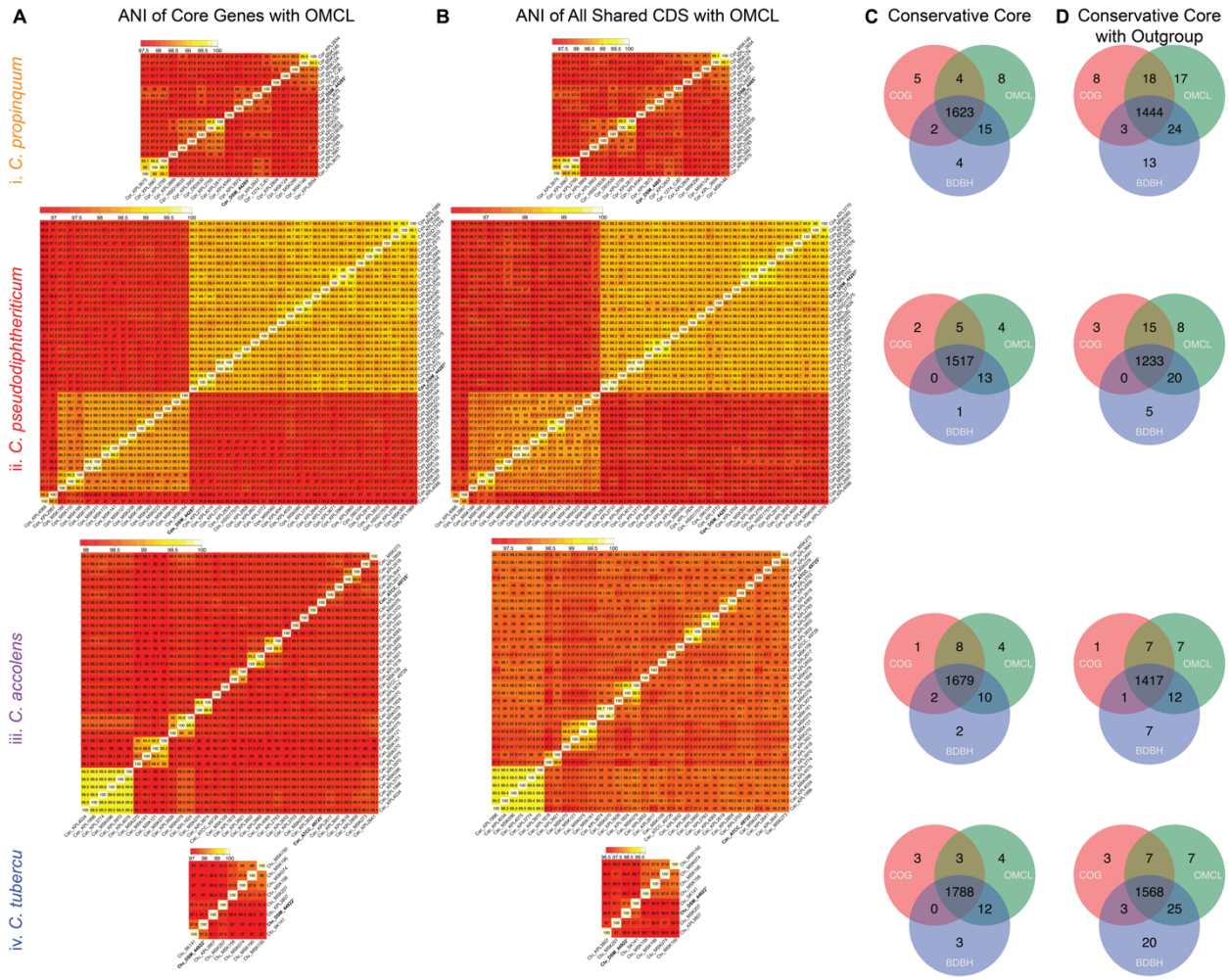

Figure S2. Species-level pairwise average nucleotide identities and conservative core GCs. (A) The shared core genes among all paired strain genomes within each species (**i-iv**) have ≥ 95% ANI (average nucleotide identity) to the type strain using the OMCL algorithm. (**B**) The ANI pairwise comparisons for all shared CDS regions are slightly less than core ANI values but still ≥ 95% among strain genomes within each species. The order of strains in A and B differ due to changes in pairwise identities because more SNPs were included in B. (**C**) The shared conservative core single-copy GCs determined by the consensus of BDBH, COG triangle, and OMCL for each of the

Corynebacterium species. (**D**) The conservative core CGs for each species plus the type strain of its closest relative in the five-species phylogenomic tree (**Fig. S1B**). Between 112 and 240 GCs were absent from the conservative core of the outgroup for each species, with the fewest absent in the outgroup for *C. pseudodiphtheriticum* and the most absent in the outgroup for *C. tuberculostearicum*.

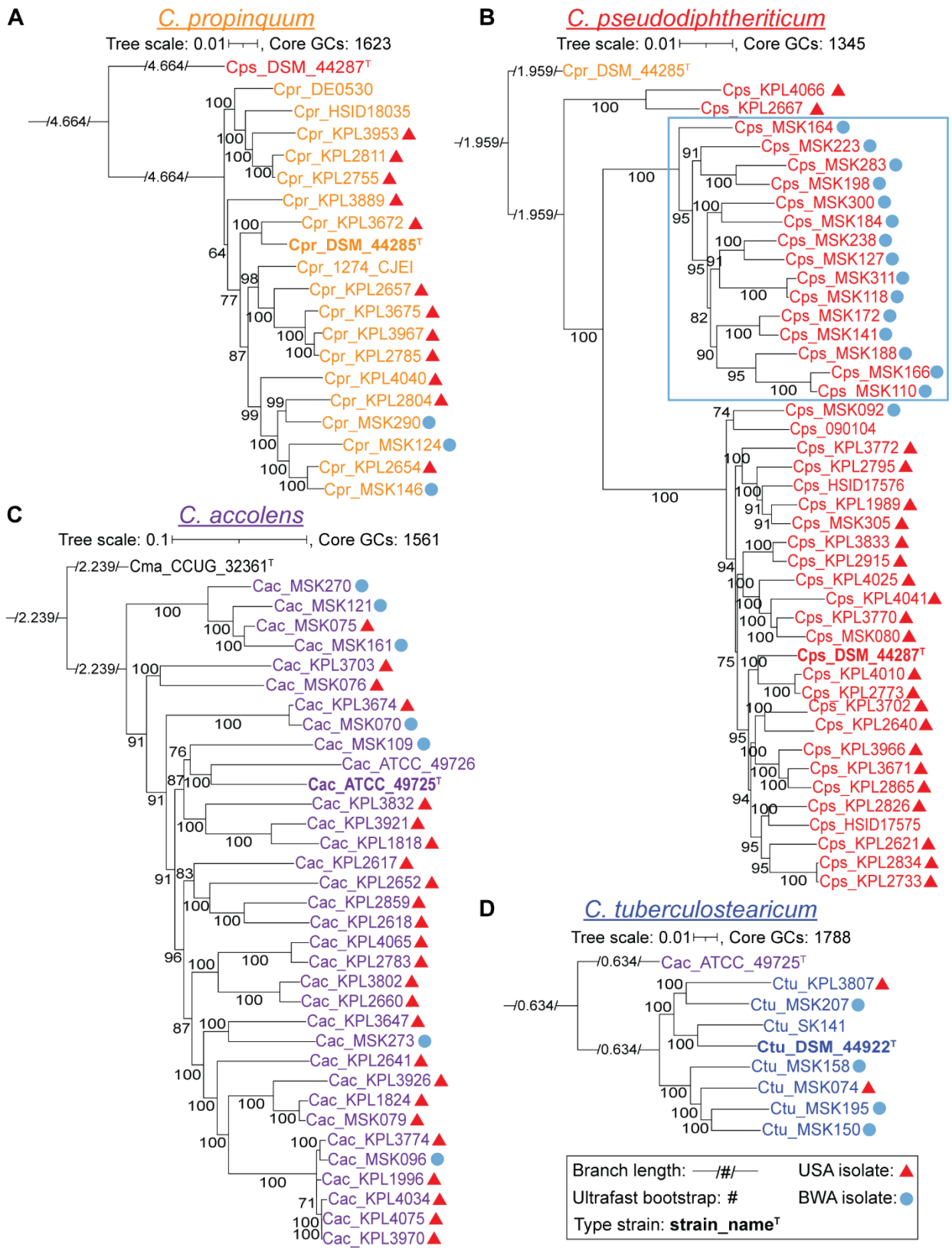
A
C. propinquum
Tree scale: 0.01, Core GCs: 1623
Cps_DSM_44287T
Cpr_DE0530
Cpr_HSID18035
Cpr_KPL3953
Cpr_KPL2811
Cpr_KPL2755
Cpr_KPL3889
Cpr_KPL3672
Cpr_DSM_44285T
Cpr_1274_CJEI
Cpr_KPL2657
Cpr_KPL3675
Cpr_KPL3967
Cpr_KPL2785
Cpr_KPL4040
Cpr_KPL2804
Cpr_MSK290
Cpr_MSK124
Cpr_KPL2654
Cpr_MSK146
B
C. pseudodiphtheriticum
Tree scale: 0.01, Core GCs: 1345
Cpr_DSM_44285T
Cps_KPL4066
Cps_KPL2667
Cps_MSK164
Cps_MSK223
Cps_MSK283
Cps_MSK198
Cps_MSK300
Cps_MSK184
Cps_MSK238
Cps_MSK127
Cps_MSK311
Cps_MSK118
Cps_MSK172
Cps_MSK141
Cps_MSK188
Cps_MSK166
Cps_MSK110
Cps_MSK092
Cps_090104
Cps_KPL3772
Cps_KPL2795
Cps_HSID17576
Cps_KPL1989
Cps_MSK305
Cps_KPL3833
Cps_KPL2915
Cps_KPL4025
Cps_KPL4041
Cps_KPL3770
Cps_MSK080
Cps_DSM_44287T
Cps_KPL4010
Cps_KPL2773
Cps_KPL3702
Cps_KPL2640
Cps_KPL3966
Cps_KPL3671
Cps_KPL2865
Cps_KPL2826
Cps_HSID17575
Cps_KPL2621
Cps_KPL2834
Cps_KPL2733
C
C. accolens
Tree scale: 0.1, Core GCs: 1561
Cma_CCUG_32361T
Cac_MSK270
Cac_MSK121
Cac_MSK075
Cac_MSK161
Cac_KPL3703
Cac_MSK076
Cac_KPL3674
Cac_MSK070
Cac_MSK109
Cac_ATCC_49726
Cac_ATCC_49725T
Cac_KPL3832
Cac_KPL3921
Cac_KPL1818
Cac_KPL2617
Cac_KPL2652
Cac_KPL2859
Cac_KPL2618
Cac_KPL4065
Cac_KPL2783
Cac_KPL3802
Cac_KPL2660
Cac_KPL3647
Cac_MSK273
Cac_KPL2641
Cac_KPL3926
Cac_KPL1824
Cac_MSK079
Cac_KPL3774
Cac_MSK096
Cac_KPL1996
Cac_KPL4034
Cac_KPL4075
Cac_KPL3970
D
C. tuberculostearicum
Tree scale: 0.01, Core GCs: 1788
Cac_ATCC_49725T
Ctu_KPL3807
Ctu_MSK207
Ctu_SK141
Ctu_DSM_44922T
Ctu_MSK158
Ctu_MSK074
Ctu_MSK195
Ctu_MSK150
Branch length: /#/
Ultrafast bootstrap: #
Type strain: strain_nameT
USA isolate:
BWA isolate:

Figure 1. Species-specific phylogenomic trees show a geographic pattern of clades for *C. pseudodiphtheriticum*. Each panel shows a core-genome-based maximum-likelihood species-specific phylogeny. The majority (86%) of the MSK-named strains are from Botswana (blue circles), whereas all KPL-named strains are from the USA (red triangles). (**A**) Phylogeny of 19 *C. propinquum* strains based on 1,623 core GCs shows two major clades (BIC value 9762417.2123). (**B**) Phylogeny of 43 *C. pseudodiphtheriticum* strains based on 1,345 core GCs shows three major clades, one of which is entirely composed of strains from Botswana (15/15, outlined in light blue), whereas the other two have a majority of the USA nasal strains (red triangles), with 2/2 and 20/22, respectively (BIC value 10177769.6675). The branching pattern separating the Botswana and USA clades was well-supported with ultrafast bootstrap values ≥ 95% (61). (**C**) Phylogeny of 34 *C. accolens* strains based on 1,561 core GCs with the majority collected in the USA shows most Botswanan strains dispersed throughout (BIC value 10700765.2332). (**D**) Phylogeny of eight *C. tuberculostearicum* strains based on 1,788 core GCs with 6 nasal isolates from Botswana and the USA (BIC value 10452720.3067). For each species-specific phylogeny, the type strain from the most closely related species (**Fig. S1B**) serves as the outgroup. Each phylogeny was made from all shared conservative core GCs for a given species (**Fig. S2C**), including the subset of GCs that were absent in the corresponding outgroup (**Fig. S2D**), to provide the highest possible resolution among the strains within each species. A large majority of the branches have highly supported ultrafast bootstrap values with the lowest at 64 on an ancestral branch in the *C. propinquum* phylogeny. Type strains are indicated in bold with a superscript T. Ancestral branch lengths are indicated numerically within a visually shortened branch to

fit on the page. Phylogenies were generated with IQ-Tree v2.1.3 using model finder, edge-linked-proportional partition model, and 1,000 ultrafast rapid bootstraps.

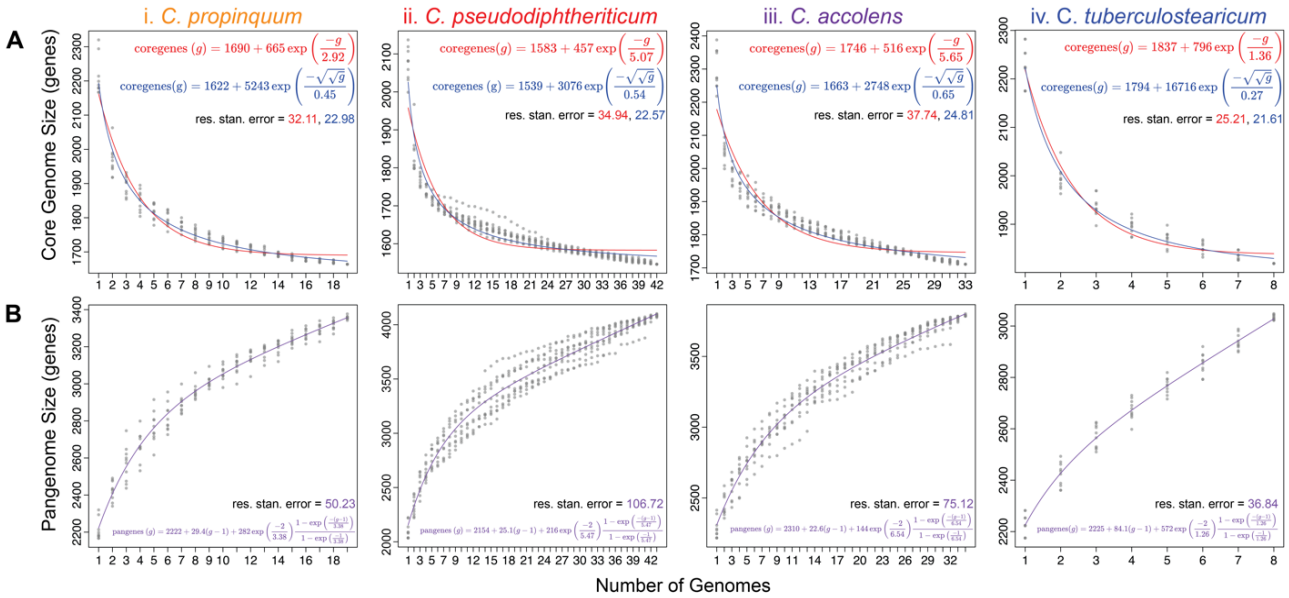

Figure 2. The four nasal *Corynebacterium* species have core genomes that have leveled off and pangenomes that remain open. (**A**) All four species have a core genome that has leveled off using a Tettelin curve fit model. (**Ai**) The *C. propinquum* core genome (n = 19) leveled off at ~12 genomes. (**Aii**) The *C. pseudodiphtheriticum* core genome (n = 42) leveled off at ~19 genomes. (**Aiii**) The *C. accolens* core genome (n = 33) leveled off at ~ 21 genomes. (**Aiv**) The *C. tuberculostearicum* core genome (n = 8) leveled off at ~7 genomes. Two best fit curve line models are shown for the core genome: Tettelin (red) and Willenbrock (blue). (**B**) The pangenomes for the four *Corynebacterium* species (i-vi) remain open as indicated by the continuous steep slope of the best fit line shown in purple. Core and pangenome size estimations were calculated from 10 random genome samplings (represented by gray dots) using the OMCL algorithm predicted GCs with GET_HOMOLOGUES v24082022.

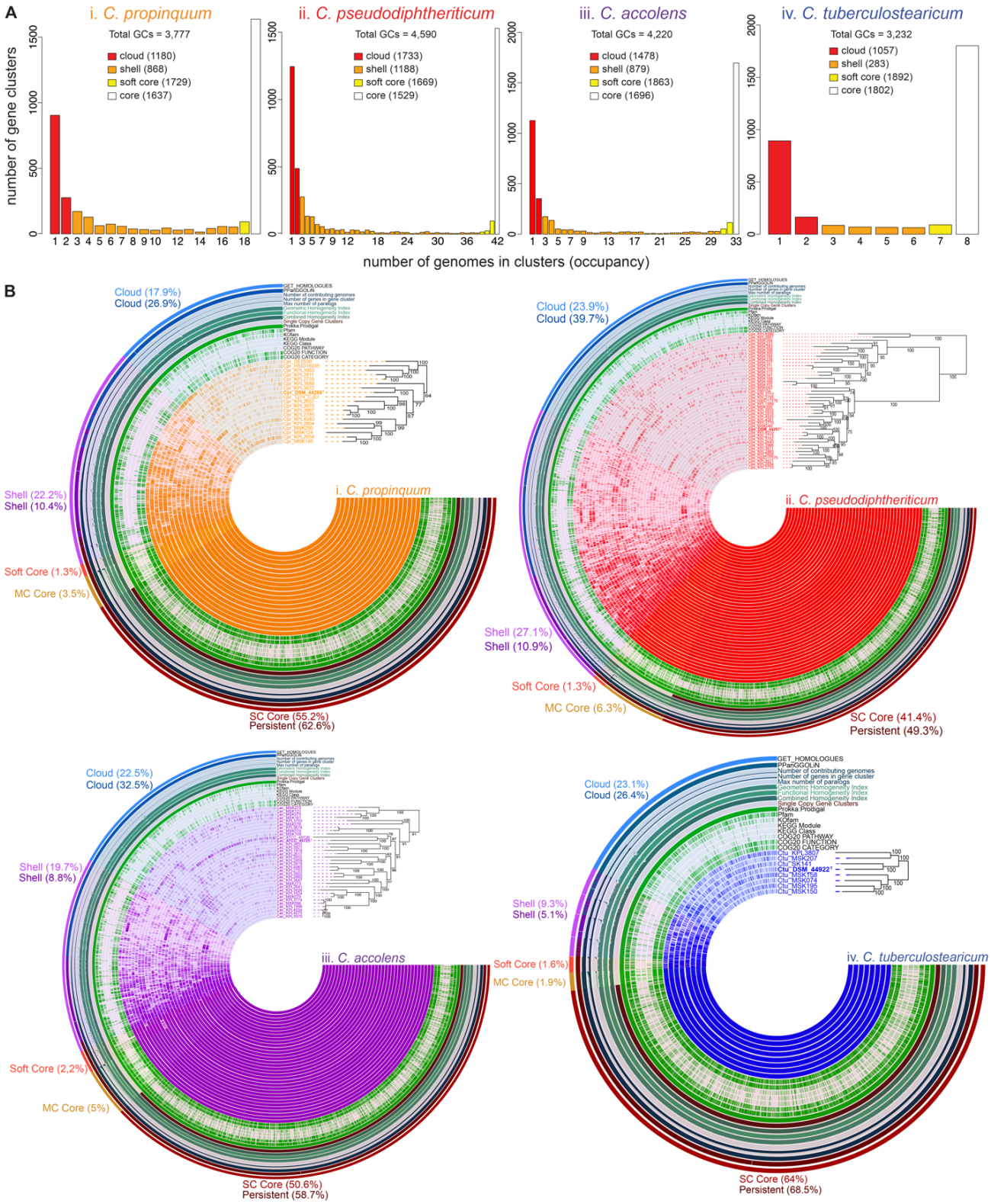
A
i. C. propinquum
Total GCs = 3,777
cloud (1180)
shell (868)
soft core (1729)
core (1637)
ii. C. pseudodiphtheriticum
Total GCs = 4,590
cloud (1733)
shell (1188)
soft core (1669)
core (1529)
iii. C. accolens
Total GCs = 4,220
cloud (1478)
shell (879)
soft core (1863)
core (1696)
iv. C. tuberculostearicum
Total GCs = 3,232
cloud (1057)
shell (283)
soft core (1892)
core (1802)
number of gene clusters
number of genomes in clusters (occupancy)
B
Cloud (17.9%)
Cloud (26.9%)
Shell (22.2%)
Shell (10.4%)
Soft Core (1.3%)
MC Core (3.5%)
SC Core (55.2%)
Persistent (62.6%)
i. C. propinquum
Cloud (23.9%)
Cloud (39.7%)
Shell (27.1%)
Shell (10.9%)
Soft Core (1.3%)
MC Core (6.3%)
SC Core (41.4%)
Persistent (49.3%)
ii. C. pseudodiphtheriticum
Cloud (22.5%)
Cloud (32.5%)
Shell (19.7%)
Shell (8.8%)
Soft Core (2,2%)
MC Core (5%)
SC Core (50.6%)
Persistent (58.7%)
iii. C. accolens
Cloud (23.1%)
Cloud (26.4%)
Shell (9.3%)
Shell (5.1%)
Soft Core (1.6%)
MC Core (1.9%)
SC Core (64%)
Persistent (68.5%)
iv. C. tuberculostearicum
GET_HOMOLOGUES
PPanGGOLIN
Number of contributing genomes
Number of genes in gene cluster
Max number of paralogs
Geometric Homogeneity Index
Functional Homogeneity Index
Combined Homogeneity Index
Single Copy Gene Clusters
Prokka Prodigal
Pfam
KOfam
KEGG Module
KEGG Class
COG20 PATHWAY
COG20 FUNCTION
COG20 CATEGORY

Figure S3. Three different analysis platforms estimated a similar pangenome for each individual *Corynebacterium* species. (**A**) Representation of the pangenome estimated by GET_HOMOLOGUES with COG triangle and OMCL of (**i**) *C. propinquum*, 19 genomes; (**ii)** *C. pseudodiphtheriticum*, 42 genomes; (**iii**) *C. accolens*, 33 genomes; and (**iv**) *C. tuberculostearicum,* 8 genomes. (**B**) Using pangenomes clustered with anvi'o, we constructed a concentric dendrogram for each species (**i-vi**) ordered to match the species-specific phylogenies in Figure 1. The GCs present in the core/persistent genome consistently accounted for over half of the pangenome in each of the nasal *Corynebacterium* species. The outermost concentric ring indicates anvi'o-defined GCs (with percentages) in the single copy core (dark red), multicopy core (beige), soft core (red), shell (light purple), and cloud (light blue) based on GET_HOMOLOGUES definition of each partition with anvi'o allowing further division of the core into single copy and multicopy core. The next to outermost ring indicates anvi'o-defined GCs (with percentages) assigned by PPanGGOLiN to persistent (dark maroon), shell (purple), and cloud (blue). The average core+soft core or persistent, shell, and cloud sizes across the four species using GET_HOMOLOGUES definitions were 58.58%, 19.58%, and 21.85%, respectively, compared to 56.63%, 10.13%, and 31.38% as assigned by PPanGGOLiN. The differences between the two algorithms were 1.95% for core, 9.45% for shell, and 9.53% for cloud. GET_HOMOLOGUES defines the pangenome compartments as GCs shared across a certain number of genomes, whereas PPanGGOLiN uses both presence and analysis for genomic neighborhoods to infer GCs in the persistent genome, which likely explains these differences.

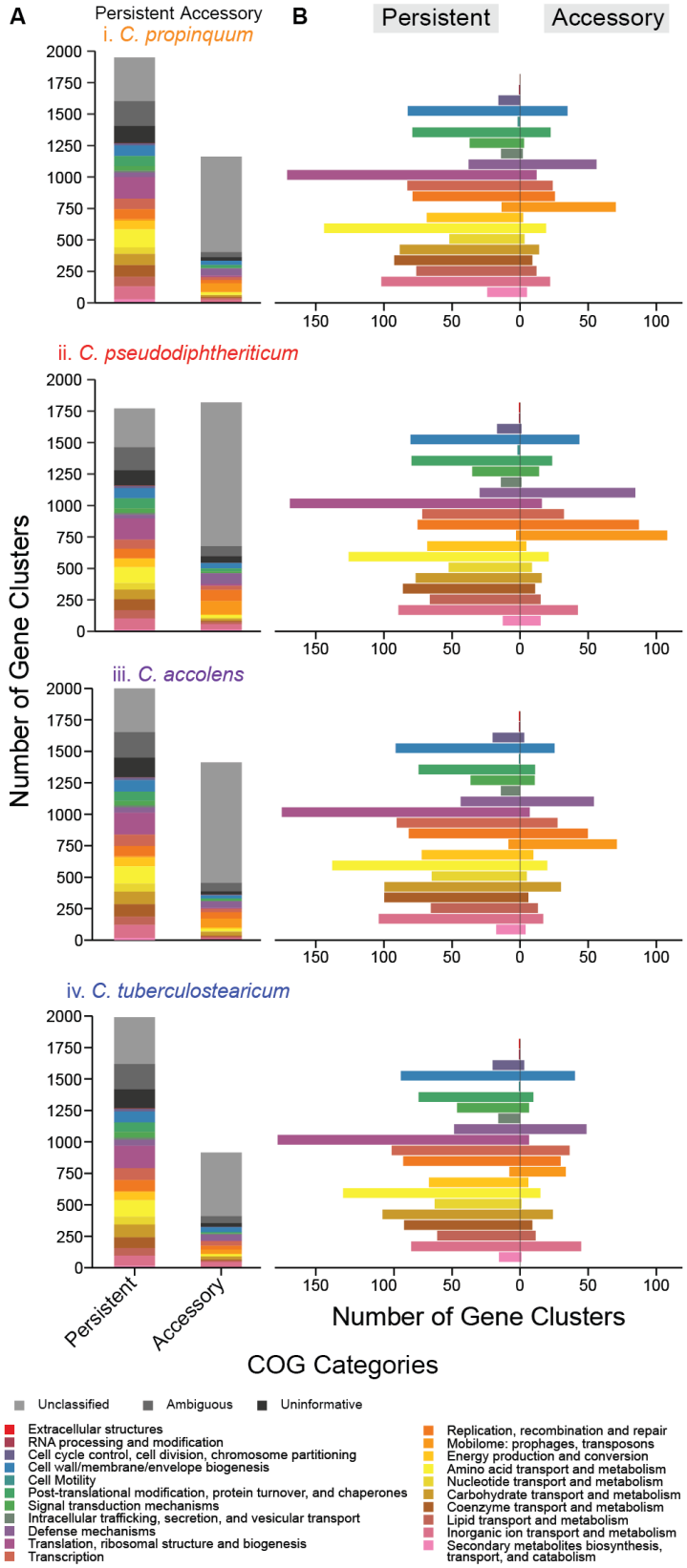
A
Persistent Accessory
i. C. propinquum
ii. C. pseudodiphtheriticum
iii. C. accolens
iv. C. tuberculostearicum
Number of Gene Clusters
Persistent
Accessory
COG Categories
B
Persistent
Accessory
Number of Gene Clusters
Unclassified
Ambiguous
Uninformative
Extracellular structures
RNA processing and modification
Cell cycle control, cell division, chromosome partitioning
Cell wall/membrane/envelope biogenesis
Cell Motility
Post-translational modification, protein turnover, and chaperones
Signal transduction mechanisms
Intracellular trafficking, secretion, and vesicular transport
Defense mechanisms
Translation, ribosomal structure and biogenesis
Transcription
Replication, recombination and repair
Mobilome: prophages, transposons
Energy production and conversion
Amino acid transport and metabolism
Nucleotide transport and metabolism
Carbohydrate transport and metabolism
Coenzyme transport and metabolism
Lipid transport and metabolism
Inorganic ion transport and metabolism
Secondary metabolites biosynthesis, transport, and catabolism

Figure 3. GCs assigned to COG metabolism categories are overrepresented in the persistent compared to the accessory genomes of each species indicating limited strain-specific metabolism. We identified the COG functional annotations for GCs using anvi'o and then used PPanGGOLiN to assign GCs to the persistent vs. accessory genome. (**A**) Over one-third of the GCs in each species (**i-iv**) were assigned as uninformative (black), ambiguous (dark gray), or unclassified (gray) across both the persistent and accessory genome. The combined percentage of each of these categories out of all the genes per species was 38.1% *Cpr*, 37.9% *Cps*, 37.1% *Cac*, and 38.3% *Ctu*. For each species, the percentage of GCs with an informative COG assignment was higher in the persistent genome, 64.9% *Cpr* (1262), 65.3% *Cps* (1156), 64.7% *Cac* (1300), and 63.5% *Ctu* (1264), than in the accessory genome, with 28.9% *Cpr* (336), 29.9% *Cps* (543), 25.7% *Cac* (363), and 35.6% Ctu (326). (**B**) Functional enrichment of GCs in the persistent vs. the accessory genome for the different COG categories. Metabolic COG categories, e.g., those involved in energy production (pale orange), or in amino acid (yellow), nucleotide (gold), carbohydrate (khaki), and lipid metabolism (dark salmon), were enriched in the persistent genome of each species. In contrast, mobilome (bright orange) and to a lesser extent defense mechanisms were enriched in the accessory genomes. Each *Corynebacterium* species shared similar COG functional enrichment ratios of GCs in its persistent vs. its accessory genome.

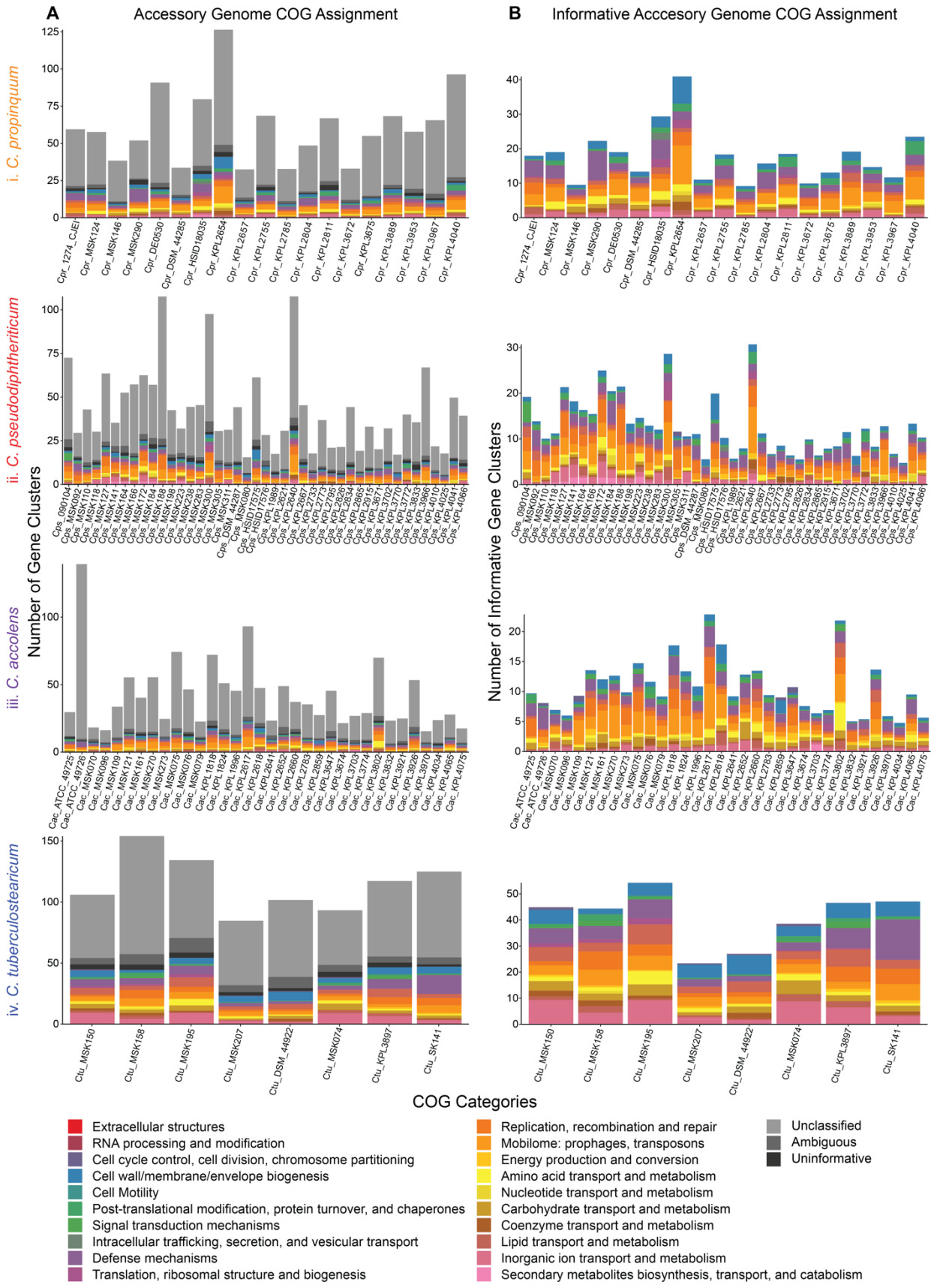
A
Accessory Genome COG Assignment
B
Informative Acccesory Genome COG Assignment
i. C. propinquum
ii. C. pseudodiphtheriticum
iii. C. accolens
iv. C. tuberculostearicum
Number of Gene Clusters
Number of Informative Gene Clusters
COG Categories
Extracellular structures
RNA processing and modification
Cell cycle control, cell division, chromosome partitioning
Cell wall/membrane/envelope biogenesis
Cell Motility
Post-translational modification, protein turnover, and chaperones
Signal transduction mechanisms
Intracellular trafficking, secretion, and vesicular transport
Defense mechanisms
Translation, ribosomal structure and biogenesis
Replication, recombination and repair
Mobilome: prophages, transposons
Energy production and conversion
Amino acid transport and metabolism
Nucleotide transport and metabolism
Carbohydrate transport and metabolism
Coenzyme transport and metabolism
Lipid transport and metabolism
Inorganic ion transport and metabolism
Secondary metabolites biosynthesis, transport, and catabolism
Unclassified
Ambiguous
Uninformative

Figure S4. The size of the accessory genome varies between strains within each nasal *Corynebacterium* species. We used anvi'o to identify COG functional annotations and PPanGGOLiN to assign GCs to the persistent vs. accessory genome. (**A**) For each species (**i-vi**), most of the GCs in each strain's accessory genome had either no annotation ("unclassified"), an ambiguous COG categorization ("ambiguous"), or belonged to an uninformative S or R COG category ("uninformative"). The calculated average percentages for unclassified, ambiguous, and uninformative categories per species were (**i**) 65.2%, 3.5%, and 2.4% for *C. propinquum*; (**ii**) 62.8%, 4.4%, and 2.9% for *C. pseudodiphtheriticum*; (**iii**) 67.6%, 4.7%, and 2.0% for *C. accolens*; and (**iv**) 55.1%, 6.2%, and 3.1% for *C. tuberculostearicum.* The accessory genome of *C. accolens* had the highest percentage of COGS belonging to these three categories and *C. tuberculostearicum* had the lowest. Averages of the informative assigned COG annotations (colored categories) in the accessory genome were calculated for each species as follows: (**i**) 28.9% for *C*. *propinquum*, (**ii**) 29.9% for *C. pseudodiphtheriticum*, (**iii**) 25.7% for *C. accolens*, and (**iv**) 35.6% for *C. tuberculostearicum*. (**B**) There was a relatively proportional distribution of accessory informative functional GCs among each set of genomes. The size of the accessory genome varied between strains from each of the four species. (**Ai**) For *C. propinquum,* KPL2654 and KPL4040 had the largest accessory sizes, whereas KPL2785 and KPL3672 had the smallest. (**Aii**) For *C. pseudodiphtheriticum,* KPL2640 and MSK188 had the largest accessory sizes, whereas MSK080 and KPL3070 had the smallest. (**Aiii**) For *C. accolens,* ATCC_49726 and KPL2617 had the largest accessory sizes, whereas MSK096 and KPL3970 had the

smallest. (**Aiv**) For *C. tuberculostearicum* MSK158 and MSK195 had the largest accessory sizes, whereas MSK207 and MSK074 had the smallest.

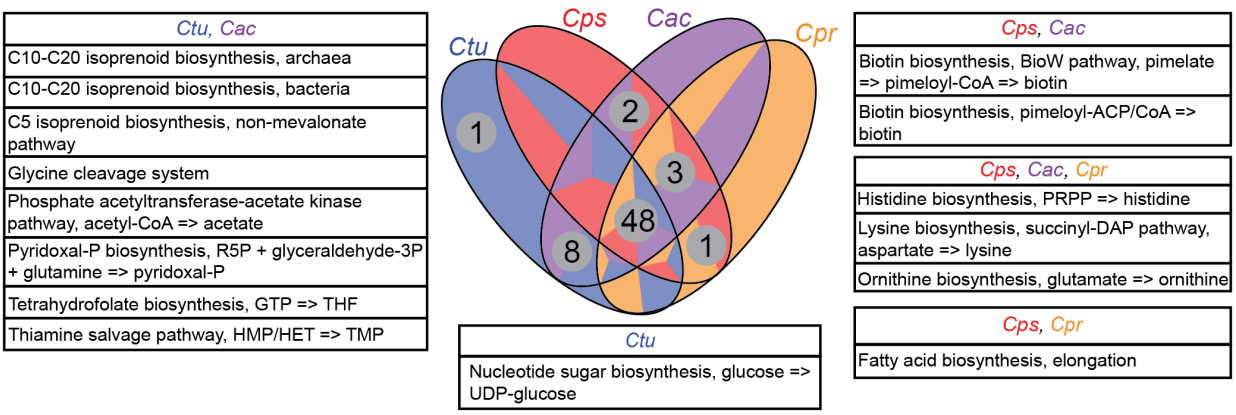

Figure 4. These four common human-nasal-associated *Corynebacterium* species have a largely shared metabolic capacity. The Venn diagram summarizes the results of an enrichment analysis of complete KEGG modules (stepwise completion score = 1) by species using anvi'o. Modules that both had an adjusted q-value > 1e-9 and were complete in at least 87% of the analyzed genomes were categorized as shared between the four *Corynebacterium*. Modules with an adjusted q-value < 1e-9 were considered enriched in their associated group of ≤ 3 species and are shown in boxes surrounding the Venn diagram. Species labels: *C. propinquum* (*Cpr*), *C. pseudodiphtheriticum (Cps), C. accolens (Cac),* and *C. tuberculostearicum (Ctu*).

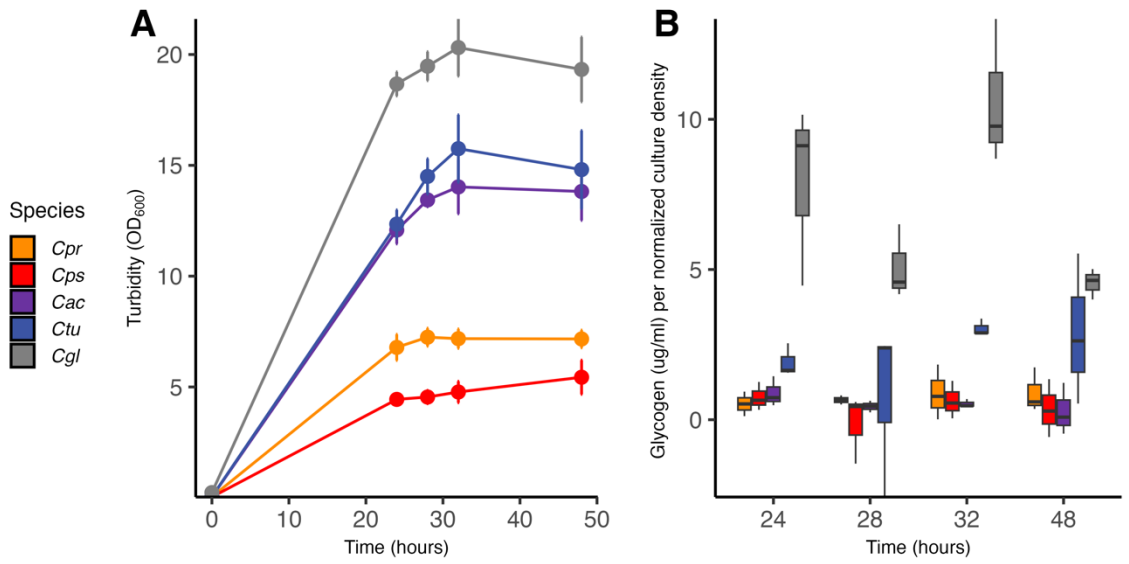

Figure 5. *C. tuberculostearicum* accumulates intracellular glycogen. (**A**) Growth curves for each of the nasal *Corynebacterium* species at 34°C in a MOPs-buffered CDM with all 20 amino acids and 5% glucose, with *C. glutamicum* as a positive control for the assay. *C. propinquum* and *C. pseudodiphtheriticum* reached stationary phase at a lower optical density at wavelength 600 nm (OD_{600}) than did *C. tuberculostearicum* and *C. accolens*, with *C. glutamicum*^{T} reaching the highest. (**B**) Overall, *C. tuberculostearicum* accumulated more intracellular glycogen than the other three nasal species (*p*-value range 0.033 to 0.009), and less than *C. glutamicum* (p = 6.64 x 10^{-10}). Intracellular glycogen content was quantified in µg/ml at timepoints between 24 and 48 hours. Statistics were done using a linear mixed model with species as a fixed effect and time point as a random effect. Boxplots show the median with first and third quartiles. Data are from n = 3 independent experiments. Species labels: *C. propinquum* (*Cpr*), *C. pseudodiphtheriticum (Cps), C. accolens (Cac), C. tuberculostearicum (Ctu*), and *C. glutamicum* (*Cgl*).

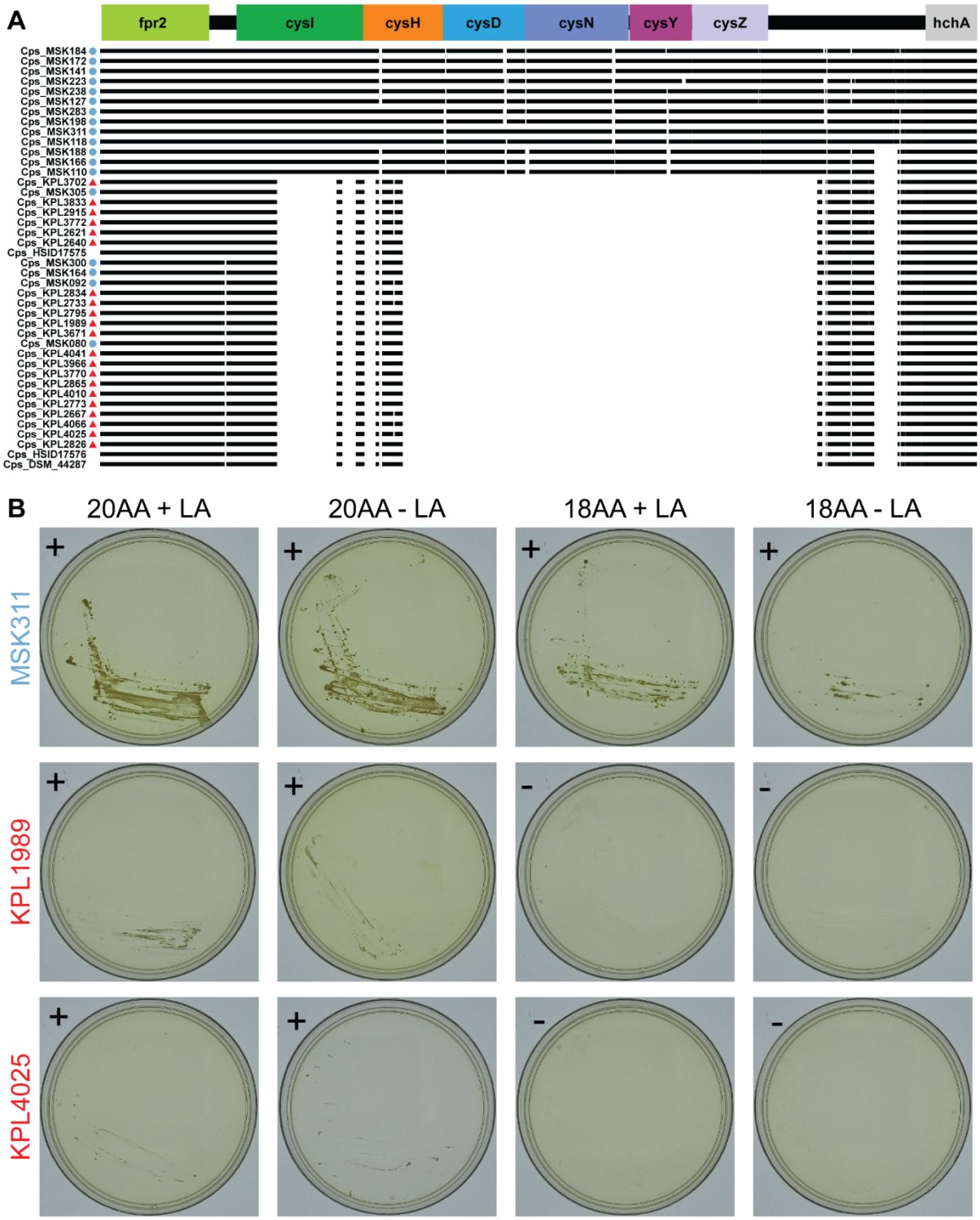
A
fpr2
cysI
cysH
cysD
cysN
cysY
cysZ
hchA
Cps_MSK184
Cps_MSK172
Cps_MSK141
Cps_MSK223
Cps_MSK238
Cps_MSK127
Cps_MSK283
Cps_MSK198
Cps_MSK311
Cps_MSK118
Cps_MSK188
Cps_MSK166
Cps_MSK110
Cps_KPL3702
Cps_MSK305
Cps_KPL3833
Cps_KPL2915
Cps_KPL3772
Cps_KPL2621
Cps_KPL2640
Cps_HSID17575
Cps_MSK300
Cps_MSK164
Cps_MSK092
Cps_KPL2834
Cps_KPL2733
Cps_KPL2795
Cps_KPL1989
Cps_KPL3671
Cps_MSK080
Cps_KPL4041
Cps_KPL3966
Cps_KPL3770
Cps_KPL2865
Cps_KPL4010
Cps_KPL2773
Cps_KPL2667
Cps_KPL4066
Cps_KPL4025
Cps_KPL2826
Cps_HSID17576
Cps_DSM_44287
B
20AA + LA
20AA - LA
18AA + LA
18AA - LA
MSK311
KPL1989
KPL4025
+
+
+
+
+
+
-
-
+
+
-
-

Figure 6. *C. pseudodiphtheriticum* strains from the Botswanan clade in Figure 1B can perform assimilatory sulfate reduction. (**A**) Most of the Botswanan *C. pseudodiphtheriticum* strains encode genes with KO annotations equivalent to those in the *C. glutamicum*^{T} *fpr2-cysIXHDNYZ* operon, which is required for assimilatory sulfate reduction. Figure represents the MAFFT multiple sequence alignment with strain genomes from Botswana (blue circles) and from USA (red triangles). (**B**) The Botswanan *C. pseudodiphtheriticum* strain MSK311, which encodes the *fpr2cysIXHDNYZ* operon, grew in chemically defined medium with sulfate as the only source of sulfur (KS-CDM 18AA - LA) indicating ability to assimilate sulfate, whereas the USA strains KPL1989 and KPL4025, which lack this operon, did not. Representative strains from the Botswanan (blue font) and USA (red font) clades in Figure 1B were grown on KS-CDM agarose with 2% glucose, supplemented with either 20 amino acids (20AA), including 2mM cysteine and 4mM methionine, or 18 amino acids (18AA), excluding cysteine and methionine; both with and without lipoic acid (LA, an additional source of sulfur). Images were captured after 8 days of growth at 34°C with 5% CO_2 and humidification. Data are from four independent experiments with images from one experiment here and three others in Figure S5A. (+) = growth, (-) = no growth.

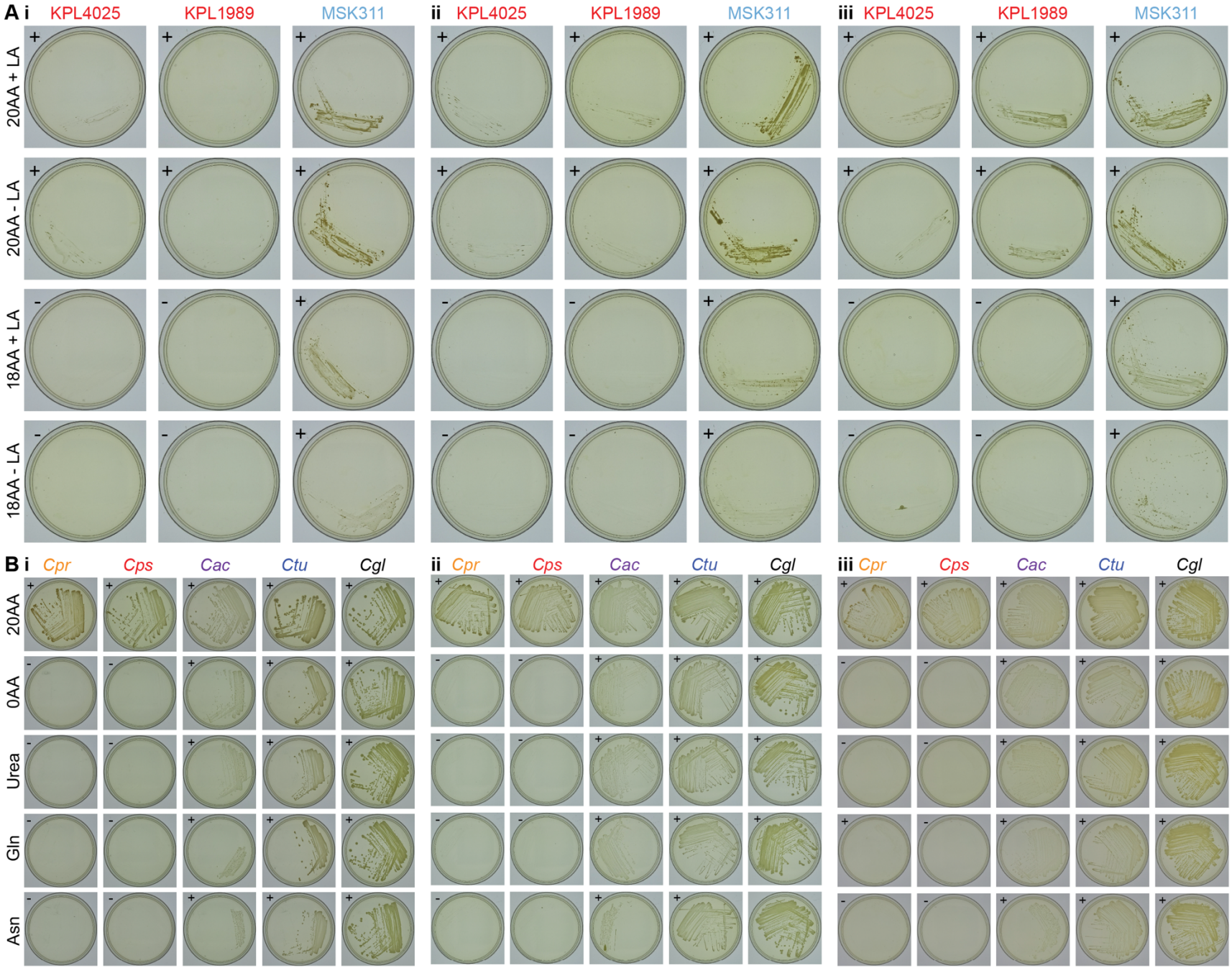
A
i
KPL4025
KPL1989
MSK311
ii
KPL4025
KPL1989
MSK311
iii
KPL4025
KPL1989
MSK311
20AA + LA
20AA - LA
18AA + LA
18AA - LA
B
i
Cpr
Cps
Cac
Ctu
Cgl
ii
Cpr
Cps
Cac
Ctu
Cgl
iii
Cpr
Cps
Cac
Ctu
Cgl
20AA
0AA
Urea
Gln
Asn

Figure S5. Results of additional growth experiments from Figures 6 (A) and 7 (B). (**A)** The Botswanan *C. pseudodiphtheriticum* strain MSK311, which encodes the *fpr2cysIXHDNYZ* operon, grew on chemically defined agarose medium with sulfate as the only source of sulfur (KS-CDM 18AA - LA), whereas the USA strains KPL1989 and KPL4025, which lack this operon, did not. (**B**) *C. accolens* (*Cac*) and *C. tuberculostearicum* (*Ctu*), as well as *C. glutamicum* (*Cgl*), grew on MOPS-buffered CDM agarose medium in the absence of all 20 amino acids, whereas *C*. *propinquum* (*Cpr*) and *C*. *pseudodiphtheriticum* (*Cps*) did not. All images captured after 8 days of growth at 34°C with 5% CO_2 with a humidification pan. (+) = growth, (-) = no growth.

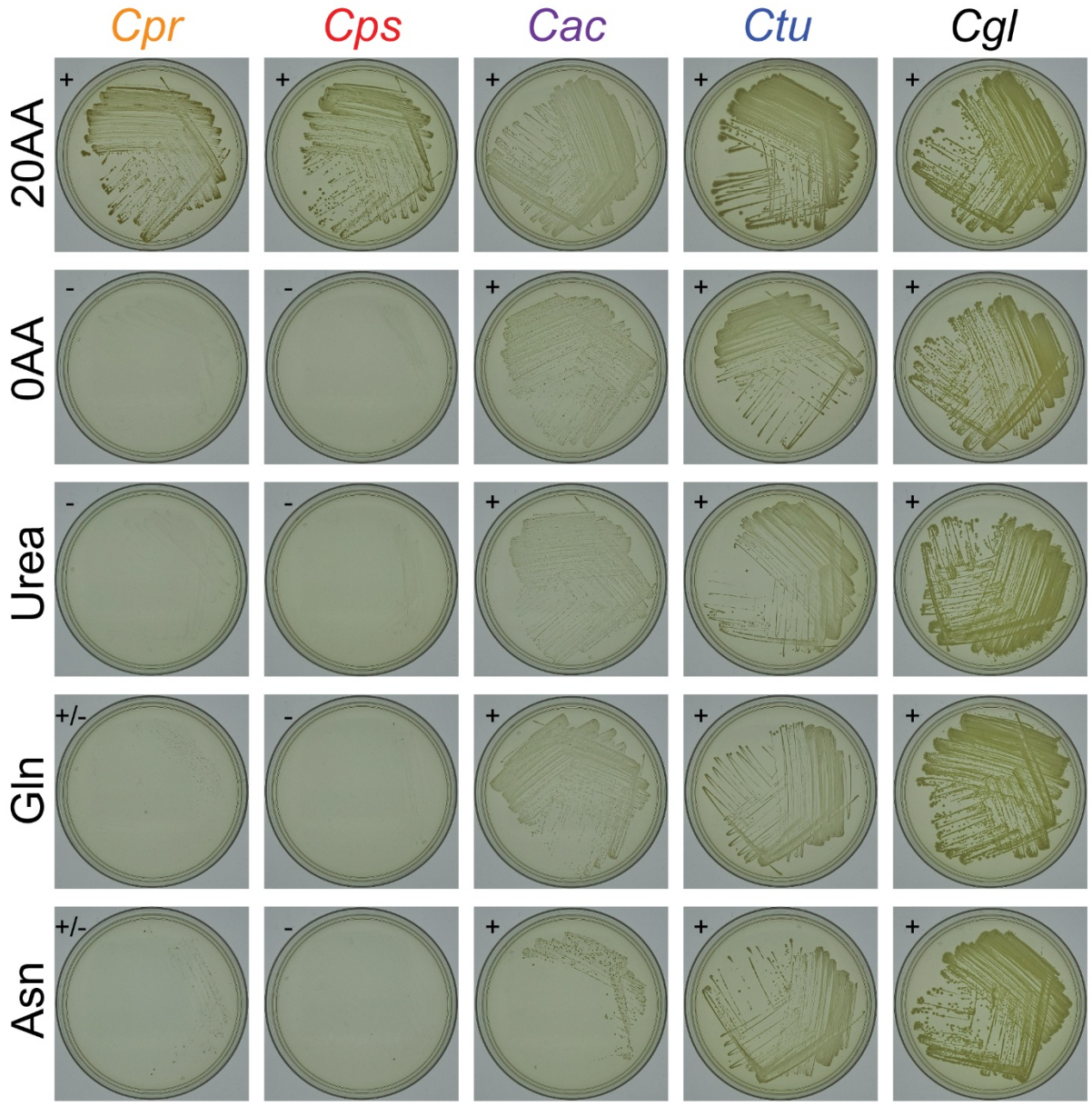

Figure 7. *C. accolens* and *C. tuberculostearicum* grow in the absence of all 20 amino acids on MOPS-buffered CDM agarose. Strains were grown on MOPS-buffered base CDM agarose with 2% glucose supplemented with 20 amino acids (20AA) vs. 0 amino acids (0 AA), and also in the absence of amino acids supplemented with either 5

mM Urea, 10 mM glutamine (Gln), or 10 mM asparagine (Asn) in *n* = 4 independent experiments. Shown are images from 1 experiment photographed after 8 days of growth at 34°C with 5% CO_2 and humidification; remaining data are in Figure S5B. (+) = growth, (-) = no growth. Species labels: *C. propinquum* (*Cpr*)*, C. pseudodiphtheriticum (Cps), C. accolens (Cac), C. tuberculostearicum (Ctu*), and *C. glutamicum* (*Cgl*).

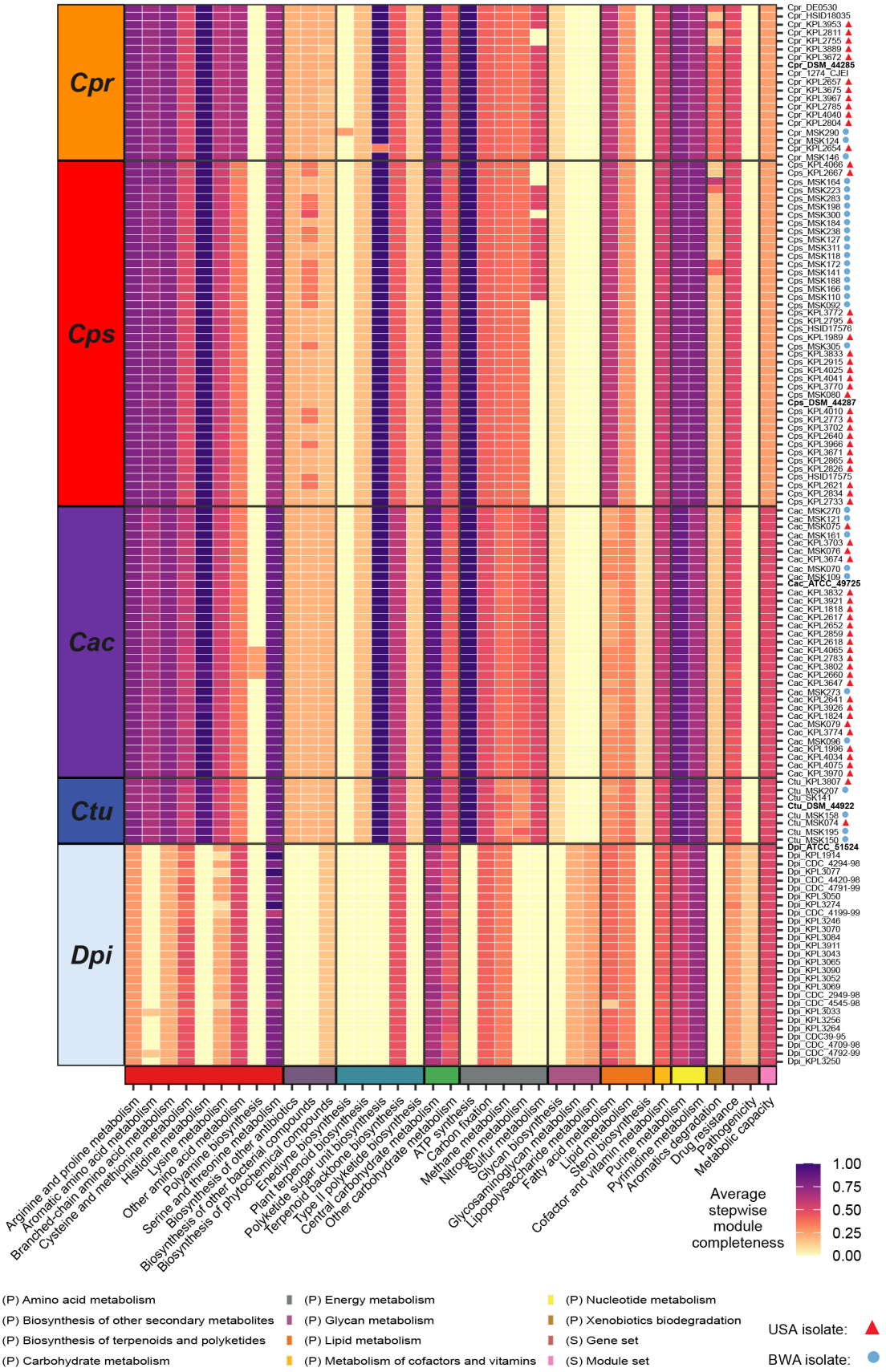
Cpr
Cps
Cac
Ctu
Dpi
Cpr_DE0530
Cpr_HSID18035
Cpr_KPL3953
Cpr_KPL2811
Cpr_KPL2755
Cpr_KPL3889
Cpr_KPL3672
Cpr_DSM_44285
Cpr_1274_CJEI
Cpr_KPL2657
Cpr_KPL3675
Cpr_KPL3967
Cpr_KPL2785
Cpr_KPL4040
Cpr_KPL2804
Cpr_MSK290
Cpr_MSK124
Cpr_KPL2654
Cpr_MSK146
Cps_KPL4066
Cps_KPL2667
Cps_MSK164
Cps_MSK223
Cps_MSK283
Cps_MSK198
Cps_MSK300
Cps_MSK184
Cps_MSK238
Cps_MSK127
Cps_MSK311
Cps_MSK118
Cps_MSK172
Cps_MSK141
Cps_MSK188
Cps_MSK166
Cps_MSK110
Cps_MSK092
Cps_KPL3772
Cps_KPL2795
Cps_HSID17576
Cps_KPL1989
Cps_MSK305
Cps_KPL3833
Cps_KPL2915
Cps_KPL4025
Cps_KPL4041
Cps_KPL3770
Cps_MSK080
Cps_DSM_44287
Cps_KPL4010
Cps_KPL2773
Cps_KPL3702
Cps_KPL2640
Cps_KPL3966
Cps_KPL3671
Cps_KPL2865
Cps_KPL2826
Cps_HSID17575
Cps_KPL2621
Cps_KPL2834
Cps_KPL2733
Cac_MSK270
Cac_MSK121
Cac_MSK075
Cac_MSK161
Cac_KPL3703
Cac_MSK076
Cac_KPL3674
Cac_MSK070
Cac_MSK109
Cac_ATCC_49725
Cac_KPL3832
Cac_KPL3921
Cac_KPL1818
Cac_KPL2617
Cac_KPL2652
Cac_KPL2859
Cac_KPL2618
Cac_KPL4065
Cac_KPL2783
Cac_KPL3802
Cac_KPL2660
Cac_KPL3647
Cac_MSK273
Cac_KPL2641
Cac_KPL3926
Cac_KPL1824
Cac_MSK079
Cac_KPL3774
Cac_MSK096
Cac_KPL1996
Cac_KPL4034
Cac_KPL4075
Cac_KPL3970
Ctu_KPL3807
Ctu_MSK207
Ctu_SK141
Ctu_DSM_44922
Ctu_MSK158
Ctu_MSK074
Ctu_MSK195
Ctu_MSK150
Dpi_ATCC_51524
Dpi_KPL1914
Dpi_CDC_4294-98
Dpi_KPL3077
Dpi_CDC_4420-98
Dpi_CDC_4791-99
Dpi_KPL3050
Dpi_KPL3274
Dpi_CDC_4199-99
Dpi_KPL3246
Dpi_KPL3070
Dpi_KPL3084
Dpi_KPL3911
Dpi_KPL3043
Dpi_KPL3065
Dpi_KPL3090
Dpi_KPL3052
Dpi_KPL3069
Dpi_CDC_2949-98
Dpi_CDC_4545-98
Dpi_KPL3033
Dpi_KPL3256
Dpi_KPL3264
Dpi_CDC39-95
Dpi_CDC_4709-98
Dpi_CDC_4792-99
Dpi_KPL3250
Arginine and proline metabolism
Aromatic amino acid metabolism
Branched-chain amino acid metabolism
Cysteine and methionine metabolism
Histidine metabolism
Lysine metabolism
Other amino acid metabolism
Polyamine biosynthesis
Serine and threonine metabolism
Biosynthesis of other antibiotics
Biosynthesis of other bacterial compounds
Biosynthesis of phytochemical compounds
Enediyne biosynthesis
Plant terpenoid biosynthesis
Polyketide sugar unit biosynthesis
Terpenoid backbone biosynthesis
Type II polyketide biosynthesis
Central carbohydrate metabolism
Other carbohydrate metabolism
ATP synthesis
Carbon fixation
Methane metabolism
Nitrogen metabolism
Sulfur metabolism
Glycan biosynthesis
Glycosaminoglycan metabolism
Lipopolysaccharide metabolism
Fatty acid metabolism
Lipid metabolism
Sterol biosynthesis
Cofactor and vitamin metabolism
Purine metabolism
Pyrimidine metabolism
Aromatics degradation
Drug resistance
Pathogenicity
Metabolic capacity
Average stepwise module completeness
1.00
0.75
0.50
0.25
0.00
(P) Amino acid metabolism
(P) Biosynthesis of other secondary metabolites
(P) Biosynthesis of terpenoids and polyketides
(P) Carbohydrate metabolism
(P) Energy metabolism
(P) Glycan metabolism
(P) Lipid metabolism
(P) Metabolism of cofactors and vitamins
(P) Nucleotide metabolism
(P) Xenobiotics biodegradation
(S) Gene set
(S) Module set
USA isolate:
BWA isolate:

Figure 8. Each of the four nasal *Corynebacterium* species encode for an increased metabolic capacity compared to *D. pigrum*. This heatmap shows stepwise module completeness averaged by KEGG module subcategory (y axis labels) for each of four nasal *Corynebacterium* species (avg. genome size 2.3 - 2.5 Mb) and for *D. pigrum* (avg. genome size 1.9 Mb). Average stepwise completion scores were calculated including only modules detected in at least one of the analyzed genomes. Color legend on the bottom represents KEGG module categories and corresponds with the colors in Table 3. (P) and (S) indicate Pathway and Signature modules respectively. Species labels: *C. propinquum* (*Cpr*)*, C. pseudodiphtheriticum (Cps), C. accolens (Cac), C. tuberculostearicum (Ctu*), and *D. pigrum* (*Dpi*).

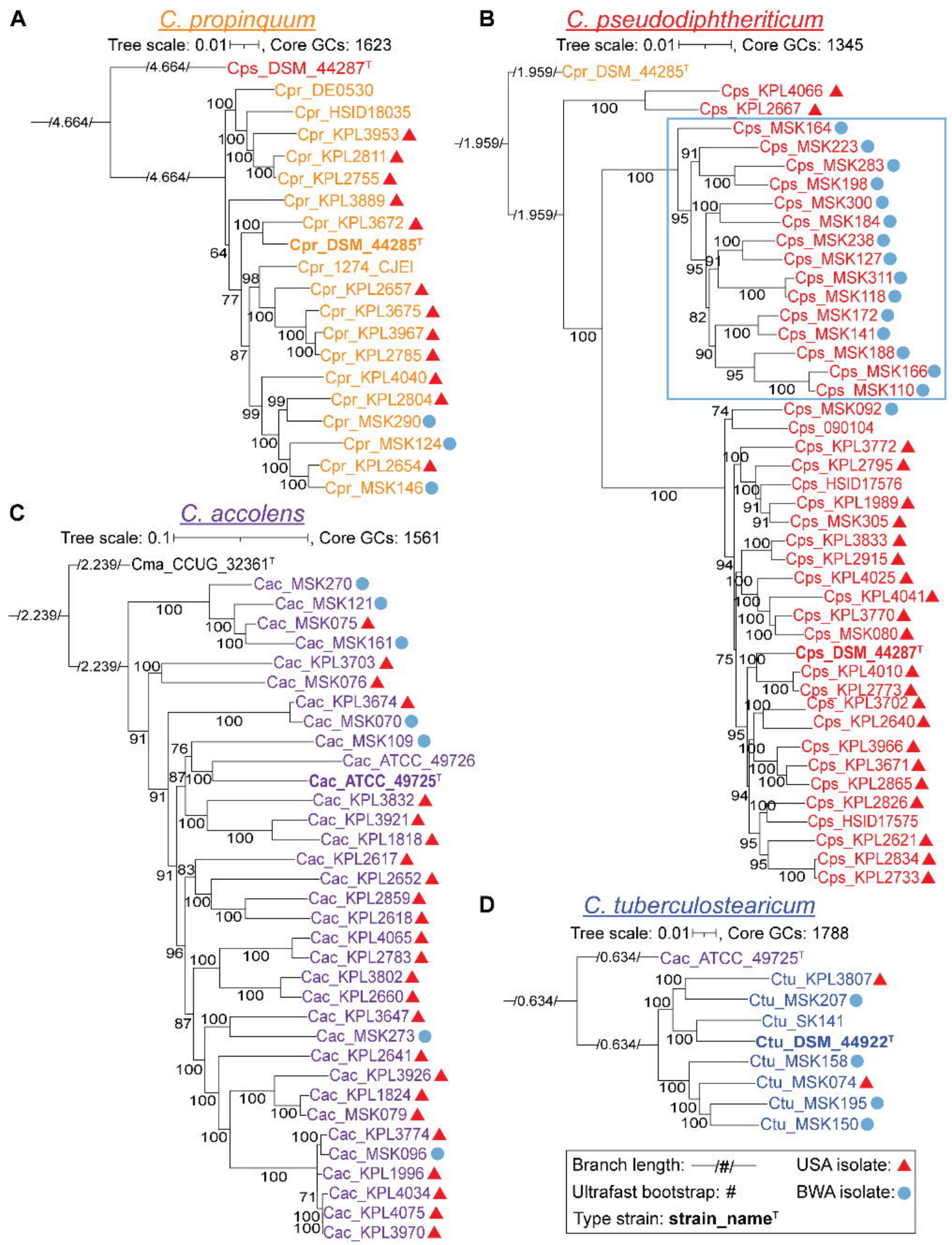
A
C. propinquum
Tree scale: 0.01, Core GCs: 1623
Cps_DSM_44287T
Cpr_DE0530
Cpr_HSID18035
Cpr_KPL3953
Cpr_KPL2811
Cpr_KPL2755
Cpr_KPL3889
Cpr_KPL3672
Cpr_DSM_44285T
Cpr_1274_CJEI
Cpr_KPL2657
Cpr_KPL3675
Cpr_KPL3967
Cpr_KPL2785
Cpr_KPL4040
Cpr_KPL2804
Cpr_MSK290
Cpr_MSK124
Cpr_KPL2654
Cpr_MSK146
B
C. pseudodiphtheriticum
Tree scale: 0.01, Core GCs: 1345
Cpr_DSM_44285T
Cps_KPL4066
Cps_KPL2667
Cps_MSK164
Cps_MSK223
Cps_MSK283
Cps_MSK198
Cps_MSK300
Cps_MSK184
Cps_MSK238
Cps_MSK127
Cps_MSK311
Cps_MSK118
Cps_MSK172
Cps_MSK141
Cps_MSK188
Cps_MSK166
Cps_MSK110
Cps_MSK092
Cps_090104
Cps_KPL3772
Cps_KPL2795
Cps_HSID17576
Cps_KPL1989
Cps_MSK305
Cps_KPL3833
Cps_KPL2915
Cps_KPL4025
Cps_KPL4041
Cps_KPL3770
Cps_MSK080
Cps_DSM_44287T
Cps_KPL4010
Cps_KPL2773
Cps_KPL3702
Cps_KPL2640
Cps_KPL3966
Cps_KPL3671
Cps_KPL2865
Cps_KPL2826
Cps_HSID17575
Cps_KPL2621
Cps_KPL2834
Cps_KPL2733
C
C. accolens
Tree scale: 0.1, Core GCs: 1561
Cma_CCUG_32361T
Cac_MSK270
Cac_MSK121
Cac_MSK075
Cac_MSK161
Cac_KPL3703
Cac_MSK076
Cac_KPL3674
Cac_MSK070
Cac_MSK109
Cac_ATCC_49726
Cac_ATCC_49725T
Cac_KPL3832
Cac_KPL3921
Cac_KPL1818
Cac_KPL2617
Cac_KPL2652
Cac_KPL2859
Cac_KPL2618
Cac_KPL4065
Cac_KPL2783
Cac_KPL3802
Cac_KPL2660
Cac_KPL3647
Cac_MSK273
Cac_KPL2641
Cac_KPL3926
Cac_KPL1824
Cac_MSK079
Cac_KPL3774
Cac_MSK096
Cac_KPL1996
Cac_KPL4034
Cac_KPL4075
Cac_KPL3970
D
C. tuberculostearicum
Tree scale: 0.01, Core GCs: 1788
Cac_ATCC_49725T
Ctu_KPL3807
Ctu_MSK207
Ctu_SK141
Ctu_DSM_44922T
Ctu_MSK158
Ctu_MSK074
Ctu_MSK195
Ctu_MSK150
Branch length: /#/
Ultrafast bootstrap: #
Type strain: strain_nameT
USA isolate:
BWA isolate:

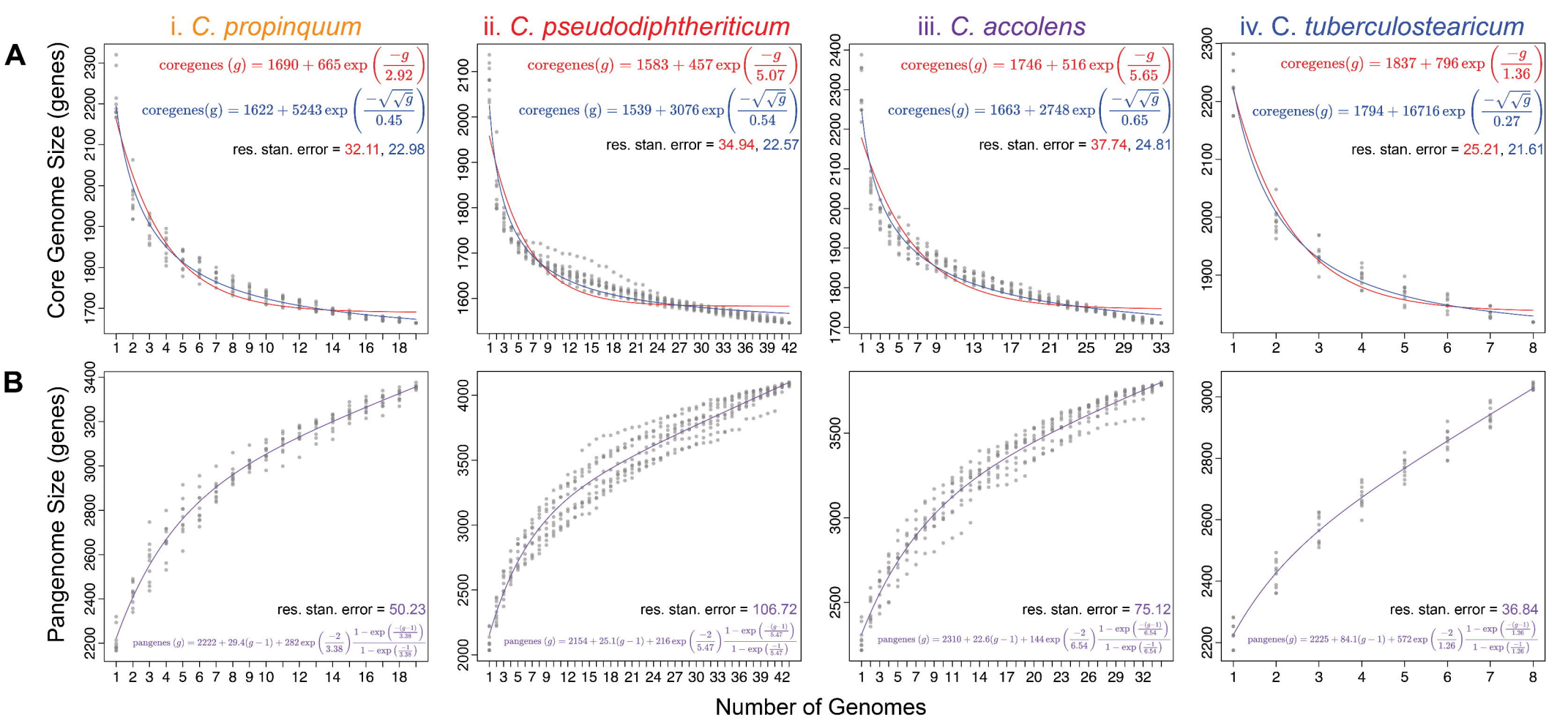
A
B
i. C. propinquum
ii. C. pseudodiphtheriticum
iii. C. accolens
iv. C. tuberculostearicum
Core Genome Size (genes)
Pangenome Size (genes)
Number of Genomes
coregenes (g) = 1690 + 665 exp(−g / 2.92)
coregenes(g) = 1622 + 5243 exp(−√√g / 0.45)
res. stan. error = 32.11, 22.98
coregenes (g) = 1583 + 457 exp(−g / 5.07)
coregenes (g) = 1539 + 3076 exp(−√√g / 0.54)
res. stan. error = 34.94, 22.57
coregenes(g) = 1746 + 516 exp(−g / 5.65)
coregenes(g) = 1663 + 2748 exp(−√√g / 0.65)
res. stan. error = 37.74, 24.81
coregenes(g) = 1837 + 796 exp(−g / 1.36)
coregenes(g) = 1794 + 16716 exp(−√√g / 0.27)
res. stan. error = 25.21, 21.61
res. stan. error = 50.23
pangenes (g) = 2222 + 29.4(g − 1) + 282 exp(−2 / 3.38) (1 − exp(−(g−1)/3.38)) / (1 − exp(−1/3.38))
res. stan. error = 106.72
pangenes (g) = 2154 + 25.1(g − 1) + 216 exp(−2 / 5.47) (1 − exp(−(g−1)/5.47)) / (1 − exp(−1/5.47))
res. stan. error = 75.12
pangenes (g) = 2310 + 22.6(g − 1) + 144 exp(−2 / 6.54) (1 − exp(−(g−1)/6.54)) / (1 − exp(−1/6.54))
res. stan. error = 36.84
pangenes(g) = 2225 + 84.1(g − 1) + 572 exp(−2 / 1.26) (1 − exp(−(g−1)/1.26)) / (1 − exp(−1/1.26))

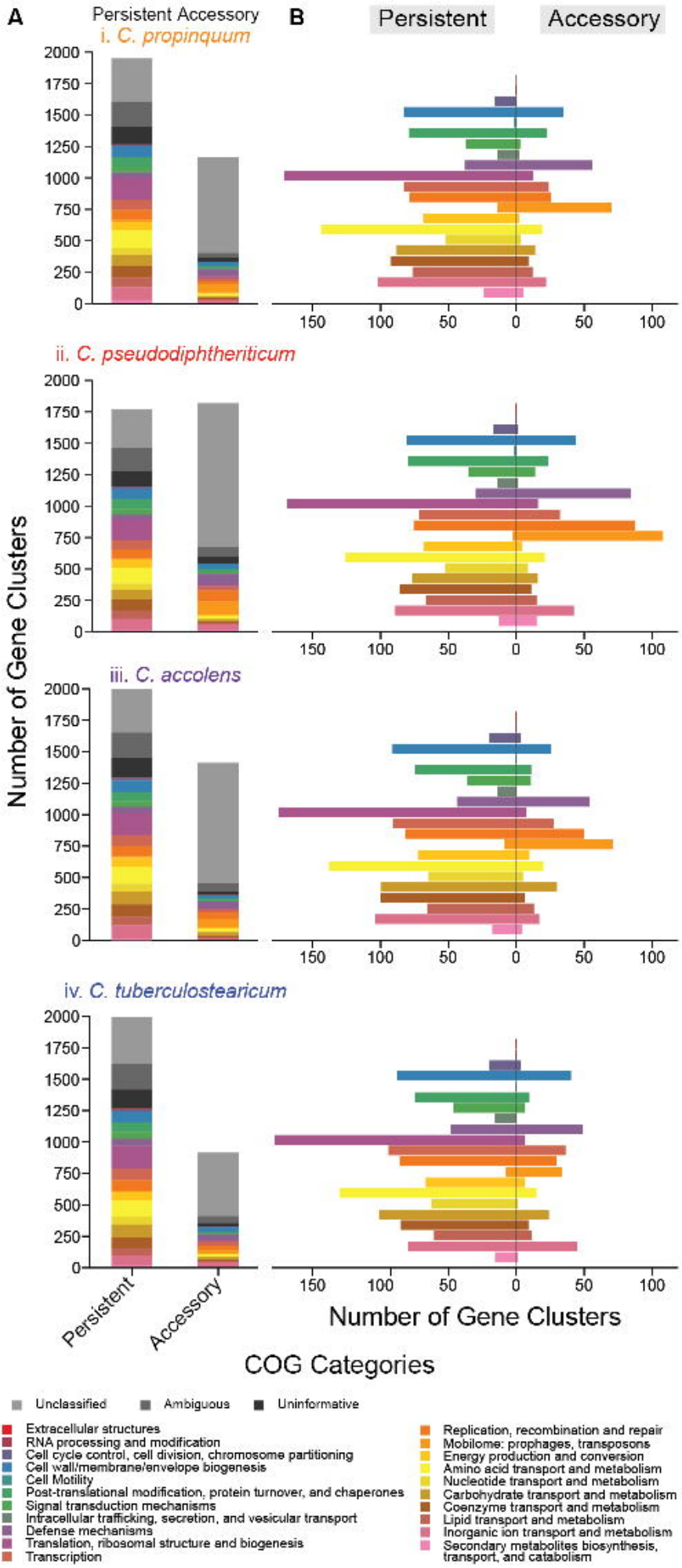
A
Persistent Accessory
B
Persistent
Accessory
i. C. propinquum
ii. C. pseudodiphtheriticum
iii. C. accolens
iv. C. tuberculostearicum
Number of Gene Clusters
Persistent
Accessory
Number of Gene Clusters
COG Categories
Unclassified
Ambiguous
Uninformative
Extracellular structures
RNA processing and modification
Cell cycle control, cell division, chromosome partitioning
Cell wall/membrane/envelope biogenesis
Cell Motility
Post-translational modification, protein turnover, and chaperones
Signal transduction mechanisms
Intracellular trafficking, secretion, and vesicular transport
Defense mechanisms
Translation, ribosomal structure and biogenesis
Transcription
Replication, recombination and repair
Mobilome: prophages, transposons
Energy production and conversion
Amino acid transport and metabolism
Nucleotide transport and metabolism
Carbohydrate transport and metabolism
Coenzyme transport and metabolism
Lipid transport and metabolism
Inorganic ion transport and metabolism
Secondary metabolites biosynthesis, transport, and catabolism

Ctu, *Cac*
C10-C20 isoprenoid biosynthesis, archaea
C10-C20 isoprenoid biosynthesis, bacteria
C5 isoprenoid biosynthesis, non-mevalonate pathway
Glycine cleavage system
Phosphate acetyltransferase-acetate kinase pathway, acetyl-CoA => acetate
Pyridoxal-P biosynthesis, R5P + glyceraldehyde-3P + glutamine => pyridoxal-P
Tetrahydrofolate biosynthesis, GTP => THF
Thiamine salvage pathway, HMP/HET => TMP

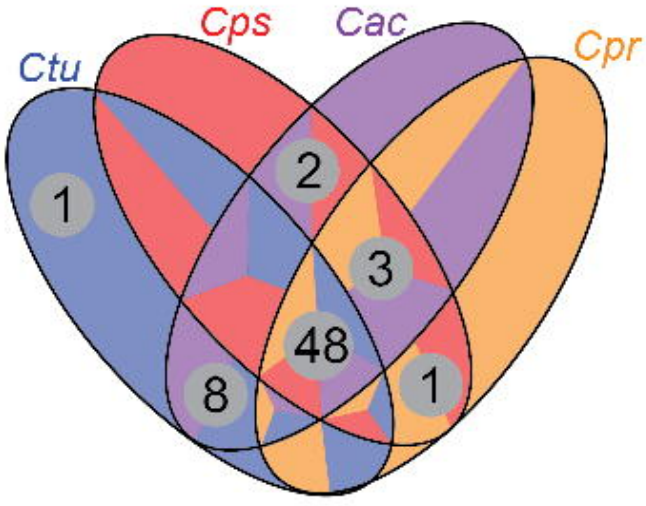

Ctu
Nucleotide sugar biosynthesis, glucose => UDP-glucose

Cps, *Cac*
Biotin biosynthesis, BioW pathway, pimelate => pimeloyl-CoA => biotin
Biotin biosynthesis, pimeloyl-ACP/CoA => biotin

Cps, *Cac*, *Cpr*
Histidine biosynthesis, PRPP => histidine
Lysine biosynthesis, succinyl-DAP pathway, aspartate => lysine
Ornithine biosynthesis, glutamate => ornithine

Cps, *Cpr*
Fatty acid biosynthesis, elongation

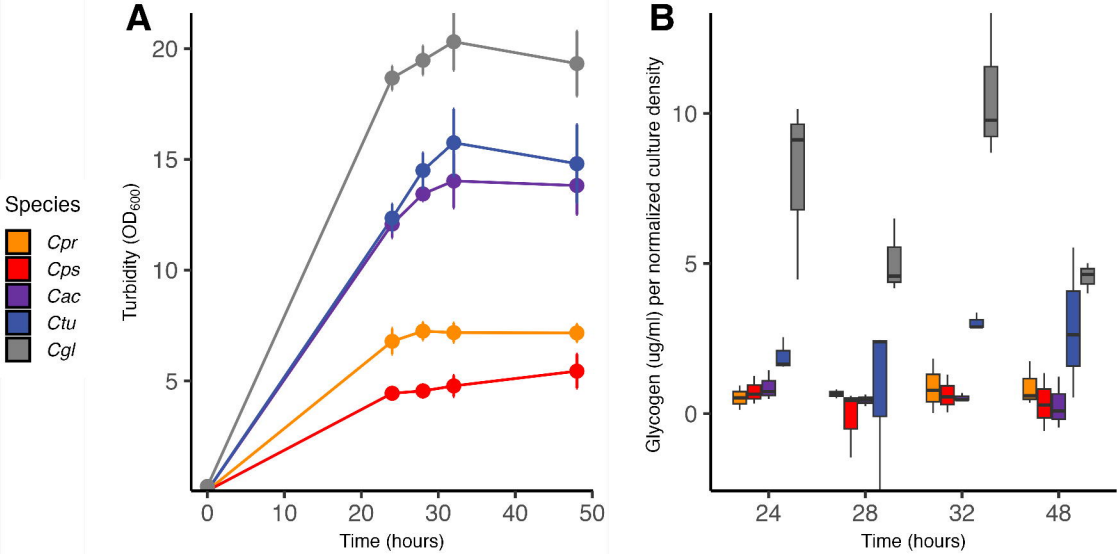
A
B
Species
Cpr
Cps
Cac
Ctu
Cgl
Turbidity (OD600)
Time (hours)
Glycogen (ug/ml) per normalized culture density
Time (hours)

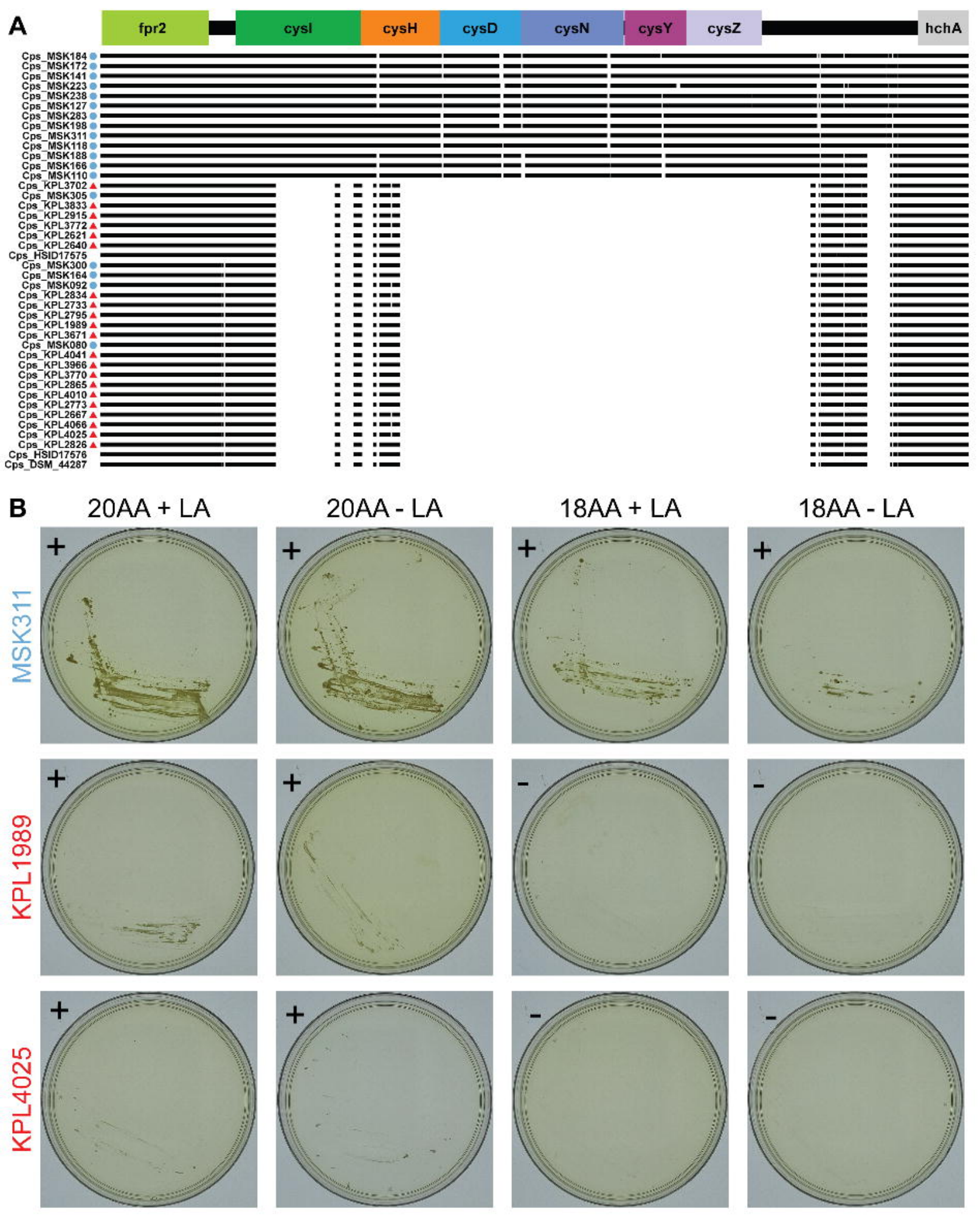
A
fpr2
cysI
cysH
cysD
cysN
cysY
cysZ
hchA
Cps_MSK184
Cps_MSK172
Cps_MSK141
Cps_MSK223
Cps_MSK238
Cps_MSK127
Cps_MSK283
Cps_MSK198
Cps_MSK311
Cps_MSK118
Cps_MSK188
Cps_MSK166
Cps_MSK110
Cps_KPL3702
Cps_MSK305
Cps_KPL3833
Cps_KPL2915
Cps_KPL3772
Cps_KPL2621
Cps_KPL2640
Cps_HSID17575
Cps_MSK300
Cps_MSK164
Cps_MSK092
Cps_KPL2834
Cps_KPL2733
Cps_KPL2795
Cps_KPL1989
Cps_KPL3671
Cps_MSK080
Cps_KPL4041
Cps_KPL3966
Cps_KPL3770
Cps_KPL2865
Cps_KPL4010
Cps_KPL2773
Cps_KPL2667
Cps_KPL4066
Cps_KPL4025
Cps_KPL2826
Cps_HSID17576
Cps_DSM_44287
B
20AA + LA
20AA - LA
18AA + LA
18AA - LA
MSK311
KPL1989
KPL4025
+
+
+
+
+
+
-
-
+
+
-
-

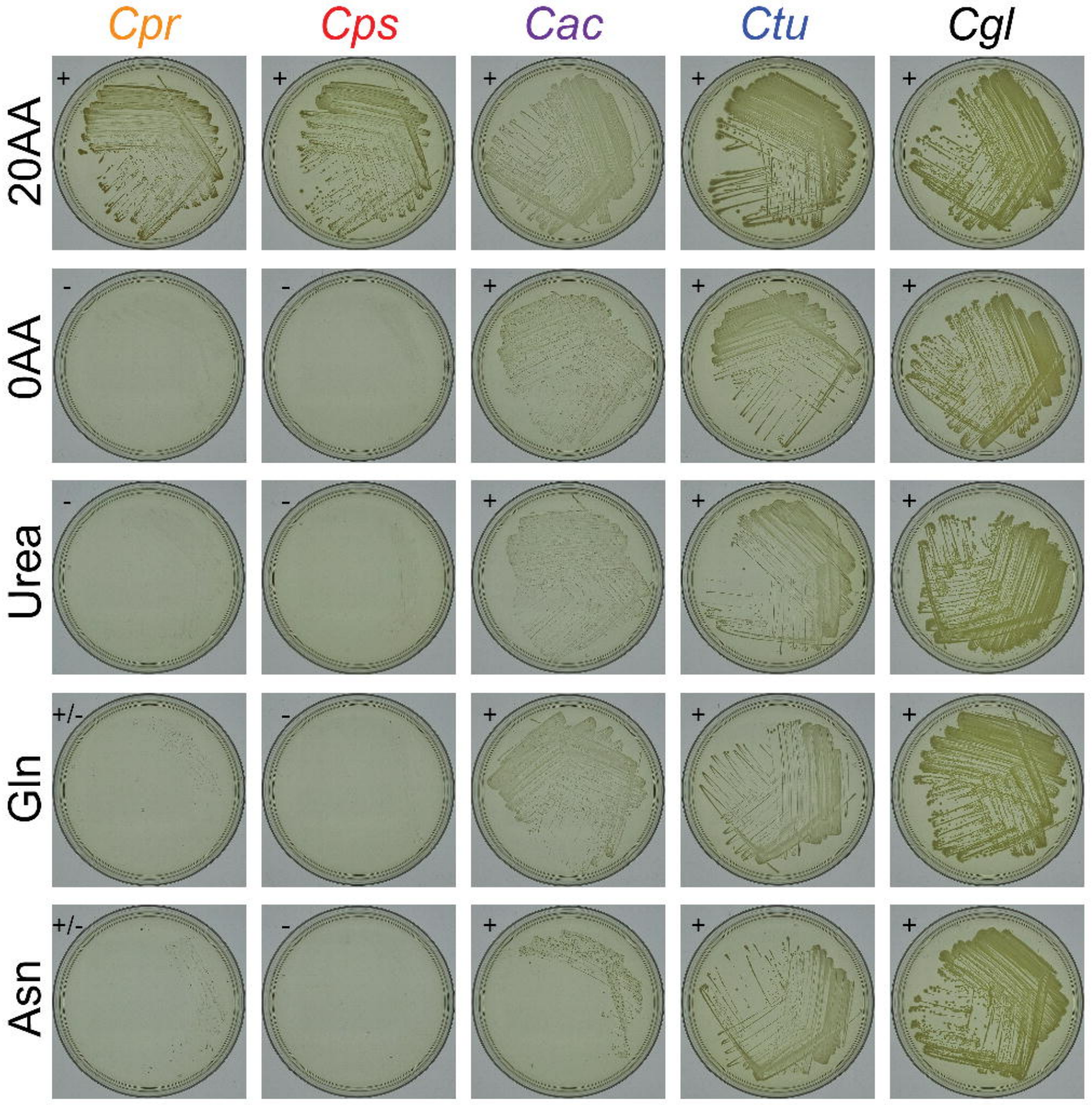
Cpr
Cps
Cac
Ctu
Cgl
20AA
0AA
Urea
Gln
Asn
+
-
+/-

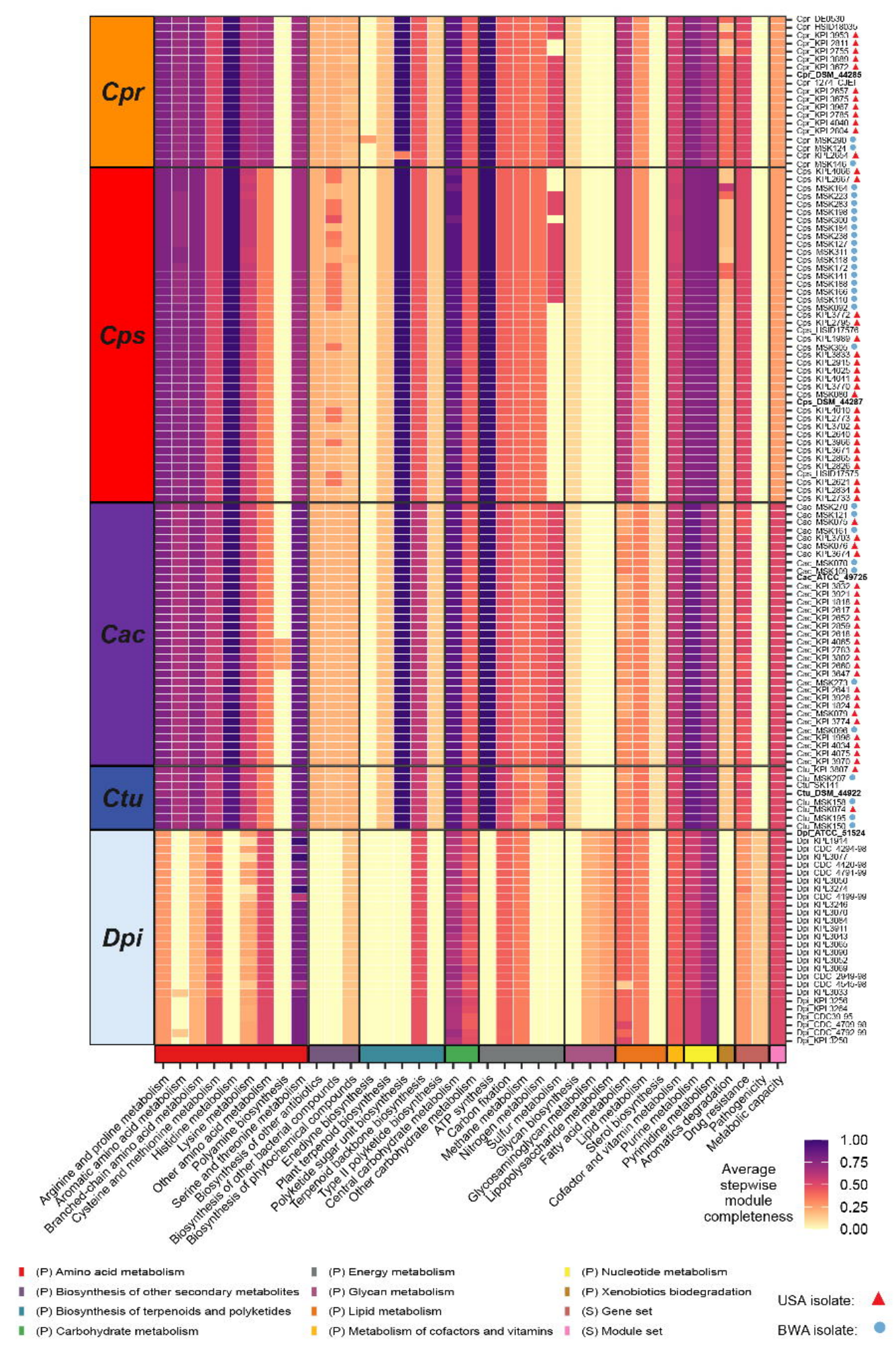
Cpr
Cps
Cac
Ctu
Dpi
Arginine and proline metabolism
Aromatic amino acid metabolism
Branched-chain amino acid metabolism
Cysteine and methionine metabolism
Histidine metabolism
Lysine metabolism
Other amino acid metabolism
Polyamine biosynthesis
Serine and threonine metabolism
Biosynthesis of other bacterial antibiotics
Biosynthesis of phytochemical compounds
Enediyne biosynthesis
Plant terpenoid biosynthesis
Polyketide sugar unit biosynthesis
Terpenoid backbone biosynthesis
Type II polyketide biosynthesis
Central carbohydrate metabolism
Other carbohydrate metabolism
ATP synthesis
Carbon fixation
Methane metabolism
Nitrogen metabolism
Sulfur metabolism
Glycan biosynthesis
Glycosaminoglycan metabolism
Lipopolysaccharide metabolism
Fatty acid metabolism
Lipid metabolism
Sterol biosynthesis
Cofactor and vitamin metabolism
Purine metabolism
Pyrimidine metabolism
Aromatics degradation
Drug resistance
Pathogenicity
Metabolic capacity
Average stepwise module completeness
1.00
0.75
0.50
0.25
0.00
(P) Amino acid metabolism
(P) Biosynthesis of other secondary metabolites
(P) Biosynthesis of terpenoids and polyketides
(P) Carbohydrate metabolism
(P) Energy metabolism
(P) Glycan metabolism
(P) Lipid metabolism
(P) Metabolism of cofactors and vitamins
(P) Nucleotide metabolism
(P) Xenobiotics biodegradation
(S) Gene set
(S) Module set
USA isolate:
BWA isolate: